Universidad del País Vasco
Euskal Herriko Unibertsitatea

ANALYTICAL ASSAYS BASED ON MODULATION OF QUANTUM DOTS *IN SITU*

Rūta Grinytė

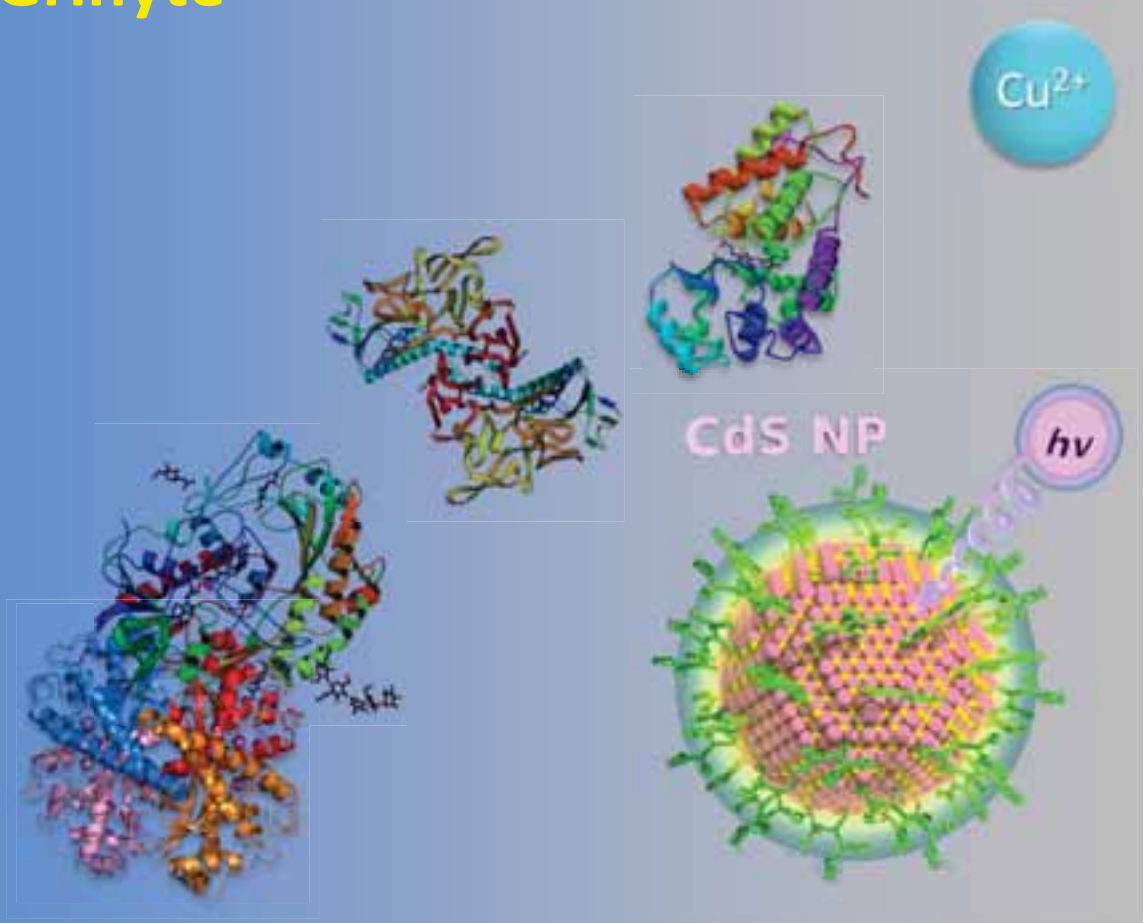

Donostia-San Sebastian | 2017

Universidad del País Vasco Euskal Herriko Unibertsitatea

CIC biomaGUNE

Analytical assays based on modulation of quantum dots *in situ*

Dissertation submitted to the

Department of Science and Technology of Polymers

University of the Basque Country (UPV/EHU)

for the degree of

Doctor in Applied Chemistry and Polymeric Materials

Presented by

Rūta Grinytė

Thesis supervisor: Dr. Valery Pavlov

University tutor: Dr. Isabel Goñi

AUTORIZACION DEL/LA DIRECTOR/A DE TESIS

PARA SU PRESENTACION

Dr/a. Valery Pavlov con N.I.F. X8155789N como Director/a de la Tesis Doctoral: *Ensayos analíticos basados en la modulación in situ de quantum dots* realizada en el Programa de Doctorado Química Aplicada y Materiales Poliméricos por el Doctorando Don/ña. Ruta Grinyte, autorizo la presentación de la citada Tesis Doctoral, dado que reúne las condiciones necesarias para su defensa.

En San Sebastian a 13 de enero de 2017

EL/LA DIRECTOR/A DE LA TESIS

Valery Pavlov

Fdo.: _____

AUTORIZACION DEL PONENTE DE TESIS

PARA SU PRESENTACION

Dr/a. Isabel Goñi como Ponente de la Tesis Doctoral: *Ensayos analíticos basados en la modulación in situ de quantum dots* realizada en el Programa de Doctorado Química Aplicada y Materiales Poliméricos por el Doctorando Don/ña. Ruta Grinyte, y dirigida por el Dr./a Valery Pavlov autorizo la presentación de la citada Tesis Doctoral, dado que reúne las condiciones necesarias para su defensa.

En _____a _____de _____de _____

EL PONENTE DE LA TESIS

Isabel Goñi

Fdo.: _____

AUTORIZACIÓN DE LA COMISIÓN ACADÉMICA DEL PROGRAMA DE DOCTORADO

La Comisión Académica del Programa de Doctorado en Química Aplicada y Materiales Poliméricos en reunión celebrada el día ____ de _____ de 20___, ha acordado dar la conformidad a la presentación de la Tesis Doctoral titulada: *Ensayos analíticos basados en la modulación in situ de quantum dots* dirigida por el/la Dr/a. Valery Pavlov y presentada por Don/ña. Ruta Grinyte_adscrito o adscrita al Departamento Ciencia y Tecnología de Polímeros

En _____a ___de _____de ___

EL MIEMBRO DE LA COMISIÓN ACADÉMICA RESPONSABLE DEL PROGRAMA DE DOCTORADO

Fdo.: _____

AUTORIZACIÓN DEL DEPARTAMENTO

El Consejo del Departamento de Ciencia y Tecnología de Polímeros en reunión celebrada el día ___ de _____ de _____ ha acordado dar la conformidad a la admisión a trámite de presentación de la Tesis Doctoral titulada: *Ensayos analíticos basados en la modulación in situ de quantum dots* dirigida por el/la Dr/a. Valery Pavlov y presentada por Don/ña. Ruta Grinyte ante este Departamento.

En _____ a _____ de _____ de _____

VºBº DIRECTOR/A DEL DEPARTAMENTO

Fdo.: _____

SECRETARIO/A DEL DEPARTAMENTO

Fdo.: _____

ACTA DE GRADO DE DOCTOR O DOCTORA
ACTA DE DEFENSA DE TESIS DOCTORAL

DOCTORANDO/A DON/DÑA. Ruta Grinyte

TITULO DE LA TESIS: **Ensayos analíticos basados en la modulación *in situ* de quantum dots**

El Tribunal designado por la Comisión de Postgrado de la UPV/EHU para calificar la Tesis Doctoral arriba indicada y reunido en el día de la fecha, una vez efectuada la defensa por el/la doctorando/a y contestadas las objeciones y/o sugerencias que se le han formulado, ha otorgado por_____la calificación de:
unanimidad ó mayoría

SOBRESALIENTE / NOTABLE / APROBADO / NO APTO

Idioma/s de defensa (en caso de más de un idioma, especificar porcentaje defendido en cada idioma):

Castellano _____

Euskera _____

Otros Idiomas (especificar cuál/cuales y porcentaje) _____

En _____a _____de _____de _____

EL/LA PRESIDENTE/A, EL/LA SECRETARIO/A,

Fdo.: Fdo.:

Dr/a: _____ Dr/a: _____

VOCAL 1º, VOCAL 2º, VOCAL 3º,

Fdo.: Fdo.: Fdo.:

Dr/a: _____Dr/a:_____Dr/a:_____

EL/LA DOCTORANDO/A,

Fdo.: _____

Table of Contents

Resumen

Esta tesis se centra en el estudio de la modulación del tamaño de nanopartículas semiconductoras y su aplicación al desarrollo de ensayos de fluorescencia, electroquímicos y fotoelectroquímicos. El trabajo se ha dividido en seis capítulos. El primero, consiste en una breve introducción sobre nanomateriales y su uso en biodetección. Los siguientes cinco capítulos están basados en artículos presentados y publicados en revistas científicas internacionales. Por último, la tesis termina con las conclusiones, apéndices, una lista de mis publicaciones y agradecimientos.

En el primer capítulo se introducen los términos de nanociencia y nanotecnología y sus aplicaciones. La nanociencia es el estudio de estructuras y materiales en la escala nanométrica. La nanotecnología es la manipulación de la materia en escala atómica, molecular y supramolecular. La nanociencia y nanotecnología tienen su origen en la confluencia de materias como la química, biología, física, ciencia de materiales e ingeniería. La nanoescala varía desde 100 nanómetros hasta el nivel atómico, donde un nanómetro es la millonésima parte de un milímetro. Hoy en día, la nanotecnología es una de las áreas de mayor velocidad de crecimiento de la ciencia y la tecnología., en la que se ha hecho un progreso exponencial. Los usos actuales y potenciales de la nanociencia y la nanotecnología abarcan una amplia gama de campos y podrían dividirse en cuatro grandes categorías generales: nanometrología; tecnología electrónica, nanomedicina y nanomateriales.

El capítulo continúa describiendo los nanomateriales, en particular, nanopartículas (NPs) metálicas y semiconductoras. Las NPs son cristales de tamaño nanométrico, constituidos por moléculas orgánicas estabilizadoras y átomos de metal (Au, Ag,…) o semiconductores (CdS, TiO_2). Las NPs metálicas, especialmente las NPs de metales nobles, como la plata, el oro, el plomo, etc., muestran características físicas, químicas y biológicas características que las hacen altamente aplicables en el área terapéutica, sistema de administración de fármacos, en hipertermia / terapia fototérmica, imagen biomédica, y biodetección.

En comparación con las NPs metálicas, la principal ventaja de las NPs semiconductoras es su capacidad intrínseca de ser fotoexcitadas, y de emitir fotones

por la recombinación de parejas electron/agujero por lo que estas partículas fluorescentes se denominan en la literatura como puntos cuánticos (en inglés, *quantum dots*, QDs). Los QDs son cristales nanométricos de semiconductores inorgánicos o nanocristales semiconductores con excelentes propiedades ópticas y electrónicas en comparación con otros macro-objetos semiconductores. los QD presentan algunas ventajas comparados con colorantes orgánicos fluorescentes: espectros de emisión gaussianos estrechos y ajustables en tamaño con un amplio ancho de banda de excitación; los QD son excepcionalmente brillantes, debido a los altos rendimientos cuánticos fluorescentes; de larga duración y mayor resistencia al fotoblanqueo; el rango de longitudes de onda es ajustable según el tamaño y los altos coeficientes de extinción molar (~ 10-100 x de los colorantes orgánicos). Hay cuatro usos principales de los QDs: (1) visualización de células bajo iluminación continúa así como adquisición de imagen multi-color. (2) formación de imágenes de tejidos profundos y para el rastreo de células cancerosas *in vivo* durante la metástasis; (3) marcadores fluorescentes en biodetección; (4) ensayos que emplean la transferencia de energía por resonancia de fluorescencia (FRET) entre QDs.

Como se ha comentado anteriormente, los nanomateriales pueden ser convenientemente empleados en bioanálisis. Sin embargo, tales sistemas de ensayo basados en NPs presintetizadas se ven obstaculizados por la adsorción inespecífica de NPs decoradas con elementos de reconocimiento sobre superficies sólidas. Los sensores basados en FRET sufren una baja relación señal / ruido debido a un atenuamiento de la fluorescencia insuficiente entre las parejas donante/aceptor. La generación de NPs *in situ* producida por un evento de reconocimiento puede hacer frente a estos inconvenientes. En la siguiente parte del primer capítulo se describen los métodos bioanalíticos basados en la modulación enzimática de NPs, que son el objeto principal de esta tesis.

El grupo del profesor Itamar Willner (Universidad Hebrea de Jerusalén) describió por primera vez el crecimiento catalítico de NPs de oro *in situ* en presencia de cofactores NAD(P)H. El desarrollo de dicho sistema introdujo nuevos ensayos enzimáticos sensibles y nuevas configuraciones de biosensores que emplean estímulos ópticos, conductores o microgravimétricos como señales de lectura. Fueron desarrollados diversos sistemas basados en el crecimiento catalítico de NPs metálicas

para el análisis de las actividades enzimáticas de lactato deshidrogenasa, glucosa oxidasa, alcohol deshidrogenasa o acetilcolina esterasa.

Se ha descrito el crecimiento catalítico de NPs semiconductoras *in situ* que mejoran la sensibilidad de ensayos de detección analíticos. El beneficio principal de estos sistemas analíticos fue que las NPs semiconductoras fluorescentes crecidas enzimáticamente podían ser detectadas por espectroscopia de fluorescencia más sensible o fotoelectroquímica que mejora los límites de detección de los ensayos. Se demostró que los iones sulfuro, productos tiolados u ortofosfatos generados enzimáticamente podían interactuar con iones de cadmio añadidos exógenamente para producir NPs de CdS esféricas. Se publicaron distintos ensayos para acetilcolina esterasa, fosfatasa alcalina, S-adenosil-L-homocisteína hidrolasa y metionina gamma-liasa, glucosa oxidasa, peroxidasa de rábano picante, paraoxonasa sérica y glutatión reductasa.

El primer capítulo continúa con una breve descripción de los dispositivos bioanalíticos. Los nanomateriales se han convertido en componentes importantes en los dispositivos bioanalíticos, ya que mejoran claramente los resultados en términos de sensibilidad y límites de detección hasta la detección de moléculas individuales. Las caracterısticas específicas de los nanomateriales, tales como las propiedades ópticas o electrónicas, se han utilizado ampliamente para fabricar diferentes tipos de biosensores. La señal de lectura de estos dispositivos puede estar producida por el cambio en la intensidad o posición del pico de absorción óptica o espectros de emisión de fluorescencia, resonancia de plasmón superficial (SPR), espectrometría Raman amplificada por superfice (SERS) y potencial/corriente electroquímica. Existen varios grupos diferentes de biosensores basados en nanomateriales, como SPR, SERS, fluorescencia, biosensores electroquímicos y fotoelectroquímicos.

La sección final del primer capítulo incluye las principales **hipótesis de la tesis: (1) la modulación de la forma de las CdS NPs en mezcla de reacción acuosas pueden ser provocadas por cantidades traza de analitos. (2) Los ensayos analíticos basados en la modulación del crecimiento de NPs semiconductoras serán más sensibles que los publicados previamente donde los iones S^{2-} son generados en presencia de analitos. (3) Debido a las propiedades únicas de las CdS QDs, formadas en mezcla de ensayos, menos caras que la espectroscopía de UV-vis, la detección electroquímica y**

fotoelectroquímica en vez de espectroscopía de fluorescencia puede ser aplicada para el seguimiento de la formación de CdS QDs, haciendo los ensayos más rentables y asequibles. Por tanto, esta tesis se centra en la modulación *in situ* de NPs semiconductoras (QDs) descubiertas por técnicas ópticas, electroquímicas y fotoelectroquímicas.

El segundo capítulo de la tesis describe el estudio de las propiedades fotocatalíticas de las NPs semiconductoras sintetizadas por medio de enzimas y su aplicación en la detección de actividades enzimáticas. Se demostró que las NPs semiconductoras de CdS (CdS NPs) producidas enzimáticamente son capaces de catalizar la oxidación del conocido sustrato enzimático cromógenico 3,3 ', 5,5' - tetrametilbenzidina (TMB) bajo luz UV. Estas NPs utilizan la energía de los fotones de luz UV y no requieren peróxido de hidrógeno para la oxidación de TMB. La tasa de oxidación fotocatalítica de TMB es directamente proporcional a la cantidad de CdS NPs producidas *in situ*. Estas propiedades de las CdS NPs se aplicaron al desarrollo de ensayos colorimétricos sensibles para la glucosa oxidasa (GOx) y la glutatión reductasa. Los ensayos cromogénicos desarrollados muestran una sensibilidad del mismo orden de magnitud o incluso mejor que la de los ensayos fluorogénicos correspondientes. La metodología desarrollada abre la posibilidad de utilizar un sustrato común y barato como el TMB , como compuesto cromogénico universal para su empleo en ensayos colorimétricos simples y sensibles de una serie de enzimas. El trabajo presentado en este capítulo ha sido publicado: Ruta Grinyte, Gaizka Garai-Ibabe, Laura Saa, Valeri Pavlov, Anal Chim Acta., 2015 Jun 30;881:131-8.

El tercer capítulo de la tesis describe el proceso de ataque biocatalítico (en inglés, *etching*) de CdS NPs. Bajo acción de la enzima peroxidasa de rábano picante (HRP) en presencia de diferentes concentraciones de agua oxigenada (H_2O_2), se demostró la disminución gradual del tamaño de las CdS NPs. Dicho fenómeno se comprobó por el desplazamiento del pico de emisión hacia el azul (en inglés, *blue-shift*), la disminución de la intensidad de la fluorescencia y mediante imágenes de microscopía electrónica de transmisión (TEM). Por otro lado, se aplicó por primera vez este fenómeno para la monotorización en tiempo real de la fotoluminiscencia durante el proceso de *etching* de las CdS NPs. Para este experimento, la fluorescencia se midió inmovilizando las CdS

NPs sobre la superficie de microparticulas con la posterior adición de todos los componentes. La adquisición de imágenes de las CdS NPs durante el proceso de *etching* se realizó mediante microscopía de fluorescencia de campo amplio. La presente propuesta desarrollada podría encontrar una amplia gama de aplicaciones en química analítica y abrir un nuevo camino para la modificación y modulación enzimática de dispositivos bioelectrónicos basados en NPs de semiconductores. . El trabajo presentado en este capítulo ha sido publicado: Ruta Grinyte, Laura Saa, Gaizka Garai-Ibabe, Valeri Pavlov, Chem. Commun., 2015, 51, 17152-17155.

En el cuarto capítulo de la tesis se desarrolla un nuevo inmunoensayo óptico y electroquímico para la detección de marcadores tumorales como por ejemplo la superóxido dismutasa (SOD2) basándose en la generación enzimática *in situ* e inmovilización de las CdS QDs sobre microparticulas. En dicho inmunoensayo, el analito de interés (SOD2) media en la inmovilización del anticuerpo conjugado de la fosfatasa alcalina (ALP) sobre la superficie de las microparticulas de cloruro de polivinilo. La hidrólisis enzimática de para-nitrofenilfosfato por la ALP desencadena la rápida formación de las CdS NPs estabilizadas con fosfato en la superficie de las microparticulas. Para su detección se empleó la espectroscopia de fluorescencia y voltametría de onda cuadrada (SWV). Estos nuevos inmunoensayos basados en la detección electroquímica y fluorogénica empleando CdS NPs generadas enzimáticamente, proporcionan mejores límites de detección de al menos tres órdenes de magnitud en comparación con los métodos publicados anteriormente. Esta metodología permitió la detección de SOD2 en lisados de células HepG2 (carcinoma hepatocelular humano). El trabajo presentado en este capítulo ha sido publicado: Ruta Grinyte, Javier Barroso, Marco Möler, Laura Saa, Valeri Pavlov, ACS Appl Mater Interfaces. 2016 oct DOI:10.1021/acsami.6b08362.

El quinto capítulo de la tesis describe la modulación en el crecimiento de las CdS QDs estabilizadas con cisteína mediante agua oxigenada (H_2O_2) producida enzimáticamente. El empleo de cisteína (CSH) como agente de recubrimiento posibilita la rápida formación de CdS QDs fluorescentes en soluciones acuosas a temperatura ambiente. Se demuestra que la oxidación del agente estabilizante mediante H_2O_2 causa la disminución en la velocidad de formación *in situ* de las CdS NPs estabilizadas

con CSH a partir de los iones Cd^{2+} y S^{2-}. Posteriormente, se combinó la modulación del crecimiento de las CdS NPs estabilizadas con CSH con la oxidación biocatalítica de D-glucosa (glucosa) catalizada por la glucosa oxidasa (GOx), generándose H_2O_2 en la mezcla de reacción. La aplicación de este proceso biocatalítico para el desarrollo de ensayos fluorométricos y fotoelectroquímicos (PEC) más sensibles y simples sirvió para detectar la actividad de la enzima GOx en soluciones tampón y glucosa en muestras reales de suero humano utilizando la actividad fotocatalítica de las QD producidas. . El trabajo presentado en este capítulo ha sido publicado: Ruta Grinyte, Javier Barroso, Laura Saa, Valeri Pavlov, 2016 nov DOI:10.1007/s12274-016-1378-1.

Finalmente, en el último capítulo de la tesis se presenta la modulación en el crecimiento de las CdS NPs mediante un proceso redox catalizado por iones de cobre (Cu^{2+}). Los iones Cu^{2+} catalizan la oxidación de la CSH mediante oxígeno para modular el crecimiento de las CdS NPs estabilizadas con CSH. Este nuevo proceso químico se aplicó a la detección fluorogénica y fotoelectroquímica de los iones Cu^{2+} en muestras reales de agua mineral y de grifo basándose en la actividad fotocatalítica de los NPs producidas. Se demostró que los ensayos desarrollados no sufren interferencia con otros iones que acompañan a los iones Cu^{2+} y la sensibilidad se enmarca dentro del límite estándar de la Unión Europea referente a los iones Cu^{2+} en agua potable. El trabajo presentado en este capítulo se encuentra en revisión en la siguiente revista: Ruta Grinyte, Javier Barroso, Laura Saa, Valeri Pavlov, Nano Letters.

Summary

In my thesis I studied modulating size of semiconductor nanoparticles and apply this process to development of optical, electrochemical and photoelectrochemical assays. The thesis consists of six chapters. The first chapter is a brief introduction to nanomaterials and their employment in biosensing. Following five chapters are based on articles submitted and published in the international scientific journals. The thesis ends with conclusions, appendixes of some chapters, the list of my publications and acknowledgments.

The first chapter introduces nanoscience and nanotechnology and their applications. Nanoscience is the study of structures and materials on the scale of nanometers. Nanotechnology is manipulation of matter on an atomic, molecular, and supramolecular scale. Nanoscience and nanotechnology originated at the interfaces between chemistry, biology, physics, materials science, and engineering. The nanoscale ranges from 100 nanometres down to the atomic level, where a nanometre is a millionth part of a millimeter. Today, nanotechnology is one of the fastest growing areas of science and technology, with exponential progress having being made. Current and potential uses of the nanoscience and nanotechnology cover a wide range of fields and could be broken down to four broad categories: nanometrology, electronics technology, nanomedicine and nanomaterials.

The chapter continues describing nanomaterials, in particular metal and semiconductor nanoparticles (NPs). NPs are nanometer-sized crystals composed of capping organic molecules and metal atoms (e.g. Au, Ag) or semiconductor materials (CdS, TiO_2). Metal NPs, especially noble metal NPs e.g., silver, gold, lead, etc., demonstrate characteristic physical, chemical and biological properties which make them more beneficial and broadly applied to therapeutics, drug-delivery systems, hyperthermia/photothermal therapy, biomedical imaging, and biosensing.

Compared to metal NPs, the key advantage of semiconductor NPs is their intrinsic capacity to be photoexcited and to emit photons upon recombination of electron-hole couples therefore such fluorescent particles are referred to in the literature as quantum dots (QDs). QDs are nanoscale crystals of inorganic semiconductor with

superb optical and electronic properties compared to other semiconductor macro-objects. QDs have some advantages over fluorescence organic dyes: size-tunable and narrow Gaussian emission spectra with broad excitation bandwidth; QDs are exceptionally bright, because of high fluorescent quantum yields; long-lasting and higher resistance to photobleaching; wavelength range is adjustable according to the size and high molar extinction coefficients (~10–100× that of organic dyes). There are four main biochemical applications of QDs: (1) visualization of cells under continuous illumination as well as multicolour imaging; (2) deep tissue imaging and tracking cancer cells in vivo during metastasis; (3) fluorescent labelling in biosensing; (4) assays employing fluorescence resonance energy transfer (FRET) involving QDs.

As it was mentioned before nanomaterials could be very conveniently used in bioanalysis. However, such assay systems relying on pre-synthesized NPs frequently suffer from nonspecific adsorption of NPs decorated with recognition elements on solid surfaces. FRET-based sensors suffer from low signal to noise ratio due to insufficient quenching of donor-acceptor couples. Generation of NPs in situ produced by a recognition event can address these issues. In the next part of the first chapter I will describe bioanalytical asays based on enzymatic modulation of NPs which are the main object of my thesis.

The group of professor Itamar Willner (The Hebrew University of Jerusalem) reported for the first time catalytic growth of gold NPs *in situ* in the presence of NAD(P)H cofactors. The development of such system introduced new sensitive enzyme assays and novel biosensor configurations that employ optical, conductive or microgravimetric stimuli as readout signals. A number of assays based on the catalytic growth of metal NPs by lactate dehydrogenase, glucose oxidase, alcohol dehydrogenase, acetylcholine esterase were developed.

The catalytic growth of semiconductor NPs *in situ* helping improve the sensitivity of analytical detection assays has been reported. The main benefit of those analytical systems was that enzymatically grown fluorescent semiconductor NPs could be detected by more sensitive fluorescence spectroscopy or photoelectrochemistry that improves detection limits of the assays. It was demonstrated that the enzymatically generated sulfide ions, thiolated products or orthophosphates could interact with exogenously added cadmium ions to yield spherical CdS QDs. Different assays for

acetylcholine esterase, alkaline phosphatase, S-adenosyl-L-homocysteine hydrolase and methionine gamma-lyase, glucose oxidase, horseradish peroxidase, serum paraoxonase, glutathione reductase were published.

The first chapter continues with brief description of bioanalytical devices. Nanomaterials became important components in bioanalytical devices since they readily enhance their performance in terms of sensitivity and detection limits down to single molecules detection. Specific characteristics like optical or the electronic properties of nanomaterials have been extensively used to fabricate different type of biosensors. The readout signal of these devices could be produced by the change in the intensity or peak position of optical absorption or fluorescence emission spectra, surface plasmon resonance (SPR), surface-enhanced Raman scattering (SERS), and electrochemical potential/current. There are several different groups of nanomaterial-based biosensors, like SPR, SERS, fluorescence, electrochemical and photoelectrochemical biosensors.

The final section of the first chapter includes the main **hypotheses of the thesis: (1) Modulation of the shape of CdS NPs in aqueous reaction mixtures can be triggered by trace amount of analytes. (2) The analytical assays based on modulation of the growth of semiconductor NPs will be more sensitive than the previously published assays in which S^{2-} ions are generated in the presence of analytes. (3) Due to unique properties of CdS QDs, formed in assay mixtures, less expensive UV-vis spectroscopic, electrochemical and photoelectrochemical detection instead of fluorescence spectroscopy can be applied to follow the formation of CdS QDs making assays more cost-efficient and more available.** Therefore, the PhD thesis is focused on modulation of semiconductor NPs (QDs) *in situ* discovered by optical, electrochemical and photoelectrochemical techniques.

The second chapter of the thesis covers photocatalytical properties of enzymatically grown semiconductor NPs applied to detection of enzymatic activities. It was demonstrated that enzymatically produced semiconductor CdS NPs are able to catalyze the oxydation of the well known chromogenic enzymatic substrate 3,3',5,5'-tetramethylbenzidine (TMB) by oxygen under UV light. These NPs use energy of photons from standard UV light and do not require hydrogen peroxide for oxidation of

TMB. The rate of photocatalytical oxidation of TMB is directly proportional to the quantity of CdS NPs produced *in situ*. These properties of CdS NPs were applied to development of colorimetric sensitive assays for glucose oxidase (GOx) and glutathione reductase. The developed chromogenic assays show sensitivity of the same order of magnitude or even better than that of relevant fluorogenic assays. The presented approach opens up the prospect to use inexpensive and available TMB as a universal chromogenic compound for the simple and sensitive colorimetric assays for a number of enzymes. The work presented in this chapter was published: Ruta Grinyte, Gaizka Garai-Ibabe, Laura Saa, Valeri Pavlov, Anal Chim Acta., 2015 Jun 30;881:131-8.

The third chapter of the thesis illustrates biocatalytic etching of semiconductor CdS NPs. Semiconductor CdS NPs treated with the enzyme horseradish peroxidase (HRP) in the presence of different concentrations of hydrogen peroxide (H_2O_2) rapidly decrease in size. It was proven by the blue-shift of emission peak and the decrease in the intensity of the fluorescence and by transmission electron microscopy (TEM) images. This phenomenon was also applied for the first time to monitor photoluminescence during etching of CdS NPs in real time. For this experiment CdS NPs were immobilized on the surface of microbeads and after adding all components fluorescence was measured continuously. In order to take images of CdS NPs during etching wide field fluorescence microscopy was used. The present approach discovered by us could find a broad range of applications in analytical chemistry and open up a new path for enzymatic modification and modulation of bioelectronic devices based on semiconductor NPs. The work presented in this chapter was published: Ruta Grinyte, Laura Saa, Gaizka Garai-Ibabe, Valeri Pavlov, Chem. Commun., 2015, 51, 17152-17155.

The fourth chapter of the thesis demonstrates new optical and electrochemical immunoassay for detection of tumor biomarkers such as superoxide dismutase (SOD2) employing enzymatic *in situ* generation and adsorbtion of CdS QDs onto plastic microbeads. In our immunoassay the target analyte (SOD2) mediates immobilization of alkaline phosphatase-antibody conjugate on the surface of polyvinyl chloride microbeads. The enzymatic hydrolysis of para-nitrophenylphosphate by alkaline phosphatase triggered rapid formation on the surface of microbeads of phosphate-

stabilized CdS semiconductor NPs which were detected by fluorescence spectroscopy and square-wave voltammetry. We have demonstrated that electrochemical and fluorogenic detection employing enzymatically generated CdS NPs yield new immunoassays with better detection limits in comparison with those of the previously published methods at least by three orders of magnitude. Our methodology allows for the detection of SOD2 in lysates from HepG2 (Human hepatocellular carcinoma) cells. The work presented in this chapter was previously published: Ruta Grinyte, Javier Barroso, Marco Möler, Laura Saa, Valeri Pavlov, ACS Appl Mater Interfaces. 2016 Oct DOI:10.1021/acsami.6b08362.

The fifth chapter of the thesis describes modulation of growth of cysteine-capped CdS QDs with enzymatically produced H_2O_2. The use of cysteine (CSH) as a capping agent allows for rapid formation of fluorescent CdS QDs in aqueous solutions at room temperature. We demonstrate that the oxidation of the capping agent CSH by H_2O_2 causes the decrease in the rate of the formation of CSH-capped CdS QDs from Cd^{2+} and S^{2-} ions *in situ*. Then we combined modulation of growth of cysteine-capped CdS QDs with biocatalytic oxidation of D-glucose (glucose) catalyzed by GOx leading to the production of H_2O_2 in the reaction mixture. We applied this biocatalytic process to the development of simple sensitive fluorometric and photoelectrochemical (PEC) assays for GOx activity in buffered solutions and D-glucose in real samples of human serum using the photocatalytic activity of the resulting QDs. The work presented in this chapter was published: Ruta Grinyte, Javier Barroso, Laura Saa, Valeri Pavlov, 2016 Nov DOI:10.1007/s12274-016-1378-1.

The last chapter of the thesis reports modulating growth of CdS NPs with redox process catalyzed by copper ions (Cu^{2+}). Cu^{2+} ions catalyze the oxidation of CSH by oxygen to modulate the growth of cysteine-capped CdS NPs. This new chemical process was applied to sensitive fluorogenic and photoelectrochemical detection of Cu^{2+} ions in real samples of mineral and tap water using the photocatalytic activity of the resulting NPs. We proved that our assays did not suffer from interferences with other ions accompanying Cu^{2+} and the sensitivity of our assays meets the European Union standard limit of Cu^{2+} ions in drinking water. The work presented in this chapter was submitted to: Ruta Grinyte, Javier Barroso, Laura Saa, Valeri Pavlov Nano Letters.

1

General introduction

1.1.1. Nanoscience and Nanotechnology

“There’s Plenty of Room at the Bottom” – the famous lecture made by physics Richard Feynman in 1959 at an annual meeting of the American Physical Society at Caltech. Feynman, Richard P. (1960) There's Plenty of Room at the Bottom.[1] In this talk, Feynman laid the theoretical basics for the field now called nanotechnology when he imagined a day when it will possible to build precise machine and components of molecular size. Nowadays, Nanotechnology and nanoscience are employed in a wide group of products and services.

Nanoscience is the study of structures and materials on the scale of nanometers. Nanotechnology is manipulation of matter on an atomic, molecular, and supramolecular scale. Nanoscience and nanotechnology originated at the interfaces between chemistry, biology, physics, materials science, and engineering. The nanoscale ranges from 100 nanometres down to the atomic level, where a nanometre is a millionth part of a millimeter. For comparison, for example, a sheet of paper is about 100,000 nanometers thick. Manipulation at nanoscale range allows us to process individual natural and synthetic nanostructures where quantum effects can play a significant role. Wherefore, this opens up new opportunities to understand physical and chemical properties of natural and artificial nano-objects having impact on the early disease detection and diagnosis, prevention and treatment. Moreover, it is helping to greatly improve, even revolutionize, many products, technology, and industry sectors.

Over the past two decades, scientists and engineers have been dealing with nanoscale materials and have a clearer picture of how to create nanoscale objects with properties never visualized before. Today, nanotechnology is one of the fastest growing areas of science and technology, with exponential progress being made. The promising application of nanoscience and nanotechnology is helpful in improving the quality of human life for all segments of the population.

1.1.2. Applications of Nanoscience and Nanotechnology

Current and potential uses of the nanoscience and nanotechnology cover a wide range of fields and could be divided into four broad categories (Scheme 1)[2-5]:

Nanomaterials – one of the main products of nanotechnologies. Nanoparticles (NPs), tubes, rods, or fibres are normally defined as being smaller that 100 nanometres in at least one dimension. They have a number of applications in healthcare (for targeted drug delivery, regenerative medicine, and diagnostics), electronics, cosmetics, textiles, information technology and environmental protection (for purification of air and water with catalytic nanomaterials).

Nanometrology – is a subfield of metrology concerned with measurements at the nanoscale. Some of the most frequent techniques used in nanometrology are transmission electron microscopy, scanning electron microscopy, atomic force microscopy, and X-ray diffraction.

Electronics, optoelectronics and information and communication technologies heavily depend on the knowledge of properties of nanodevices and nanomaterials. In the course of development of these technologies new advances in nanoscience and nanotechnology, including fabrication, processing, applications, and characterization of nano-objects are made. For instance, during development of miniature, inexpensive and available electronic devices huge progress in fabrication and modification of nanomaterials and microchips has been seen.

Bio-nanotechnology and nanomedicine – the most stimulating application concerned with molecular scale properties and applications of biological nanostructures and defining diseases diagnosis, controlled drug delivery in the body and molecular imaging.

Scheme 1.1. Aplications of nanoscience and nanotechnology.

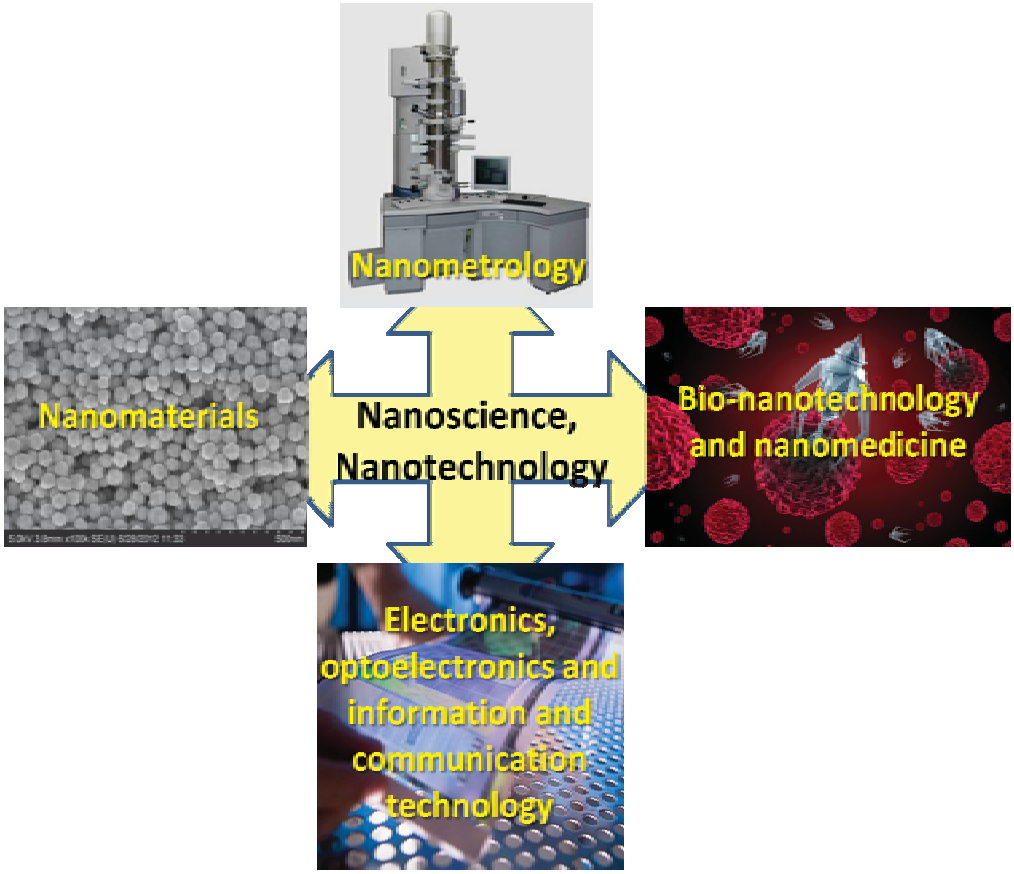

1.2. Nanomaterials: metallic and semiconductor nanoparticles

Nanomaterials with all three external dimensions at nanoscale are known as nanoparticles. These nanometer-sized crystals are composed of capping organic molecules and metal atoms (e.g. Au, Ag)[6, 7] or semiconductor materials (CdS, TiO_2) [8, 9]. . At nanoscale level physical and chemical properties of nanomaterials are govern by quantum effects. They depend on the composition, shape, environment and size of NPs. Therefore, absorption, emission spectra and catalytical activities of nanomaterials can be conveniently and easily variated by changing their size, shape and molecules in vicinity to their surface. Due to this feature nanometer-sized structures have unique electrical, optical and photophysical properties and can be very conveniently employed for transduction and amplification of electronic and photonic signals

1.2.1. Metallic nanoparticles: properties and applications

Metal NPs, especially noble metal NPs e.g., silver, gold, lead, etc. (Figure 1.1), demonstrate characteristic colors unique shape and size-dependent optical properties. These unique optical properties originate from localized surface plasmon resonance (LSPR) which is the frequency at which conduction metal electrons oscillate in the presence of the oscillating electromagnetic field of the light.[10, 11] In addition, the metals (gold, silver, copper) with free electrons exhibit plasmon resonances in the visible region of light giving rise to intense colors important for optical applications. [12, 13] In addition to significant optical properties, metal NPs demonstrate electrochemical activity and are very broadly utilized as labels to read out biorecognition events by optical and electrochemical methods. [14]

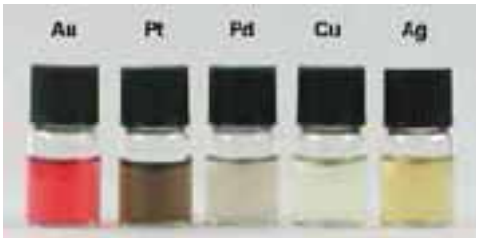

Figure 1.1. Metal nanoparticles (gold, platinum, palladium, copper, silver).[13]

Unique physical, chemical and biological properties of metal NPs depending on their geometry make them more useful than traditional organic molecules in the area of clinical applications like therapeutics, imaging and diagnosis. Moreover, metal NPs show effective anti-microbial abilities.[15] It was demonstrated that pathogenic microorganisms show less resistance to NPs compared to conventional antibiotics.[16] Nanoscale size of the particles allows them to circulate in the blood stream *in vivo* and probably reach targeted tumors. Easy synthesis and surface modification of gold NPs (AuNPs) facilitates their use as drug-delivery system carrier.[17] NPs also could be applied in hyperthermia/photothermal therapy because tumor cells are more susceptible to high temperature than normal cells. Metallic NPs demonstrate perfect properties as selective photo-dynamic therapy and hyperthermic agents.[18] Research has shown the application of magnetic fields to metallic NPs results in rapid heating.[19] It was demonstrated that this kind of heating quickly and efficiently destroy tumor cells.[20]

Metal NPs are very important nanomaterials with unique features suitable for biomedical imaging. For example gold NPs could be good contrast agents *in vivo* because of gold's high atomic number which allows high absorption and enhancement of ionizing radiation and make them visible by X-ray computer tomography.[21, 22] Moreover, metal NPs posses Raman scattering activity which could visualize intracellular molecules at the nanometer scale resolution employing surface-enhanced Raman scattering (SERS), nano-spectroscopy and nano-imaging.[23, 24]. Pre-synthesized metal NPs can be readily linked to antibodies,[25] polysaccharides, [26] RNA and DNA oligonucleotides[27, 28] for subsequent use in biosensing. Many different optical, electrochemical or acoustic detection systems based on metal NPs were published. [14]

1.2.2. Quantum Dots: properties and applications

Compared to metal NPs, the key advantage of semiconductor NPs is their intrinsic capacity to become photoexcited therefore such fluorescent particles are referred in the literature as quantum dots (QDs).[29] QDs are one of the first nanomaterials which have been integrated in bioanalysis. QDs are nanoscale crystals of inorganic semiconductor (semiconductor nanocrystals) with superb optical and electronic

properties compared to other semiconductor macro-objects. When this semiconductor NP absorbs a photon of light, an electron is promoted to the conduction band, and a region of positive charge, called the “hole,” is left behind in the valence band (Scheme 1.2).[30] Electron-hole pair is formed and due to the small size of particles it creates confinement energy.

Scheme 1.2. CdS QDs. Upon excitation with a photon, an electron-hole pair is created in a nanocrystal.

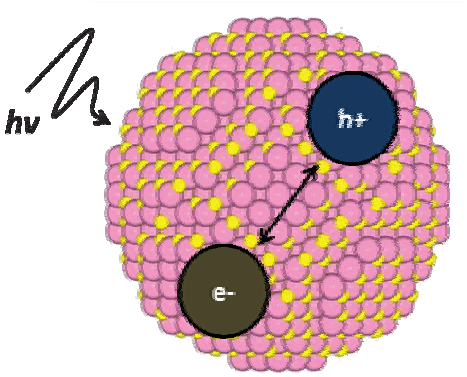

The quantum mechanical confinement causes the energy states to shift to higher levels, or blue shift. The smaller you make the nanocrystal, the higher the energy levels go. So, large diameter nanocrystals absorb and emit in the red area, small diameter nanocrystals absorb and emit in the blue area, and the wavelength of emission can be tuned by variating the size of the particles (see **Scheme 1.3.**). Changing the nanocrystal composition will change the wavelength range over which the optical properties can be tuned.[31]

Scheme 1.3. (A) Size-tunable fluorescence spectra of quantum dots; (B) Illustration of the relative particle sizes. From left to right, the particle diameters are 2.1 nm, 2.5 nm, 2.9 nm, 4.7 nm, and 7.5 nm. [31]

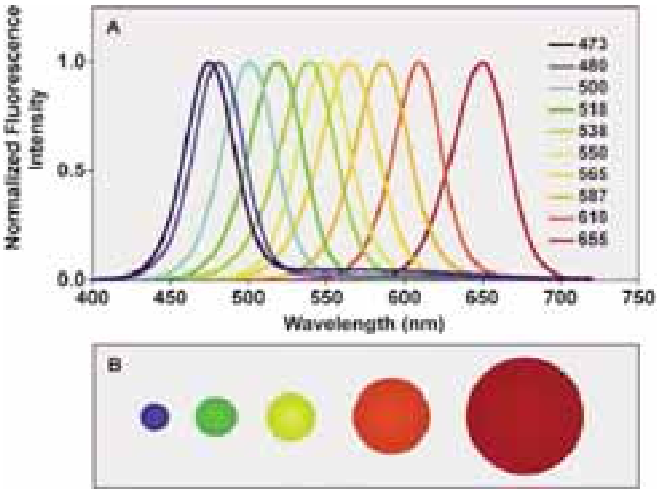

Fluorescent chemical compounds (fluorescence dyes) have been beneficial to the bioanalysis and imaging due to their characteristic high fluorescence intensity resulting in high sensitivity of detection and ease of use. However, QDs offer new benefits in bioanalysis that could overcome the limitations of organic dyes. In comparison with fluorescence organic dyes QDs have some advantages:

1. QDs have size-tunable and narrow Gaussian emission spectra with broad excitation bandwidth.
2. QDs are exceptionally bright, because of high fluorescent quantum yields. In fact, the emission of a single quantum dot can be determined visually with a fluorescent microscope.
3. QDs are long-lasting and more resistance to photobleaching.
4. Emission wavelength range is adjustable according to the size.
5. High molar extinction coefficients (~10–100× that of organic dyes).

Because of the broad benefits of QDs, the conjugates of fluorescence semiconductor NPs with recognition elements like antibodies and DNA oligonucleotides (QD-bioconjugates) have been generally used in imaging, labeling and

biosensing. There are four main uses of QDs in biochemistry. First, cellular labeling by QDs permits extended visualization of cells under continuous illumination as well as multicolour imaging, highlighting the advantages of the fluorophores.[32-37] Second, QDs spectroscopic properties can be exploited to achieve a deeper penetration than the available near-infrared dyes[38, 39] and could be applied for deep tissue imaging.[40] Moreover, QDs have been demonstrated to retain fluorescence in tissue *in vivo* for four months[41] and also could be used for tracking cancer cells *in vivo* during metastasis.[37, 42, 43] Third, QDs could be employed as fluorescent labels in biosensing, especially in assays based on detection of analytes by affinity interaction. For example, in immunoassays QDs were linked to detection antibody which was allowed to bind selectively to the captured antigen[44] or for detection of the four toxins from a single sample probed with a mixture of all four QD-antibody reagents.[45] DNA-QDs conjugates were also, used for detection of DNA like multiple genetic markers.[46] Finally, QDs are good donors for assays employing fluorescence resonance energy transfer (FRET). FRET relies on the distance-dependent transfer of energy from a donor molecule to an acceptor molecule. The transfer of energy leads to a reduction in the donor's fluorescence intensity and excited state lifetime, and an increase in the acceptor's emission intensity.[47] Bioconjugates, such as proteins, peptides, and oligonucleotides, are frequently tethered to QDs and create FRET-based sensors for detection of enzymatic activity.[48, 49] The cleavage of acceptor molecules caused by enzymes makes changes in emission spectra and was used for sensing of enzymatic activities.[50, 51] Another assays based on FRET have been reported for detection of explosives[52] or sugars[53] in which analyte displaces bounded fluorescence quencher on the specific antibody fragments decorated QDs and QD photoluminescence increases.

1.3.1. Enzymatic Growth of Nanoparticles in Bioanalysis

As it was mentioned before nanomaterials could be very conveniently used in bioanalysis. However, such assay systems relying on pre-synthesized NPs frequently suffer from nonspecific adsorption of NPs decorated with recognition elements on

solid surfaces. FRET-based sensors suffer from low signal to noise ratio due to insufficient quenching of donor-acceptor couples. Generation of NPs *in situ* produced by a recognition event can address these issues.

The group of professor Itamar Willner (The Hebrew University of Jerusalem) reported for the first time catalytic growth of AuNPs *in situ* in the presence of NAD(P)H cofactors.[54] It was demonstrated that NAD(P)H can reduce yellow $AuCl_4^-$ to the colorless Au^I species (Equation 1). Later on, Au^I species were reduced by the Au NP seeds to the Au^0 nanoparticles (Equation 2).

$$AuCl_4^- + NADH \rightarrow Au^I + 4\,Cl^- + NAD^+ + H^+ \qquad (1)$$

$$2AuCl_4^- + NADH \xrightarrow{Au-NP} 2Au^0 + NAD^+ + H^+ \qquad (2)$$

The growth solutions upon interaction with different concentration of NADH in the visible region create changes in the colors and could be detected by UV-vis spectroscopy. Futhermore, the growth of AuNPs was confirmed by scanning electron microscopy (SEM) images Figure 1.2. AuNPs-functionalized glass slides in the presence of cetyl trimethylammonium bromide (CTAB) surfactant were analyzed. As it is shown in Figure 1.2., when the concentration of NADH increases the size and the surface coverage of the Au particles on the glass surface also increases. This optical readout method by using the catalytic growth of AuNPs seeds was applied for detection of lactate in the presence of the NAD^+-dependent lactate dehydrogenase (LDH).

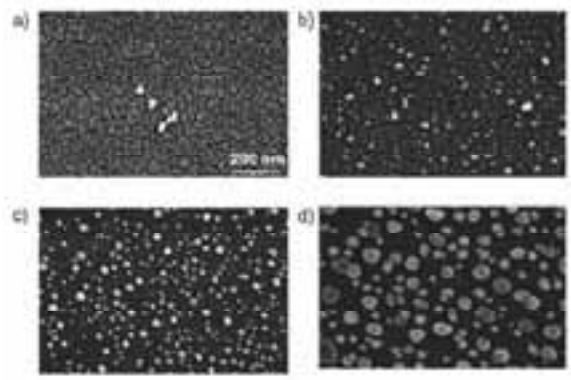

Figure 1.2. SEM images of enlarged Au particles generated on a Au nanoparticle/3-aminopropylsiloxane interface on a glass support using $AuCl_4$, CTAB, and variable concentrations of NADH. All images are on the same scale as indicated in a).[54]

The development of such system introduced new sensitive enzyme assays and novel biosensor configurations that employ optical, conductive or microgravimetric stimuli as readout signals. Another published system based on the catalytic growth of Au NPs was a glucose assay.[55] It was demonstrated that Au NP seeds act as catalysts for the reduction of $AuCl_4^-$ by H_2O_2, resulting in the enlargement of the particles which could be detected by UV-vis spectroscopy. Moreover, for sensing of ethanol by the NAD^+-dependent alcohol dehydrogenase (AlcDH), apart from the optical method, electrical detection was employed (Scheme 1.4).[56] In this system NADH cofactor produced by AlcDH induces catalytic deposition of Cu^0 on AuNPs-functionalized conductive surface. AlcDH also is able to trigger shape-controlled synthesis of the AuNPs (Scheme 1.5).[57] AlcDH produced NADH which reduces $AuCl_4^-$ at the surface of the Au NPs allowing for the colorimetric analysis of enzymatic processes because the color of the system changes from red to dark blue. Other enzymes which are able to catalyze the decomposition of enzymatic substrates to metal ion reducing agents could be used for growth of metal NPs. For example, acetylcholine esterase (AChE) produces thiocholine from acetylthiocholine which reduces $AuCl_4^-$ to stimulate the growth of AuNPs (Scheme 1.6).[58] In the presence of ascorbic acid thiocholine, produced by AChE, modulates the growth of silver-coated AuNPs. This process can be applied for optical detection of any AChE inhibitor (Scheme 1.7).[59]

Scheme 1.4. Catalytic deposition of Cu^0 on AuNPs by the NADH cofactor produced by AlcDH.[56]

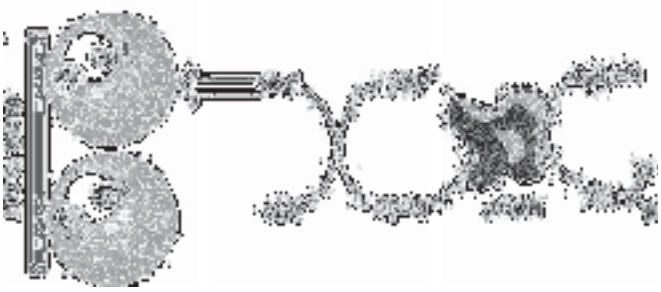

Scheme 1.5. Colorimetric detection of ethanol based on the NADH-mediated shape-controlled growth of the AuNPs.[57]

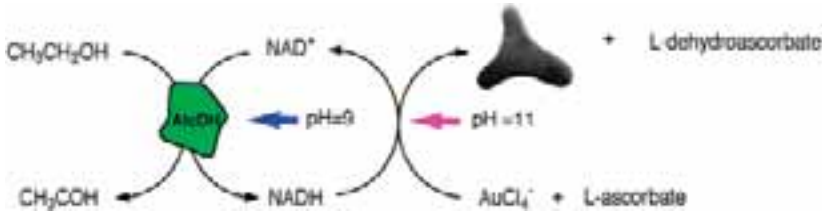

Scheme 1.6. Inhibition of the acetycholine esterase stimulated growth of AuNPs.[58]

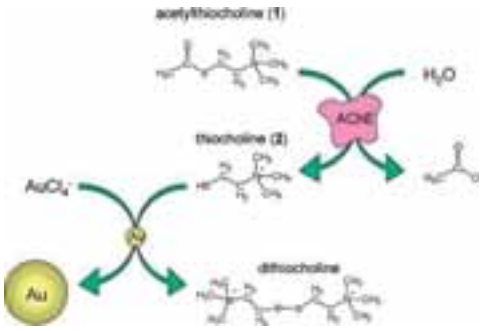

Scheme 1.7. Detection of acetylcholine esterase inhibitors by growing silver-coated AuNPs. [59]

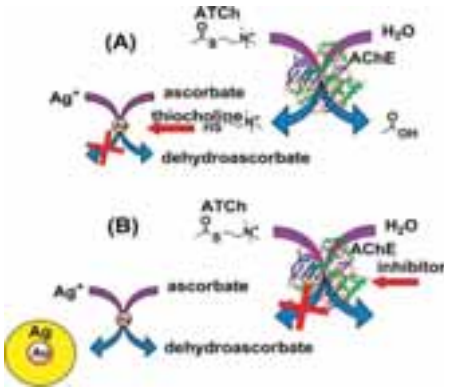

The catalytic growth of semiconductor NPs *in situ* helping improve the sensitivity of analytical detection assays has been reported. The main benefit of analytical systems was that enzymatically grown fluorescent semiconductor NPs could be detected by more sensitive optical techniques such as fluorescence spectroscopy or photoelectrochemistry significantly improving detection limits of the enzymatic assays. It was demonstrated that the enzymatically generated sulfide ions, thiolated products or orthophosphates could interact with exogenously added cadmium ions to yield spherical CdS QDs. For example, AChE hydrolyzes the artificial substrate acetylthiocholine (ATCh) yielding thiocholine, which in its turn catalyzes the hydrolysis of thiosulfate. The resulting H_2S interacts with Cd^{2+} ions to give fluorescent CdS NPs (Scheme 1.8A)[60] It was also demonstrated that alkaline phosphatase (ALP) is able to

hydrolyze thiophosphate to orthophosphate and H_2S. The latter reacts immediately with cadmium cations to give CdS QDs (Scheme 1.8B)[60] The detection limit for ALP was four times better than that of the commercial available assays. Another hydrolyzing enzyme S-adenosyl-L-homocysteine hydrolase (AHCY) decomposes S-adenosyl-L-homocysteine to L-homocysteine (Hcy). In the presence of methionine gamma-lyase (MGL) Hcy is decomposed to hydrogen sulfide which interacts with added Cd^{2+} ions to form fluorescent CdS NPs (Scheme 1.9).[61] The new fluorogenic assay for detection of MGL activity demonstrated 200-fold better sensitivity than the conventional chromogenic assay. Redox enzymes like glucose oxidase (GOx) and horseradish peroxidase (HRP) also can produce hydrogen sulfide giving CdS QDs (Scheme 1.10).[62]

Scheme 1.8. Enzymatic generation of CdS QDs for the detection of (A) AChE activity; (B) ALP activity.[60]

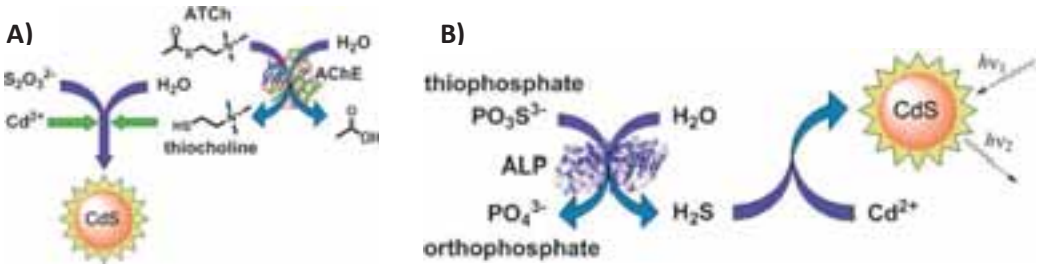

Scheme 1.9. Fluorogenic enzymatic assays for quantification of enzymatic activities of MGL and AHCY.[61]

Scheme 1.10 Enzymatic generation of CdS QDs for the detection of (A) GOx activity; (B) HRP activity.[62]

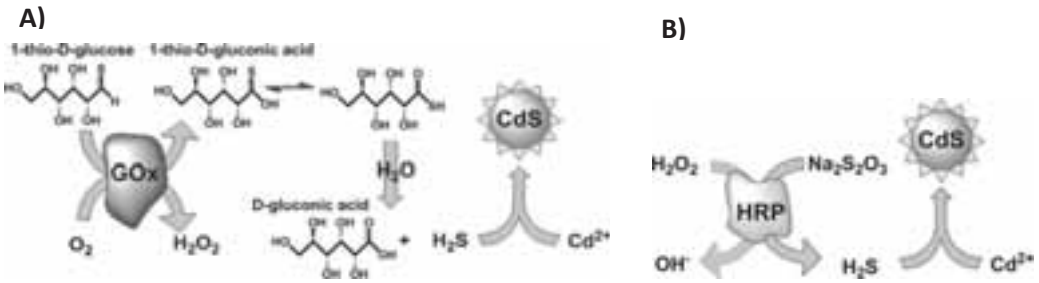

Another group of QDs-generating fluorogenic enzymatic assays relies on modulating the growth of CdS QDs with the products of biocatalytic transformation through inhibition or enhancement. For instance, an ultrasensitive assay to measure serum paraoxonase (PON1) activity was published relying on the enzymatic modulation of the growth of fluorescent CdS NPs where thiophenol, the product of enzymatic reaction, inhibits growth of CdS QDs (Scheme 1.11). [63] This assay leads to an improvement of the limit of detection by around 15 times, compared to the conventional assays to determine PON1 activity. Another fluorogenic bioanalytical system for detection of glutathione reductase activity (GR) was published elsewhere[64] in which the product of enzymatic reaction (reduced glutathione (GSH)) enhances the growth of QDs (Scheme 1.12). The sensitivity of this new assay is 3 orders of magnitude better than other fluorogenic methods previously reported. The concept of QDs formation *in situ* enhanced with the compounds generated by ALP was further expanded. In another system inorganic phosphate produced by ALP through hydrolysis of p-nitrophenyl phosphate (pNPP) stabilizes CdS QDs produced *in situ* in the presence of Cd^{2+} and S^{2-} ions (Scheme 1.13). [65] The system was applied to enzyme-linked immunosorbent assay (ELISA) being the first fluorogenic immunoassay bases on enzymatic growth of QDs *in situ*. Moreover, the sensitivity of this novel assay showed to be 1 order of magnitude better than that of the standard method based on colorimetric p-nitrophenyl phosphate assay.

Scheme 1.11. Detection of PON1 activity relying on the enzymatic modulation of growth of fluorescent CdS QDs.[63]

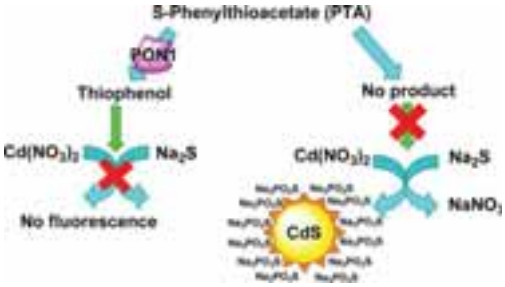

Scheme 1.12. Detection of GR activity where the enzymatic product (GSH) enhance the growth of fluorescent CdS QDs.[64]

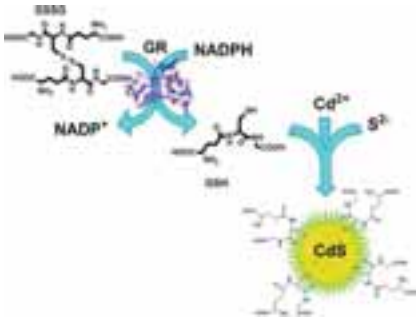

Scheme 1.13. Detection of ALP Activity by Enzymatic Growth orthophosphate stabilized-CdS QDs.[65]

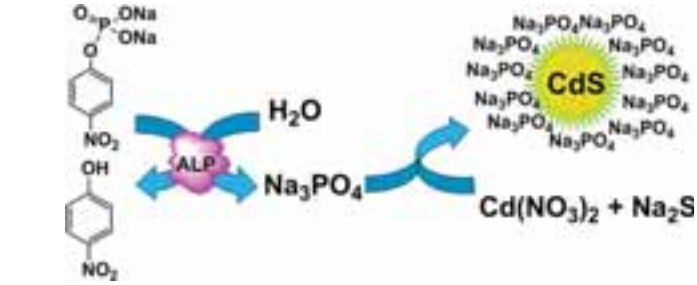

1.4. Biosensors based on nanomaterials

According to IUPAC definition biosensor is device that uses specific biochemical reactions mediated by isolated enzymes, immunosystems, tissues, organelles or whole cells to detect chemical compounds usually by electrical, thermal or optical signal.[66] Nanomaterials became important components in bioanalytical devices since they readily enhance their performance in terms of sensitivity and detection limits down to single molecules detection. Specific characteristics like optical or the electronic properties of nanomaterials have been extensively used to fabricate different type of

biosensors. The readout signal of these devices could be produced by the change in the intensity or peak position of optical absorption or fluorescence emission spectra, surface plasmon resonance (SPR), surface-enhanced Raman scattering (SERS), and electrochemical potential/current. There are several different groups of nanomaterial-based biosensors, like SPR, SERS, fluorescence, electrochemical and photoelectrochemical biosensors.

1.4.1. Surface plasmon resonance

SPR is a standard optical method for real time detection of binding interactions. SPR biosensing principle: firstly, polarized light is directed toward the sensor surface and when the analyte of interest bounds to the surface, the refractive index near the surface is altered. This modification of refractive index is registered.[67] In particular, nanomaterials are used like enhancers of the response of SPR biosensors. For example, gold spherical NPs of diameters ranging from 5 to 40 nm have been widely used to enhance the response of SPR biosensors. Furthermore, the coupling between the LSPR of AuNPs and the propagating SPR of Au films results in a greater SPR incident angle shift. During the biorecognition reaction, decorated AuNPs attached to the SPR sensor via affinity interaction make refractive index change more significant.[68, 69] The angle could be influenced by the size and shape of AuNP, [70, 71], surface/particle or interparticle distance.[72-75]

1.4.2. Surface-enhanced Raman scattering

SERS is a highly sensitive optical detection technique in which lasers are used to excite vibrational transitions in molecule adsorbed on a rough metal or on metal NPs surface. The resulting Raman spectra consist of bands corresponding to vibrational or rotational transitions specific to the molecular structure, and therefore provide chemical “fingerprints” to identify the analyte.[76, 77] Due to the possibility to detect a single molecule, SERS based devices could be used for the highly sensitive and selective detection of biological analytes. Using this technique, the detection sensitivity can be increased up to 100-1000 times higher than that of conventional Raman spectroscopy.[78, 79] AuNPs are most widely used as optical enhancing agent in SERS. For example, antibody-decorated AuNPs can generate high SERS enhancement

due to plasmonic coupling *via* controlled interaction of the NPs in response to sandwiched antibody−antigen assembly.[80] AuNPs also could be used as SERS detection probes because of the characteristic Raman peak of AuNPs whose intensity could be changed depending on a bound analyte.[78]

1.4.3. Fluorescence-based biosensors

Fluorescence-based biosensors are those devices that derive their analytical redout signal from the fluorescence emission. In these sensors single molecules could be repeatedly excited and detected to produce a bright signal easily measured even at single-cell level. There are two main types of fluorescent materials used in fluorescence-based assays and biosensors: organic fluorophores and quantum dots. Fluorescent inorganic semiconductor nanocrystals (QDs) increasingly substitute organic fluorophores and became novel fluorescence labels in biosensing with better stability and sensitivity.[81-84] For example, Mattoussi group demonstrated the use of QDs conjugated to antibody fragments to develop fluorescence nanosensor based on fluorescence resonance energy transfer (FRET) specific for the detection of the explosive 2,4,6-trinitrotoluene (TNT) in aqueous environments.[52] The group of Tang have developed a simple, fast, convenient and sensitive fluorescence biosensor for detection of organophosphorus pesticide based on fluorescence quenching of CdTe QDs in the presence of H_2O_2.[85]

1.4.4. Electrochemical biosensors

Electrochemical biosensors were the first scientifically proposed as well as productively commercialized biosensors. It is the most rapidly growing biosensors class.[86] Compared to other methods, such as spectroscopy and chromatography, the electrochemical measurements are much cheaper and simpler and easier to miniaturize, making them more suitable for point of care (POC) detection. In electrochemical biosensors the immobilized biomolecule acting as recognition element chemically or physically interacts with target analyte to produce or consume electrons or ions generating electrochemical readout signal which is used to quantify specifically analyte in the sample solution.[87] There are many types of electrochemical detection techniques depending on the type of electrochemical signal,

such as, potentiometry, amperometry, voltamperometry and electrochemical impedance spectroscopic measurements.[88] Some nanomaterials can be used for signal amplification as labels for analytes.[89] NPs in electrochemical signal amplification are broken down to main two groups operating by different mechanisms.

- First, NPs that catalyze the electrolysis of a large quantity of substrate which enhances the electrochemical signal. For example, the metal nanoparticle tags can act as catalytic sites for the electroless deposition of other metals.[90] For detecting DNA hybridization, the precipitation of silver on gold nanoparticle tags and a subsequent electrochemical stripping detection of the dissolved silver were used.[91] Another electrochemical immunoassay was based on copper-enhanced AuNPs tags for detection of hepatitis B.[92] The recognition event is amplified by the catalytic precipitation of copper on the AuNPs. The deposited copper is detected by anodic stripping voltammetry in an acidic solution.
- Second, NPs that increase the loading of electrochemically detectable species since every nanoparticle contains thousands of atoms that can be electrochemically detected. When captured biospecific molecules are labeled with electroactive NPs, the loading of electroactive species on the electrode surface significantly increases, leading to enhanced sensitivity of the biosensor. For instance, AuNPs, acting as electrochemical labels of affinity reactions, can be electrooxidated in an acidic solution and detected by electrochemical techniques.[93-96] Ag NPs function as electroactive labels that can be detected through a characteristic solid-state Ag/AgCl reaction.[97, 98] Moreover, metal sulfide NPs like ZnS, CdS and PbS in the bioconjugates could be detected directly without acid dissolution and preconcentration and could increase sensitivity to fentamolar level.[99, 100]

1.4.5. Photoelectrochemical biosensors

Photoelectrochemical (PEC) biosensors are based on photoelectrochemical process of electron excitation and transfer between the target analyte and the electrode surface under light irradiation.[101, 102] The ability to couple the photoexcitation process with electrochemical detection provides PEC sensors with the

unique advantage of being both optical and electrochemical sensors at the same time. Furthermore, low background signals, high sensitivity, simple operation, easy to miniaturize and inexpensive instruments makes PEC biosensors more attractive in these days.[103-105] The effectiveness of photo-current transfer in PEC biosensor is one of the important factors influencing PEC detection sensitivity and generally depends on the light-harvesting semiconductor materials attached on the substrate electrode. Among the various photoactive materials, semiconductor metal oxide nanostructures have of special interest because of their high chemical stability and strong photocatalytic activity. Titanium dioxide (TiO_2) is one of the most broadly employed nanostructured oxides in PEC biosensors. For example, for the sensitive detection of dopamine, TiO_2 NPs act as electron acceptor from dopamine molecule allowing to enhance photocurrent readout signal in the presence of the light.[106] In another report, a photoelectrochemical sensor for the determination of hydroquinone was developed, based on the high photoelectrocatalytic activity of hemin modified TiO_2 NPs. In this system hemin remarkably promoted the photocatalytic capacity of TiO_2 NPs to absorb the visible light.[107] Apart from metal oxide-based nanostructures, semiconductor QDs are also intensely studied because of their unique electronic and optical properties, as well as high PEC activity. As it was mentioned before, when the semiconductor QDs absorbs the photon of the light, electron-hole pair is formed and may also stimulate the generation of photocurrent. In the system published by Itamar Wilner enzymatically produced thiocholine scavenges the photogenerated valence-band holes of the QDs and enhances the formation of photocurrent.[108]

1.5. The aim of the thesis

Bioanalytical assays and devices employing metal NPs and QDs are becoming the mainstream technology for medical, forensic, and agricultural analysis. According to the literature, there is a strong growing interest in rapid development and broad application of such bioassays. The very simple idea to tether pre-synthesized QDs to biorecognition elements in order to use them as labels influenced dramatically,

imaging, biosensing and analytical chemistry and evolved into publication of incredibly huge number of articles in highly ranked international scientific journals. The introduction of new, more sophisticated concept relying on biocatalytic generation of QDs *in situ* has similar or stronger impact on biosensing. The majority of known enzymes can be taught to generate bright fluorescent semiconductor NPs upon selection of suitable experimental conditions and natural or artificial enzymatic substrates. The previously published works describing analytical assays based on enzymatic growth of CdS NPs employed biocatalytic formation of S^{2-} ions followed by addition of Cd^{2+} ions to yield CdS QDs. Those assays required significant build up of S^{2-} ions in the reaction mixture to form CdS NPs, hence the detection limits shown by those analytical assays were not satisfactory for commercial applications. On the one hand, the formation of CdS NPs from Cd^{2+} and S^{2-} can be easily modulated by trace amounts of stabilizing agents. On the other hand, the shape of preformed CdS NPs can be modified by redox processes. Potentially those modulating agents can be produced by enzymatic reactions or inorganic processes triggered by analytes of interest. In both cases the shape and the amount of CdS NPs define their chemical and physical properties which can be followed by number of laboratory techniques. **The hypotheses of the thesis are:**

(1) Modulation of the shape of CdS NPs in aqueous reaction mixtures can be triggered by trace amount of analytes.

(2) The analytical assays based on modulation of the growth of semiconductor NPs will be more sensitive than the previously published assays in which S^{2-} ions are generated in the presence of analytes.

(3) Due to unique properties of CdS QDs, formed in assay mixtures, less expensive UV-vis spectroscopic, electrochemical and photoelectrochemical detection instead of fluorescence spectroscopy can be applied to follow the formation of CdS QDs making assays more cost-efficient and more available.

Therefore, the PhD thesis is focused on modulation of semiconductor NPs (QDs) *in situ* discovered by optical, electrochemical and photoelectrochemical techniques.

1.6. References

[1] R.P. Feynman, There's Plenty of Room at the Bottom Engineering and Science, 23 (1960) 22-36.

[2] D. Bhattacharyya, S. Singh, N. Satnalika, A. Khandelwal, S.-H. Jeon, Nanotechnology, Big things from a Tiny World: a Review, Science and Technology, 2 (2009) 29-38.

[3] I.Y. Wong, S.N. Bhatia, M. Toner, Nanotechnology: emerging tools for biology and medicine, Genes & Development, 27 (2016) 2397-2408.

[4] G.A. Menezes, P.S. Menezes, C.M. Menezes, Nanoscience in diagnostics: A short review, Internet Journal of Medical Update, 6 (2011) 16-23.

[5] Nanoscience and nanotechnologies: opportunities and uncertainties, The Royal Society & The Royal Academy of Engineering, 2004, pp. 116.

[6] J. Kimling, M. Maier, B. Okenve, V. Kotaidis, H. Ballot, A. Plech, Turkevich Method for Gold Nanoparticle Synthesis Revisited, The Journal of Physical Chemistry B, 110 (2006) 15700-15707.

[7] S. Iravani, H. Korbekandi, S.V. Mirmohammadi, B. Zolfaghari, Synthesis of silver nanoparticles: chemical, physical and biological methods, Research in pharmaceutical sciences, 9 (2014) 385-406.

[8] N. Li, X. Zhang, S. Chen, X. Hou, Synthesis and characterization of CdS nanoparticles in the presence of oleic acid as solvent and stabilizer, Journal of Physics and Chemistry of Solids, 72 (2011) 1195-1198.

[9] S. Mahshid, M. Askari, M.S. Ghamsari, Synthesis of TiO2 nanoparticles by hydrolysis and peptization of titanium isopropoxide solution, Journal of Materials Processing Technology, 189 (2007) 296-300.

[10] E. Petryayeva, U.J. Krull, Localized surface plasmon resonance: Nanostructures, bioassays and biosensing A review, Analytica chimica acta, 706 (2011) 8-24.

[11] L.M. Liz-Marzán, Nanometals: Formation and color, Mater. Today, 7 (2004) 26-31.

[12] S. Eustis, M.A. El-Sayed, Why gold nanoparticles are more precious than pretty gold: Noble metal surface plasmon resonance and its enhancement of the radiative and nonradiative properties of nanocrystals of different shapes, Chemical Society Reviews, 35 (2006) 209-217.

[13] U. Kreibig, M. Vollmer, Optical Properties of Metal Clusters, Springer, Heidelberg, 1995.

[14] E. Katz, I. Willner, Integrated Nanoparticle–Biomolecule Hybrid Systems: Synthesis, Properties, and Applications, Angewandte Chemie, 43 (2004) 6042-6108.

[15] E. Weir, A. Lawlor, A. Whelan, F. Regan, The use of nanoparticles in anti-microbial materials and their characterization, The Analyst, 133 (2008) 835-845.

[16] M. Muhling, A. Bradford, J.W. Readman, P.J. Somerfield, R.D. Handy, An investigation into the effects of silver nanoparticles on antibiotic resistance of naturally occurring bacteria in an estuarine sediment, Marine environmental research, 68 (2009) 278-283.

[17] K. Kobayashi, J. Wei, R. Iida, K. Ijiro, K. Niikura, Surface engineering of nanoparticles for therapeutic applications, Polym J, 46 (2014) 460-468.

[18] R.R. Arvizo, S. Bhattacharyya, R.A. Kudgus, K. Giri, R. Bhattacharya, P. Mukherjee, Intrinsic therapeutic applications of noble metal nanoparticles: past, present and future, Chemical Society Reviews, 41 (2012) 2943-2970.

[19] M.A. El-Sayed, Some interesting properties of metals confined in time and nanometer space of different shapes, Accounts of chemical research, 34 (2001) 257-264.

[20] R.L. Manthe, S.P. Foy, N. Krishnamurthy, B. Sharma, V. Labhasetwar, Tumor Ablation and Nanotechnology, Molecular Pharmaceutics, 7 (2010) 1880-1898.

[21] J.F. Dorsey, L. Sun, D.Y. Joh, A. Witztum, G.D. Kao, M. Alonso-Basanta, S. Avery, S.M. Hahn, A. Al Zaki, A. Tsourkas, Gold nanoparticles in radiation research: potential applications for imaging and radiosensitization, Translational cancer research, 2 (2013) 280-291.

[22] S.K. Nune, P. Gunda, P.K. Thallapally, Y.Y. Lin, M.L. Forrest, C.J. Berkland, Nanoparticles for biomedical imaging, Expert opinion on drug delivery, 6 (2009) 1175-1194.

[23] J. Ando, T.A. Yano, K. Fujita, S. Kawata, Metal nanoparticles for nano-imaging and nano-analysis, Physical Chemistry Chemical Physics, 15 (2013) 13713-13722.

[24] J.C. Kah, K.W. Kho, C.G. Lee, C. James, R. Sheppard, Z.X. Shen, K.C. Soo, M.C. Olivo, Early diagnosis of oral cancer based on the surface plasmon resonance of gold nanoparticles, International journal of nanomedicine, 2 (2007) 785-798.

[25] K. Omidfar, F. Khorsand, M. Darziani Azizi, New analytical applications of gold nanoparticles as label in antibody based sensors, Biosens. Bioelectron., 43 (2013) 336-347.

[26] S. Pandey, G.K. Goswami, K.K. Nanda, Green synthesis of polysaccharide/gold nanoparticle nanocomposite: An efficient ammonia sensor, Carbohydrate polymers, 94 (2013) 229-234.

[27] A. Ogawa, RNA aptazyme-tethered large gold nanoparticles for on-the-spot sensing of the aptazyme ligand, Bioorganic & Medicinal Chemistry Letters, 21 (2011) 155-159.

[28] B. Li, Y. Du, S. Dong, DNA based gold nanoparticles colorimetric sensors for sensitive and selective detection of Ag(I) ions, Analytica chimica acta, 644 (2009) 78-82.

[29] W.J. Parak, L. Manna, L.C. Simmel, D. Gerion, P. Alivisatos, Nanoparticles: From Theory to Application, Wiley-VCH, Weinheim, 2004.

[30] S.J. Rosenthal, J.C. Chang, O. Kovtun, J.R. McBride, I.D. Tomlinson, Biocompatible quantum dots for biological applications, Chemistry & biology, 18 (2011) 10-24.

[31] A.M. Smith, S. Nie, Chemical analysis and cellular imaging with quantum dots, The Analyst, 129 (2004) 672-677.

[32] X. Wu, H. Liu, J. Liu, K.N. Haley, J.A. Treadway, J.P. Larson, N. Ge, F. Peale, M.P. Bruchez, Immunofluorescent labeling of cancer marker Her2 and other cellular targets with semiconductor quantum dots, Nature Biotechnology, 21 (2003) 41-46.

[33] K.-i. Hanaki, A. Momo, T. Oku, A. Komoto, S. Maenosono, Y. Yamaguchi, K. Yamamoto, Semiconductor quantum dot/albumin complex is a long-life and highly photostable endosome marker, Biochemical and Biophysical Research Communications, 302 (2003) 496-501.

[34] A. Sukhanova, J.r.m. Devy, L. Venteo, H. Kaplan, M. Artemyev, V. Oleinikov, D. Klinov, M. Pluot, J.H.M. Cohen, I. Nabiev, Biocompatible fluorescent nanocrystals for immunolabeling of membrane proteins and cells, Analytical Biochemistry, 324 (2004) 60-67.

[35] J.K. Jaiswal, H. Mattoussi, J.M. Mauro, S.M. Simon, Long-term multiple color imaging of live cells using quantum dot bioconjugates, Nature Biotechnology, 21 (2003) 47-51.

[36] Z. Kaul, T. Yaguchi, S.C. Kaul, T. Hirano, R. Wadhwa, K. Taira, Mortalin imaging in normal and cancer cells with quantum dot immuno-conjugates, Cell Research, 13 (2003) 503-507.

[37] A. Hoshino, K.-i. Hanaki, K. Suzuki, K. Yamamoto, Applications of T-lymphoma labeled with fluorescent quantum dots to cell tracing markers in mouse body, Biochemical and Biophysical Research Communications, 314 (2004) 46-53.

[38] M.J. Levene, D.A. Dombeck, K.A. Kasischke, R.P. Molloy, W.W. Webb, In Vivo Multiphoton Microscopy of Deep Brain Tissue, 2004, pp. 1908-1912.

[39] S.J. Rosenthal, I. Tomlinson, E.M. Adkins, S. Schroeter, S. Adams, L. Swafford, J. McBride, Y. Wang, L.J. DeFelice, R.D. Blakely, Targeting Cell Surface Receptors with Ligand-Conjugated Nanocrystals, Journal of the American Chemical Society, 124 (2002) 4586-4594.

[40] S. Kim, Y.T. Lim, E.G. Soltesz, A.M. De Grand, J. Lee, A. Nakayama, J.A. Parker, T. Mihaljevic, R.G. Laurence, D.M. Dor, L.H. Cohn, M.G. Bawendi, J.V. Frangioni, Near-infrared fluorescent type II quantum dots for sentinel lymph node mapping, Nature Biotechnology, 22 (2004) 93-97.

[41] B. Ballou, B.C. Lagerholm, L.A. Ernst, M.P. Bruchez, A.S. Waggoner, Noninvasive Imaging of Quantum Dots in Mice, Bioconjugate Chemistry, 15 (2004) 79-86.

[42] X. Gao, Y. Cui, R.M. Levenson, L.W.K. Chung, S. Nie, In vivo cancer targeting and imaging with semiconductor quantum dots, Nature Biotechnology, 22 (2004) 969-976.

[43] E.B. Voura, J.K. Jaiswal, H. Mattoussi, S.M. Simon, Tracking metastatic tumor cell extravasation with quantum dot nanocrystals and fluorescence emission-scanning microscopy, Nature Medicine, 10 (2004) 993-998.

[44] B. Sun, W. Xie, G. Yi, D. Chen, Y. Zhou, J. Cheng, Microminiaturized immunoassays using quantum dots as fluorescent label by laser confocal scanning fluorescence detection, Journal of immunological methods, 249 (2001) 85-89.

[45] E.R. Goldman, A.R. Clapp, G.P. Anderson, H.T. Uyeda, J.M. Mauro, I.L. Medintz, H. Mattoussi, Multiplexed Toxin Analysis Using Four Colors of Quantum Dot Fluororeagents, Analytical chemistry, 76 (2004) 684-688.

[46] D. Gerion, F. Chen, B. Kannan, A. Fu, W.J. Parak, D.J. Chen, A. Majumdar, A.P. Alivisatos, Room-Temperature Single-Nucleotide Polymorphism and Multiallele DNA

Detection Using Fluorescent Nanocrystals and Microarrays, Analytical chemistry, 75 (2003) 4766-4772.

[47] P. Andrew, W.L. Barnes, Förster Energy Transfer in an Optical Microcavity, 2000, pp. 785-788.

[48] W.R. Algar, K. Susumu, J.B. Delehanty, I.L. Medintz, Semiconductor Quantum Dots in Bioanalysis: Crossing the Valley of Death, Analytical chemistry, 83 (2011) 8826-8837.

[49] N. Hildebrandt, C.M. Spillmann, W.R. Algar, T. Pons, M.H. Stewart, E. Oh, K. Susumu, S.A. Díaz, J.B. Delehanty, I.L. Medintz, Energy Transfer with Semiconductor Quantum Dot Bioconjugates: A Versatile Platform for Biosensing, Energy Harvesting, and Other Developing Applications, Chemical Reviews, (2016).

[50] I.L. Medintz, A.R. Clapp, F.M. Brunel, T. Tiefenbrunn, H. Tetsuo Uyeda, E.L. Chang, J.R. Deschamps, P.E. Dawson, H. Mattoussi, Proteolytic activity monitored by fluorescence resonance energy transfer through quantum-dot-peptide conjugates, Nature materials, 5 (2006) 581-589.

[51] L. Shi, N. Rosenzweig, Z. Rosenzweig, Luminescent Quantum Dots Fluorescence Resonance Energy Transfer-Based Probes for Enzymatic Activity and Enzyme Inhibitors, Analytical chemistry, 79 (2007) 208-214.

[52] E.R. Goldman, I.L. Medintz, J.L. Whitley, A. Hayhurst, A.R. Clapp, H.T. Uyeda, J.R. Deschamps, M.E. Lassman, H. Mattoussi, A Hybrid Quantum Dot-Antibody Fragment Fluorescence Resonance Energy Transfer-Based TNT Sensor, Journal of the American Chemical Society, 127 (2005) 6744-6751.

[53] I.L. Medintz, A.R. Clapp, H. Mattoussi, E.R. Goldman, B. Fisher, J.M. Mauro, Self-assembled nanoscale biosensors based on quantum dot FRET donors, Nature materials, 2 (2003) 630-638.

[54] Y. Xiao, V. Pavlov, S. Levine, T. Niazov, G. Markovitch, I. Willner, Catalytic Growth of Au Nanoparticles by NAD(P)H Cofactors: Optical Sensors for NAD(P)+-Dependent Biocatalyzed Transformations, Angewandte Chemie, 43 (2004) 4519-4522.

[55] M. Zayats, R. Baron, I. Popov, I. Willner, Biocatalytic growth of Au nanoparticles: from mechanistic aspects to biosensors design, Nano letters, 5 (2005) 21-25.

[56] B. Shlyahovsky, E. Katz, Y. Xiao, V. Pavlov, I. Willner, Optical and electrochemical detection of NADH and of NAD+-dependent biocatalyzed processes by the catalytic deposition of copper on gold nanoparticles, Small, 1 (2005) 213-216.

[57] Y. Xiao, B. Shlyahovsky, I. Popov, V. Pavlov, I. Willner, Shape and color of au nanoparticles follow biocatalytic processes, Langmuir, 21 (2005) 5659-5662.

[58] V. Pavlov, Y. Xiao, I. Willner, Inhibition of the acetycholine esterase-stimulated growth of Au nanoparticles: nanotechnology-based sensing of nerve gases, Nano Letters, 5 (2005) 649-653.

[59] A. Virel, L. Saa, V. Pavlov, Modulated growth of nanoparticles. Application for sensing nerve gases, Analytical Chemistry, 81 (2009) 268-272.

[60] L. Saa, A. Virel, J. Sanchez-Lopez, V. Pavlov, Analytical applications of enzymatic growth of quantum dots, Chemistry, 16 (2010) 6187-6192.

[61] L. Saa, J.M. Mato, V. Pavlov, Assays for methionine gamma-lyase and S-adenosyl-L-homocysteine hydrolase based on enzymatic formation of CdS quantum dots *in situ*, Analytical Chemistry, 84 (2012) 8961-8965.

[62] L. Saa, V. Pavlov, Enzymatic growth of quantum dots: applications to probe glucose oxidase and horseradish peroxidase and sense glucose, Small, 8 (2012) 3449-3455.

[63] G. Garai-Ibabe, M. Moller, V. Pavlov, Ultrasensitive assay for detection of serum paraoxonase by modulating the growth of fluorescent semiconductor nanoparticles, Analytical Chemistry, 84 (2012) 8033-8037.

[64] G. Garai-Ibabe, L. Saa, V. Pavlov, Enzymatic product-mediated stabilization of CdS quantum dots produced *in situ*: application for detection of reduced glutathione, NADPH, and glutathione reductase activity, Analytical Chemistry, 85 (2013) 5542-5546.

[65] N. Malashikhina, G. Garai-Ibabe, V. Pavlov, Unconventional application of conventional enzymatic substrate: first fluorogenic immunoassay based on enzymatic formation of quantum dots, Analytical Chemistry, 85 (2013) 6866-6870.

[66] B. Nagel, H. Dellweg, L.M. Gierasch, Glossary for chemists of terms used in biotechnology (IUPAC Recommendations 1992), Pure and Applied Chemistry, 1992, pp. 143.

[67] E. Wijaya, C.d. Lenaerts, S. Maricot, J. Hastanin, S. Habraken, J.-P. Vilcot, R. Boukherroub, S. Szunerits, Surface plasmon resonance-based biosensors: From the development of different SPR structures to novel surface functionalization strategies, Current Opinion in Solid State and Materials Science, 15 (2011) 208-224.

[68] T. Špringer, M.L. Ermini, B. Špačková, J. Jablonku, J. Homola, Enhancing Sensitivity of Surface Plasmon Resonance Biosensors by Functionalized Gold Nanoparticles: Size Matters, Analytical chemistry, 86 (2014) 10350-10356.

[69] L.A. Lyon, M.D. Musick, M.J. Natan, Colloidal Au-Enhanced Surface Plasmon Resonance Immunosensing, Analytical chemistry, 70 (1998) 5177-5183.

[70] D.E. Mustafa, T. Yang, Z. Xuan, S. Chen, H. Tu, A. Zhang, Surface Plasmon Coupling Effect of Gold Nanoparticles with Different Shape and Size on Conventional Surface Plasmon Resonance Signal, 2010, pp. 221-231.

[71] S.J. Chen, F.C. Chien, G.Y. Lin, K.C. Lee, Enhancement of the resolution of surface plasmon resonance biosensors by control of the size and distribution of nanoparticles, Optics Letters, 29 (2004) 1390-1392.

[72] W.P. Hu, S.J. Chen, K.T. Huang, J.H. Hsu, W.Y. Chen, G.L. Chang, K.A. Lai, A novel ultrahigh-resolution surface plasmon resonance biosensor with an Au nanocluster-embedded dielectric film, Biosensors and Bioelectronics, 19 (2004) 1465-1471.

[73] J. Matsui, K. Akamatsu, N. Hara, D. Miyoshi, H. Nawafune, K. Tamaki, N. Sugimoto, SPR Sensor Chip for Detection of Small Molecules Using Molecularly Imprinted Polymer with Embedded Gold Nanoparticles, Analytical chemistry, 77 (2005) 4282-4285.

[74] L. He, E.A. Smith, M.J. Natan, C.D. Keating, The Distance-Dependence of Colloidal Au-Amplified Surface Plasmon Resonance, The Journal of Physical Chemistry B, 108 (2004) 10973-10980.

[75] E. Hutter, J.H. Fendler, D. Roy, Surface Plasmon Resonance Studies of Gold and Silver Nanoparticles Linked to Gold and Silver Substrates by 2-Aminoethanethiol and 1,6-Hexanedithiol, The Journal of Physical Chemistry B, 105 (2001) 11159-11168.

[76] J. Choo, Biosensors Using Surface-Enhanced Raman Scattering, in: D. Li (Ed.) Encyclopedia of Microfluidics and Nanofluidics, Springer US, Boston, MA, 2014, pp. 1-6.

[77] K.C. Bantz, A.F. Meyer, N.J. Wittenberg, H. Im, O. Kurtulus, S.H. Lee, N.C. Lindquist, S.-H. Oh, C.L. Haynes, Recent progress in SERS biosensing, Physical Chemistry Chemical Physics, 13 (2011) 11551-11567.

[78] X. Fu, Z. Cheng, J. Yu, P. Choo, L. Chen, J. Choo, A SERS-based lateral flow assay biosensor for highly sensitive detection of HIV-1 DNA, Biosensors and Bioelectronics, 78 (2016) 530-537.

[79] J. Yoon, N. Choi, J. Ko, K. Kim, S. Lee, J. Choo, Highly sensitive detection of thrombin using SERS-based magnetic aptasensors, Biosensors and Bioelectronics, 47 (2013) 62-67.

[80] Y. Wang, L.-J. Tang, J.-H. Jiang, Surface-Enhanced Raman Spectroscopy-Based, Homogeneous, Multiplexed Immunoassay with Antibody-Fragments-Decorated Gold Nanoparticles, Analytical chemistry, 85 (2013) 9213-9220.

[81] D. Geissler, L.J. Charbonniere, R.F. Ziessel, N.G. Butlin, H.G. Lohmannsroben, N. Hildebrandt, Quantum dot biosensors for ultrasensitive multiplexed diagnostics, Angewandte Chemie, 49 (2010) 1396-1401.

[82] R. Freeman, T. Finder, L. Bahshi, I. Willner, ÎB-Cyclodextrin-Modified CdSe/ZnS Quantum Dots for Sensing and Chiroselective Analysis, Nano letters, 9 (2009) 2073-2076.

[83] A.M. Dennis, G. Bao, Quantum Dot-Fluorescent Protein Pairs as Novel Fluorescence Resonance Energy Transfer Probes, Nano letters, 8 (2008) 1439-1445.

[84] Z. Li, Y. Wang, J. Wang, Z. Tang, J.G. Pounds, Y. Lin, Rapid and Sensitive Detection of Protein Biomarker Using a Portable Fluorescence Biosensor Based on Quantum Dots and a Lateral Flow Test Strip, Analytical chemistry, 82 (2010) 7008-7014.

[85] X. Meng, J. Wei, X. Ren, J. Ren, F. Tang, A simple and sensitive fluorescence biosensor for detection of organophosphorus pesticides using H2O2-sensitive quantum dots/bi-enzyme, Biosensors and Bioelectronics, 47 (2013) 402-407.

[86] C. Zhu, G. Yang, H. Li, D. Du, Y. Lin, Electrochemical Sensors and Biosensors Based on Nanomaterials and Nanostructures, Analytical chemistry, 87 (2015) 230-249.

[87] A. Touhami, Biosensors and Nanobiosensors: Design and Applications, in: A. Seifalian, A. de Mel, D.M. Kalaskar (Eds.) Nanomedicine, One Central Press, London, 2014.

[88] D.R. Thévenot, K. Toth, R.A. Durst, G.S. Wilson, Electrochemical biosensors: recommended definitions and classification1, Biosensors and Bioelectronics, 16 (2001) 121-131.

[89] M. Holzinger, A. Le Goff, S. Cosnier, Nanomaterials for biosensing applications: a review, 2014.

[90] A.-N. Kawde, J. Wang, Amplified Electrical Transduction of DNA Hybridization Based on Polymeric Beads Loaded with Multiple Gold Nanoparticle Tags, Electroanalysis, 16 (2004) 101-107.
[91] J. Wang, R. Polsky, D. Xu, Silver-Enhanced Colloidal Gold Electrochemical Stripping Detection of DNA Hybridization, Langmuir, 17 (2001) 5739-5741.
[92] G. Shen, Y. Zhang, Highly sensitive electrochemical stripping detection of hepatitis B surface antigen based on copper-enhanced gold nanoparticle tags and magnetic nanoparticles, Analytica chimica acta, 674 (2010) 27-31.
[93] Q. Xu, F. Yan, J. Lei, C. Leng, H. Ju, Disposable Electrochemical Immunosensor by Using Carbon Sphere/Gold Nanoparticle Composites as Labels for Signal Amplification, Chemistry – A European Journal, 18 (2012) 4994-4998.
[94] K. Omidfar, H. Zarei, F. Gholizadeh, B. Larijani, A high-sensitivity electrochemical immunosensor based on mobile crystalline material-polyvinyl alcohol nanocomposite and colloidal gold nanoparticles, Analytical Biochemistry, 421 (2012) 649-656.
[95] L. Authier, C.l. Grossiord, P. Brossier, B.t. Limoges, Gold Nanoparticle-Based Quantitative Electrochemical Detection of Amplified Human Cytomegalovirus DNA Using Disposable Microband Electrodes, Analytical chemistry, 73 (2001) 4450-4456.
[96] A. Ambrosi, M.T. Castañeda, A.J. Killard, M.R. Smyth, S. Alegret, A. Merkoçi, Double-Codified Gold Nanolabels for Enhanced Immunoanalysis, Analytical chemistry, 79 (2007) 5232-5240.
[97] B.P. Ting, J. Zhang, Z. Gao, J.Y. Ying, A DNA biosensor based on the detection of doxorubicin-conjugated Ag nanoparticle labels using solid-state voltammetry, Biosensors and Bioelectronics, 25 (2009) 282-287.
[98] J. Zhang, B.P. Ting, N.R. Jana, Z. Gao, J.Y. Ying, Ultrasensitive Electrochemical DNA Biosensors Based on the Detection of a Highly Characteristic Solid-State Process, Small, 5 (2009) 1414-1417.
[99] J.A. Hansen, R. Mukhopadhyay, J.Ã. Hansen, K.V. Gothelf, Femtomolar Electrochemical Detection of DNA Targets Using Metal Sulfide Nanoparticles, Journal of the American Chemical Society, 128 (2006) 3860-3861.
[100] L.-N. Feng, Z.-P. Bian, J. Peng, F. Jiang, G.-H. Yang, Y.-D. Zhu, D. Yang, L.-P. Jiang, J.-J. Zhu, Ultrasensitive Multianalyte Electrochemical Immunoassay Based on Metal Ion

Functionalized Titanium Phosphate Nanospheres, Analytical chemistry, 84 (2012) 7810-7815.

[101] A. Devadoss, P. Sudhagar, C. Terashima, K. Nakata, A. Fujishima, Photoelectrochemical biosensors: New insights into promising photoelectrodes and signal amplification strategies, Journal of Photochemistry and Photobiology C: Photochemistry, 24 (2015) 43-63.

[102] W.-W. Zhao, J.-J. Xu, H.-Y. Chen, Photoelectrochemical bioanalysis: the state of the art, Chemical Society Review, 44 (2015) 729-741.

[103] P. Wang, W. Dai, L. Ge, M. Yan, S. Ge, J. Yu, Visible light photoelectrochemical sensor based on Au nanoparticles and molecularly imprinted poly(o-phenylenediamine)-modified TiO2 nanotubes for specific and sensitive detection chlorpyrifos, The Analyst, 138 (2013) 939-945.

[104] G.-C. Fan, L. Han, H. Zhu, J.-R. Zhang, J.-J. Zhu, Ultrasensitive Photoelectrochemical Immunoassay for Matrix Metalloproteinase-2 Detection Based on CdS:Mn/CdTe Cosensitized TiO2 Nanotubes and Signal Amplification of SiO2@Ab2 Conjugates, Analytical chemistry, 86 (2014) 12398-12405.

[105] Q. Shen, L. Han, G. Fan, E.S. Abdel-Halim, L. Jiang, J.-J. Zhu, Highly sensitive photoelectrochemical assay for DNA methyltransferase activity and inhibitor screening by exciton energy transfer coupled with enzyme cleavage biosensing strategy, Biosensors and Bioelectronics, 64 (2015) 449-455.

[106] P. Gao, H. Ma, J. Yang, D. Wu, Y. Zhang, B. Du, D. Fan, Q. Wei, Anatase TiO2 based photoelectrochemical sensor for the sensitive determination of dopamine under visible light irradiation, New Journal of Chemistry, 39 (2015) 1483-1487.

[107] Y. Zhu, K. Yan, Z. Xu, J. Zhang, Hemin Modified TiO2 Nanoparticles with Enhanced Photoelectrocatalytic Activity for Electrochemical and Photoelectrochemical Sensing, 2016, pp. B526-B532.

[108] V. Pardo-Yissar, E. Katz, J. Wasserman, I. Willner, Acetylcholine Esterase-Labeled CdS Nanoparticles on Electrodes: Photoelectrochemical Sensing of the Enzyme Inhibitors, Journal of the American Chemical Society, 125 (2003) 622-623.

2

Application of photocatalytic cadmium sulfide nanoparticles to detection of enzymatic activities of glucose oxidase and glutathione reductase using oxidation of 3,3',5,5'-tetramethylbenzidine (TMB)

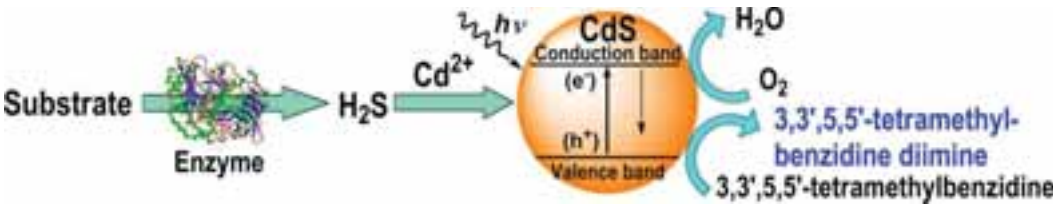

It was found out that semiconductor CdS nanoparticles (NPs) are able to catalyze photooxidation of the well known chromogenic enzymatic substrate TMB by oxygen. The photocatalytical oxidation of TMB does not require hydrogen peroxide and its rate is directly proportional to the quantity of CdS NPs produced in situ through the interaction of Cd^{2+} and S^{2-} ions in an aqueous medium. This phenomenon was applied to development of colorimetric sensitive assays for glucose oxidase and glutathione reductase based on enzymatic generation of CdS NPs acting as light-powered catalysts. Sensitivity of the developed chromogenic assays was of the same order of magnitude or even better than that of relevant fluorogenic assays. The present approach opens the possibility for the design of simple and sensitive colorimetric assays for a number of enzymes using inexpensive and available TMB as a universal chromogenic compound.

The work presented in this chapter was previously published: Ruta Grinyte, Gaizka Garai-Ibabe, Laura Saa, Valeri Pavlov, Analytica Chimica Acta 881 (2015) 131–138.

2.1. Introduction

In bioanalysis detection of analytes of interest is performed employing biological components for instance enzymes, antibodies, DNA and RNA oligonucleotides. These biopolymers have been designed by nature to specifically interact with targets via hydrogen bonding and electrostatic attraction. A recognition event should be transduced into some weak measurable signal which requires frequently amplification. Different physical techniques such as surface plasmon resonance, Raman spectroscopy, quartz crystal microbalance, electrochemistry and extremely popular UV–Vis and fluorescence spectroscopy are applied to follow the amplified signal.

Metallic and semiconductor nanoparticles (NPs) can be very conveniently employed for signal transduction and signal amplification by physical methods. Their chemical and physical properties are defined by three dimensional structure of NPs, therefore very slight changes in shape and size lead to drastic variation in absorption and emission spectra. Usually, pre-synthesized inorganic NPs tethered to an analyte through recognition elements report a recognition event as labels via optical, electrochemical or acoustic signal detection.[1] Amplification of signal is frequently achieved by *in situ* growth of metal or semiconductor NPs from initial seeds proceeding from a recognition event.[2, 3] Labels prepared of inorganic metal and semiconductor NPs found broad application to discovery of affinity interaction in biosensors and ELISA type assays. Metal NPs can be readily linked to antibodies,[4] polysaccharides, RNA and DNA oligonucleotides [5-7] for subsequent use in bioanalytical assays. The labels fabricated from semiconductor NPs confer more sensitivity to assays due their intrinsic fluorescence. Semiconductor NPs can be photo-excited producing electron/hole couples, which recombine to yield emission of light. Quantum effects in inorganic NPs give rise to fluorescence, therefore such fluorescent particles are referred to in the literature as quantum dots (QDs).[8] Their advantages over organic fluorophores include, higher brightness, narrow and symmetric emission, resistance to photo-bleaching and longer life time.[9] Traditionally, semiconductor NPs have been employed as labels tethered to antibodies in immunosorbent assays [10] or to DNA oligonucleotides in DNA biosensors.[11] QDs are also good donors for assays employing fluorescence resonance energy transfer (FRET) in which cleavage of

acceptor molecules caused by enzymes was used for sensing of enzymatic activities. The performance of immunosorbent and DNA bio-assays based on QD labels is hindered by nonspecific adsorption of NPs decorated with sensing elements on solid surfaces. On the other hand, enzymatic assays based on bio-catalytic modulation of FRET between QDs and quenchers suffer from low signal to noise ratio due to insufficient quenching of donor couples. Generation of NPs *in situ* triggered by a recognition event can address these shortages. A number of analytical enzymatic systems producing gold and silver NPs were described in the literature. It was shown that the enzymatically reduced cofactor nicotinamide adenide dinucleotide (NADH) converts $AuCl_4^-$ ions to gold NPs. This biocatalytic system was applied to optical detection of lactate and alcohol taking advantage of corresponding dehydrogenases.[2] In another electrochemical assay NADH produced by alcohol dehydrogenase reduces Cu^{2+} enlarging gold seeding NPs immobilized on the electrode surface.[12] Glucose oxidase is another redox enzyme capable to trigger formation of metal NPs. This enzyme catalyzes oxidation of glucose with $AuCl_4^-$, mediated by poly-pyridyl osmium complex, yielding gold NPs.[13] Hydrolyzing enzymes also can be taught to generate metal NPs. For example, alkaline phosphatase catalyzes hydrolysis of 3-indoxyl phosphate producing products which are able to reduce silver ions into a metallic deposit.[14] Acetylcholine esterase accelerates decomposition of acetylthiocholine to give acetate and thiocholine. This product of the enzymatic reaction reduces $AuCl_4^-$ producing gold NPs [15] and modulates growth of silver NPs.[3] Actually, any enzyme catalyzing the synthesis of compounds with capacity to reduce metal salts can promote formation of metal NPs. The sensitivity of the related bio-analytical assays based on enzymatic generation of metal NPs is limited by the sensitivity of UV-Visible absorbance spectroscopy employed to follow the read-out signal. Analytical assays employing enzymatic formation of fluorescent semiconductor NPs are much more sensitive because they take advantage of much more sensitive fluorescence spectroscopy.

Our laboratory has introduced application of *in situ* growth of QDs to development of flourogenic enzymatic assays.[16] This concept is based on registration of fluorescence originating from CdS QDs influenced by products of an enzymatic reaction. Those fluorogenic assays showed low detection limits and high signal to noise

ratio, but unfortunately the read-out signal was not stable with time. The size of semiconductor QDs defines quantum effects governing fluorescence emission. The enzymatically driven growth of semiconductor NPs leads to the increase in their diameter and significant decrease in their brightness with time, resulting in relatively high standard deviation. On the other hand, fluorescent spectrometers require a source of excitation light, they are quite expensive and cannot be easily miniaturized. In order to overcome these shortages one needs to combine the advantage of enzymatic growth of QDs with the generation of a stable reporter molecule readily detectable by an inexpensive UV-Vis spectrometer. In this manuscript we report a new methodology allowing measurement of enzymatic activities using UV-spectroscopy with the sensitivity usually demonstrated by fluorescence spectroscopy. We found out that CdS QDs, grown under the influence of products of biocatalytical transformations, are photo-catalysts enhancing oxidation of commercially available enzymatic chromogenic substrates such as 3,3',5,5'-tetramethylbenzidine (TMB) and 2,2'-azino-bis(3-ethylbenzothiazoline-6-sulphonic acid) (ABTS). Due to photocatalytical transformation of colorless TMB or ABTS molecules into colored oxidation products UV-Vis spectroscopy may be applied to follow enzymatic generation of QDs. In order to demonstrate application in bioanalysis of chromogenic dye oxidation catalyzed by QDs we developed two enzymatic assays in which NPs produced by glucose oxidase (GOx) or glutathione reductase (GR) act as light-powered catalysts.

2.2. Materials and methods

2.2.1. Materials

Glucose oxidase type VII from Aspergillus niger, 1-thio-β-D-glucose, L-glutathione reduced, L-glutathione oxidized, GR (from Baker's yeast), β-nicotinamide adenine dinucleotide 2′-phosphate reduced tetrasodium salt hydrate (NADPH), 2,2′-azino-bis(3-ethylbenzothiazoline-6-sulfonate) (ABTS), sodium sulfide and cadmium nitrate were obtained from Sigma-Aldrich. Anhydrous D-(+)-glucose were purchased from Panreac and 3,3',5,5'-tetramethylbenzidine (TMB) were obtained from Fluka. Absorbance spectra measurements were performed on a Varioskan Flash microplate reader (Thermo Scientific) using transparent microwell plates at room temperature (RT).

2.2.2. Methods

2.2.2.1. TMB oxidation by CdS quantum dots

The determination of TMB oxidation by CdS quantum dots was performed by modulating growth of CdS QDs. The system was composed of 100 µL citrate buffer (10 mM, pH 3.5) containing, Na_2S (1 mM), and $Cd(NO_3)_2$ (10 mM). The mixtures were incubated for 5 min at room temperature. TMB was dissolved in DMSO and then diluted by citrate buffer (10 mM, pH 3.5) to a final concentration 2.4 mM. 100 µL of this TMB solution was added to the samples and absorbance spectra were recorded after 3 min incubation under 365 nm wavelength UV lamp. The fluorescence emission spectra of the resulting suspensions were recorded at λex = 320 nm.

2.2.2.2. Quantum Dot and TMB-Based Glucose Oxidase Assay with 1-Thio-β-D–glucose

Varying amounts of 1-thio-β-D-glucose were incubated with different amounts of GOx in citrate buffer (10 mM, pH 3.5) for 40 min at room temperature. After that, $Cd(NO_3)_2$ (2.5 µL , 0.2 M) was added to the samples (97.5 µL). Subsequently, 100 µL of TMB (2.4 mM) was added to the samples. The absorbance spectra of the resulting suspensions were recorded after 3 min incubation under 365 nm UV lamp. All measurements were carried out in triplicates; the error bars represent the standard deviation of three independent measurements. Furthermore, quantification of glucose in human plasma was performed by the standard edition method. Commercial human plasma (Sigma-Aldrich) was centrifuged using an Amicon Ultra filter with a 30000 molecular weight cutoff. After filtering, the plasma was spiked with different concentrations of glucose and the glucose concentration of the mixtures was determined. The dilution factor of plasma in the assay was 1:50.

2.2.2.3. CdS QD and TMB oxidation-mediated determination of reduced glutathione (GSH)

To determine the GSH concentration in aqueous media by TMB oxidation catalyzed with grown in situ CdS QDs, the assay system was composed of 100 µL citrate−phosphate buffer (25%, pH 7.5) containing varying amounts of GSH (from 5 to

200 µM), Na_2S (0.25 mM), and $Cd(NO_3)_2$ (0.25 mM). The mixtures were incubated for 5 min at RT. Afterwards, 100 µL of TMB (2.4 mM) in 0.1 M citric acid was added to the samples. The absorbance spectra of the resulting suspensions were recorded after 3 min incubation under 365 nm UV lamp. All measurements were carried out in triplicates; the error bars represent the standard deviation of three independent measurements.

2.2.2.4. Quantum Dot and TMB-based determination of glutathione disulfide (GSSG) and glutathione reductase (GR)

For determination of GSSG, GR (200 pM) was incubated with 35 µM NADPH and varying concentrations of GSSG (from 1 to 25 µM) in 92.5 µL of citrate–phosphate buffer (25%, pH 7.5) at RT for 30 min. Afterward, 2.5 µL of 10 mM Na_2S and 5 µL of 5 mM $Cd(NO_3)_2$ were added to the mixtures. After 5 min, 100 µL of TMB (2.4 mM) in 0.1 M citric acid was added to the samples. The mixture was incubated for 3 min under 365 nm UV light lamp and absorbance spectra were record. For the quantification of total glutathione in human plasma was performed by the standard edition method. Pooled human plasma (Sigma-Aldrich) was spiked with different concentrations of glutathione and the total glutathione concentration of the mixtures was determined. The dilution factor of plasma in the assay was 1:4.

2.3. Results and Discussion

2.3.1. Photocatalytical oxidation of TMB with CdS NPs

It is known that semiconductor NPs adsorb light with energies at or above their characteristic band gap energy (Eg). Absorption of a photon results in excitation of an electron e- from the valence band to the conduction band accompanied by formation of a hole, h+, behind in the valence band. At the surface of semiconductor NPs electrons and holes are able to take part in redox half-reactions.[17] NPs have very high surface area to volume ratios and consequently they demonstrate very good efficiency of the photocatalytical processes.

The employment of semiconductor NPs for removal of organic pollutants from water by photocatalitic oxidation with oxygen has been described in the literature.[18-

20] Thus we suggest the following mechanism of TMB photo-oxidation by CdS NPs presented in Scheme 2.1. When a CdS NP is illuminated with UV light a photon excites an electron producing a hole. Due to the position of the valence band edge of CdS, the produced hole acts as a potent oxidant able to convert colorless TMB into 3,3',5,5'-tetramethylbenzidine diimine at the surface of the CdS nanoparticle. The redox process proceeds through removal of the photo-generated electron from the CdS nanoparticle using oxygen as the electron accepter.

Scheme 2.1. Diagram of photocatalytical oxidation of TMB with CdS NPs.

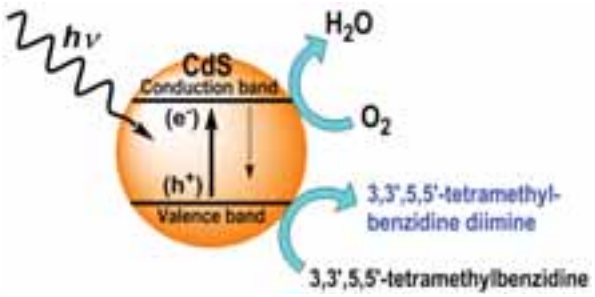

In the present work we show that the irradiation of TMB by UV light in the presence of CdS QDs, formed in situ by the interaction of Cd^{2+} and S^{2-} ions, results in formation of a colored reaction product with two absorbance peaks at 650 nm and 370 nm (Figure 2.1). This spectrum is characteristic for 3,3',5,5'-tetramethylbenzidine diimine, the oxidation product usually obtained in the course of enzymatic oxidation of TMB with hydrogen peroxide, catalyzed by horseradish peroxidase.[21]

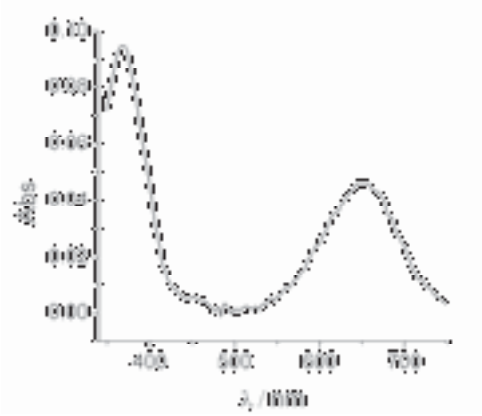

Figure 2.1. Absorbance spectra of TMB produce by phootoxidation with CdS QDs.

A number of control experiments in which one of the components was missing have been carried out. Figure 2.2A represents experimental results of those experiments. Curve d corresponds to the absorbance spectra of the system containing all components of the assay, i.e., Na_2S, $Cd(NO_3)_2$ and TMB under irradiation with 365 nm light. The absorbance spectra of this curve shows the peak at 650 nm corresponding to peak of 3,3',5,5'-tetramethylbenzidine diimine. Without UV light, the assay mixture containing only CdS quantum dots and TMB showed no significant absorbance peak (curve c). In order to exclude the possibility that the absorbance peak observed at 650 nm under the UV light was caused by non-specific photoreaction of TMB, the assay was performed in the absence of CdS QDs, i.e. under the UV light with TMB only. Curve a displays no significant absorbance peak at 650 nm. When CdS quantum dots were incubated under the UV light in the absence of TMB no detectable absorbance peak was measured (curve b). To confirm that under our experimental conditions S^{2-} anions readily interact with Cd^{2+} forming fluorescent CdS nanocrystals emission spectra were measured (Figure 2.2B). The CdS quantum dots grown in the presence of TMB showed much higher emission peak (curve a) than TMB alone (curve b).

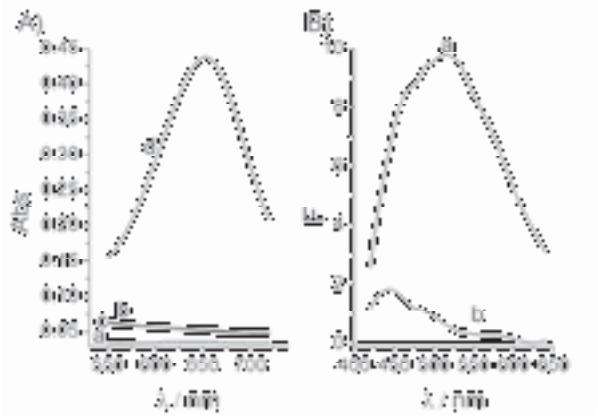

Figure 2.2. (A) Absorbance spectra of color reaction in the presence of a) only TMB (1.2 mM); b) Na_2S (0.5 mM) and $Cd(NO_3)_2$ (5mM); c) Na_2S (0.5 mM), $Cd(NO_3)_2$ (5 mM) and TMB (1.2 mM) in the dark; d) Na_2S (0.5 mM), $Cd(NO_3)_2$ (5 mM) and TMB (1.2 mM) under UV light. (B) Emission spectra of CdS quantum dots (a) and TMB only (b) under the same conditions λ_{ex}=390.

Transmission Electron Microscopy (TEM) was used to confirm the existence of CdS QDs in the reaction mixture (Figure 2.3). This technique revealed the presence of spheroidal QDs with a medium diameter 2.6 ± 0.4 nm (Figure 2.3B).

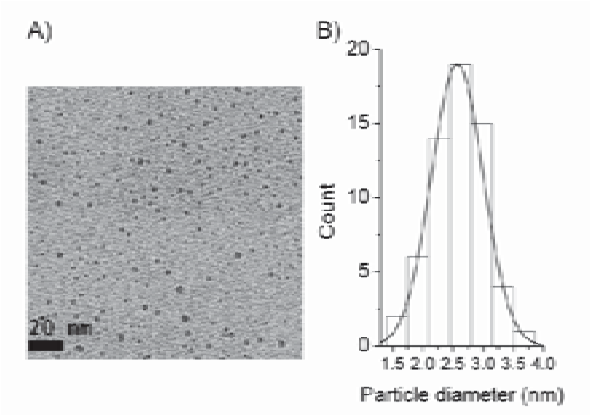

Figure 2.3. (A) TEM image of CdS QDs after TMB oxidation. (B) Size distribution of the CdS QDs.

Some additional experiments were carried out to confirm the mechanism of the photoreaction (Figure 2.4). The effect of varying TMB concentrations on the amount of photo-oxidation product produced after incubation during 3 min at a fixed amount of CdS QDs was studied. The resulting calibration curve showed saturation of the reaction rate starting from 0.5 mM of TMB. Fitting of the experimental data to the Michaelis-Menten model of catalysis gave the apparent the Michaelis-Menten constant of 60 µM

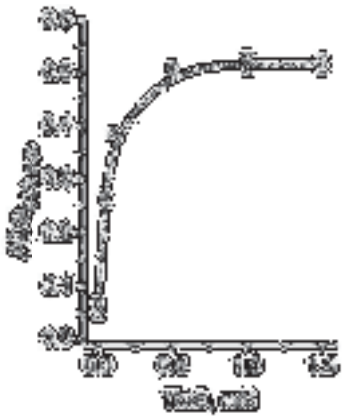

Figure 2.4. Effect of different concentrations of TMB on UV absorbance at 650 nm in the system composed of Cd(NO3)2 (5 mM), Na2S (0.5 mM).

computed by nonlinear regression method. In the presence of lone ions (Cd^{2+} or S^{2-} only), no photo-oxidation of TMB was observed (Figure 2.5, curves b and c correspondingly) whereas in the presence of both Cd^{2+} and S^{2-} ions photo-oxidation of TMB was evident (Figure 2.5 curve a). Curve d of Figure 2.5 corresponds to TMB only.

So, it was proved that CdS NPs are able to catalyze photo-oxidation of TMB under given experimental conditions.

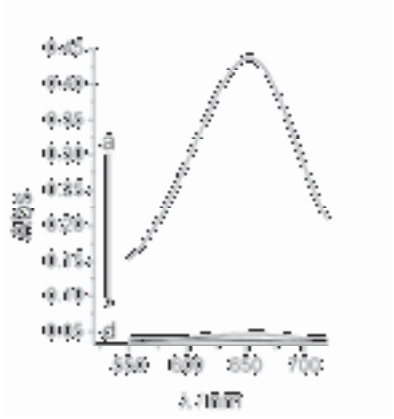

Figure 2.5. UV-Vis absorption spectra in the presence of a) $Cd(NO_3)_2$ (5 mM), Na_2S (0.5 mM) and TMB (1.2 mM); b) $Cd(NO_3)_2$ (5 mM) and TMB (1.2 mM); c) Na_2S (0.5 mM) and TMB (1.2 mM); d) only TMB (1.2 mM).

The effect of exogenous hydrogen peroxide on the rate of photocatalytical oxidation of TMB by CdS QDs was studied. As shown in Figure 2.6, increase in the concentration of hydrogen peroxide did not cause any significant changes in the rate of photocatalytical oxidation of TMB in the presence of QDs (curve a) or in the absence of them (curve b). Thus, CdS QDs do not have peroxidase-like activity detectable by UV-spectroscopy.

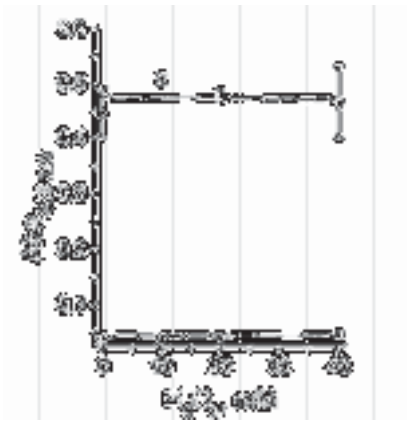

Figure 2.6. Calibration curve of H_2O_2 in the presence of a) $Cd(NO_3)_2$ (5 mM), Na_2S (0.5 mM), TMB (1.2 mM); b) only TMB (1.2 mM).

We studied the effect of pH and buffer concentration influence on the rate of photocatalitical oxidation of TMB by CdS NPs. As shown in Figure 2.7, the optimum pH is 3.5. The influence of the concentration of buffer was performed also. Figure 2.7B demonstrates that it is important to dilute citrate buffer to have 10 mM.

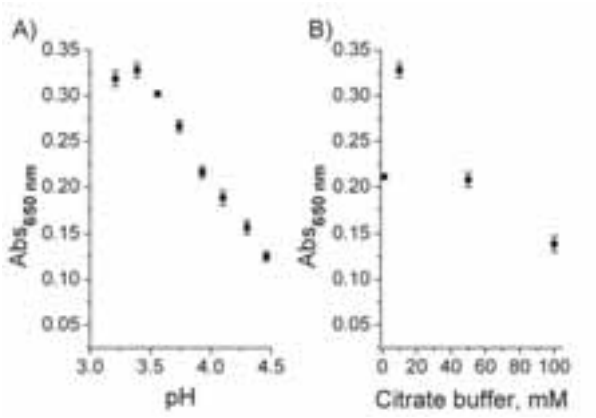

Figure 2.7. Absorbance spectra of TMB (A) in different ph; (B) in different concentration of citrate buffer.

Photocatalytical activity of QDs also was checked with another commonly employed chromogenic dye ABTS. Figure 2.8 demonstrates that CdS QDs also catalyze photo-oxidation of ABTS, but the signal/background ratio is not so high as in case of TMB. Therefore TMB was selected as a proper chromogenic dye for the subsequent experiments.

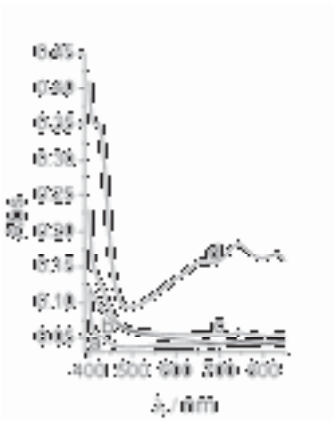

Figure 2.8. Absorbance spectra of color reaction in the presence of a) only ABTS (2.5 mM); b) Na_2S (1 mM) and $Cd(NO_3)_2$ (10 mM); c) Na_2S (1 mM), $Cd(NO_3)_2$ (10mM) and ABTS (2.5 mM) in the dark; d) Na_2S (1 mM), $Cd(NO_3)_2$ (10 mM) and ABTS (2.5 mM) under the UV light.

Oxidation of TMB catalyzed by CdS NPs does not occur under ambient laboratory light. It requires illumination with a portable ultraviolet lamp, therefore the reproducibility and stability of the read-out signal in analytical assays based on formation of CdS QDs *in situ* should be promising for development of new light-powered biosensing techniques.

2.3.2. Chromogenic detection of GOx activity using photocatalytical oxidation of TMB enhanced by enzymaticaly produced CdS

The proposed colorimetric method could be applied to bioanalytical assays taking advantage of enzymatic generation of quantum dots such as detection of glucose oxidase.[22] The operation principle of the chromogenic assay for evaluation of enzymatic activity of glucose oxidase (GOx) is demonstrated in Scheme 2.2. GOx catalyzes oxidation of 1-thio-ß-D-glucose to the final product H_2S. The latter in the presence of the excess of Cd^{2+} ions and citrate, acting as a stabilizer, forms CdS QDs.

Scheme 2.2. Chromogenic detection of GOx activity using photocatalytical oxidation of TMB enhanced by enzymaticaly produced CdS NPs

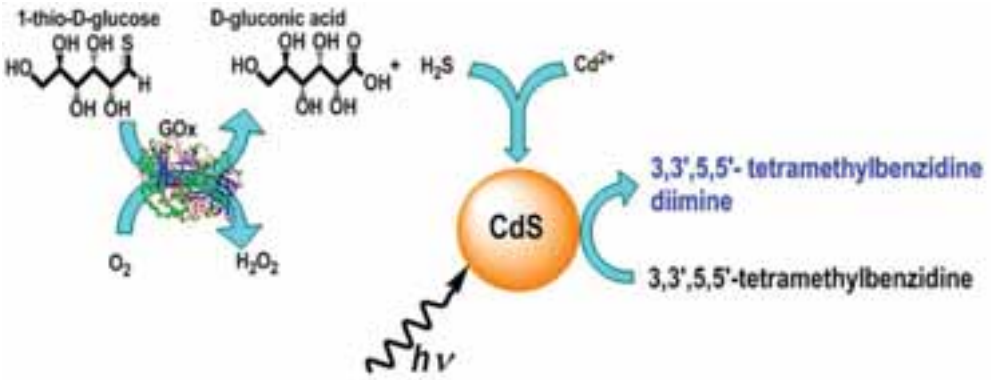

The resulting semiconductors NPs catalyze formation of the colored product 3,3',5,5'-tetramethylbenzidine diimine from TMB under UV light. In order to increase the yield of CdS NPs produced in response to sulfide ions the optimum concentration of Cd^{2+} ions was determined (2.5 mM) and used in subsequent experiments (Figure 2.9).

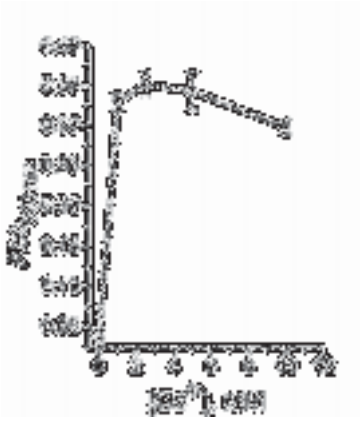

Figure 2.9. Calibration curve of Cd in GOx analtycal assay containing GOx 60 µg/mL and 1-thio-ß-D-glucose 0.5 mM.

The influence of varying 1-thio-ß-D-glucose concentrations on the quantity of 3,3',5,5'-tetramethylbenzidine diimine produced by enzymatically generated CdS nanocrystals was studied by UV-Visible spectroscopy. As shown in Figure 2.10A, the increase in 1-thio-ß-D-glucose concentration is directly related with the increase in the intensity of absorption peaks monitored in the range from 550 to 720 nm. Figure 2.10B demonstrates the calibration curve obtained by plotting the intensities of observed absorption peaks at 650 nm (Abs650 nm) against the substrate concentrations. The curve shows linearity from 0 to 0.15 mM and the saturation starting from 0.3 mM of substrate concentration. It means that the amount of oxidized TMB generated by CdS is directly related with the quantity of 1-thio-ß-D-glucose in the assay mixture. Enzymaticaly generated CdS nanocrystals oxidize TMB leading to a color change.

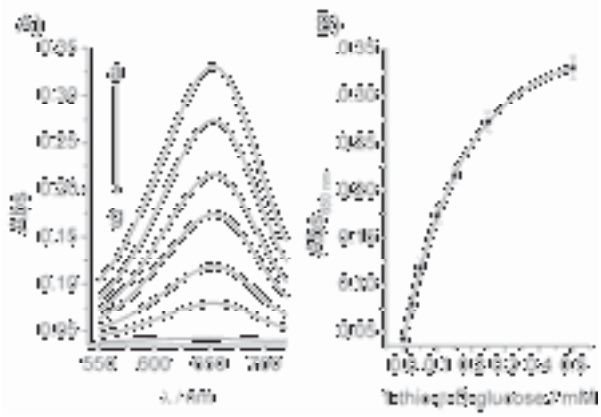

Figure 2.10. A) UV-vis absorption spectra of the system containing GOx (60 µg mL-1), $Cd(NO_3)_2$ (2.5mM), TMB (1.2mM) and different concentrations of 1-thio-ß-D-glucose: a) 0.5 mM, b) 0.25 mM; c) 0.15 mM; d) 0.1 mM; e) 0.05 mM; f) 0.025 mM; g) 0 mM. B) Calibration curve of 1-thio-ß-D-glucose at λ = 650 nm.

According to the calibration curve the limit of 1-thio-ß-D-glucose detection was 10 µM. The IUPAC definition was used to determine the limit of detection.[23] The detection limit of the enzymatic fluorogenic assay for 1-thio-ß-D-glucose by following fluorescence of CdS QDs was the same 10 µM.[22] Thus, this chromogenic assay taking advantage of this amplification cascade showed detection limit not worse than that of the fluorometric test. Within a particular range of substrate concentration this biocatalytic reaction was consistent with typical Michaelis-Menten kinetics. The experimental data were fitted by non linear regression method according to the Michaelis-Menten equation Abs650= Absmax650 [S]/(K_M + [S]), where [S] is the concentration of 1-thio-ß-D-glucose and K_M is the apparent Michaelis-Menten constant equal to 213.8 ± 14.6 µM.

Figure 2.11 shows the absorbance spectra of oxidized TMB in the presence of a fixed 0.5 mM 1-thio-ß-D-glucose concentration and different concentrations of GOx. In this case, we observed that the increase in amounts of enzyme was correlated linearly with the increase in the absorbance peak intensity. To the best of our knowledge we present here the first chromogenic test for rapid and specific detection of thio-ß-D-glucose. The standard assay for detection of GOx activity requires the second enzyme horseradish peroxidase (HRP) which catalysis oxidation of hydrogen peroxide by chromogenic substrates like o-Dianisidine or Ampliflu^{TM} Red. Only three published assays don't require the presence of HRP for chomogenic detection of GOx activity.

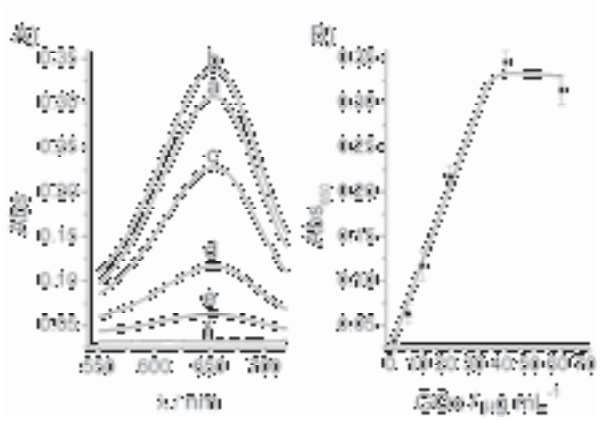

Figure 2.11. A) UV-vis absorption spectra of the system containing 1-thio-ß-D-glucose (0.5 mM), $Cd(NO_3)_2$ (2.5 mM), TMB (1.2 mM) and different concentrations of GOx: a) 60 µg mL^{-1} b) 40 µg mL^{-1}; c) 20 µg mL^{-1}; d) 10 µg mL^{-1}; e) 5 µg mL^{-1}; f) 0 µg mL^{-1}. B) Calibration curve of GOx at λ_{abs} = 650 nm.

They are based on formation or modulation of gold nanoparticles grown *in situ* under the influence of the enzymatic products. The assay based on enzymatic grows of Au NPs from $AuCl_4^-$ reduced by H_2O_2 generated by GOx suffers from very bad signal-noise ratio.[24] The similar assay mediated by $[Os(bpy)_2PyCO_2H]^{2+}$ showed improved signal to noise ratio but it requires complicated synthesis of this mediator from expensive precurses.[13] The third assay is based on modulated aggregation of presynthesized gold NPs caused the product of enzymatic oxidation which are not stable under physiologic conditions, so those previously published HRP free assays cannot be applied for detection of analytes in real body fluids.[25]

To confirm that enzymatically generated CdS QDs can oxidize TMB the effect of the natural substrate ß-D-glucose on the enzymatic system was studied. The natural substrate and the artificial one 1-thio-ß-D-glucose compete for binding with FAD, the active center of GOx. The fixed concentration of 1-thio-ß-D-glucose and constant amount of GOx. was used during the experiments. Increase in the concentration of ß-D-glucose leads to the decline in the concentration of produced H_2S, to the decrease in amount of formed CdS QDs and finally to the reduction of TMB oxidation rate. The influence of varying concentrations of ß-D-glucose on the absorbance signal is presented in Figure 2.12. The decrease in absorbance peaks in Figure 2.12A is correlated with the increase in concentration of ß-D-glucose as expected due to diminished formation of H_2S and CdS QDs. The smaller is amount of semiconductor

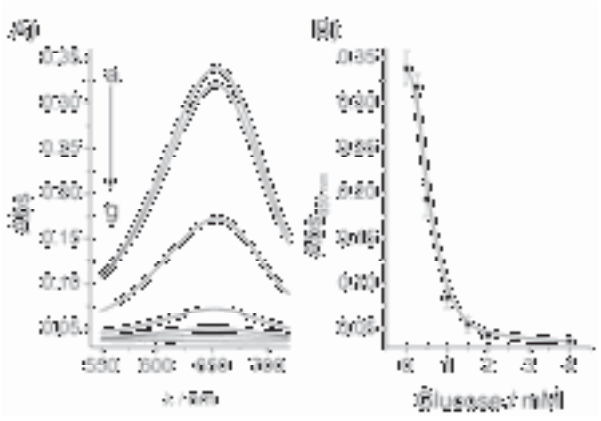

Figure 2.12. (A) UV-vis absorption spectra of the system containing GOx (40 µg mL^{-1}), 1-thio-ß-D-glucose (0.5 mM), $Cd(NO_3)_2$ (2.5mM), TMB (1.2mM) and different concentrations of ß-D-glucose: a) 0 mM, b) 0.25 mM; c) 0.5 mM; d) 1 mM; e) 1.5 mM; f) 2 mM; g) 4 mM. (B) Calibration curve of ß-D-glucose at λ_{abs} = 650 nm.

NPs in the assay mixture, the slower is the rate of TMB photo-oxidation. This simple colorimetric method could be potentially used by for determination of ß-D-glucose. The detection limit of the chromogenic assay calculated from the calibration plot, according to IUPAC definition, was 0.3 mM of ß-D-glucose. This value has the same order of magnitude as the detection limit of the fluorogenic assay (0.4 mM) employing measurement of fluorescence arising from CdS QDs formed *in situ.*[22]

Furthermore, we applied our assay for detection of ß-D-glucose in human plasma by the standard addition method. According to this method the same amount of plasma sample was split in separated eppendorfs. Varying standard amounts of ß-D-glucose were injected in to the samples with human plasma. The results were plotted with the concentration standard added in the x-axis and the obtained absorbance readings in the y-axis of calibration line. The linear regression was carried out to calculate the position of the recalculated calibration line, which showed the concentration of ß-D-glucose in diluted real samples (Figure 2.13). Taking into consideration all dilutions of the samples, the found concentration of ß-D-glucose was 5.7 ± 0.9 mM. It lies within the range of previously reported healthy students.[26, 27]

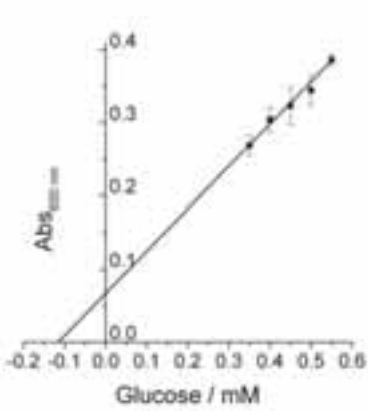

Figure 2.13. Quantification of glucose in human plasma with the method of standard addition. The system contained GOx 40 µg mL^{-1}, 1-thio-ß-D-glucose 0.5 mM, $Cd(NO_3)_2$ (2.5 mM) and TMB (1.2 mM).

2.3.3. Chromogenic detection of GR activity using photocatalytical oxidation of TMB enhanced by enzymaticaly produced CdS

The proposed colorimetric technique can be applied also to analytical assays in which the growth of semiconductor NPs *in situ* is modulated by products of enzymatic

reactions such as reduction of glutathione disulfide (GSSG) to glutathione (GSH) catalyzed by glutathione reductase (GR). In human cells glutathione has multiple functions, including protection of cells from oxidative stress.[28] GSH is able to stabilize CdS NPs produced by the interaction of Cd^{2+} with S^{2-} ions. CdS NPs stabilized with GSH demonstrate photocatalytical properties with respect to oxidation of TMB as shown in Scheme 2.3.

Scheme 2.3. Chromogenic detection of GR activity using photocatalytical oxidation of TMB enhanced by enzymaticaly produced CdS NPs.

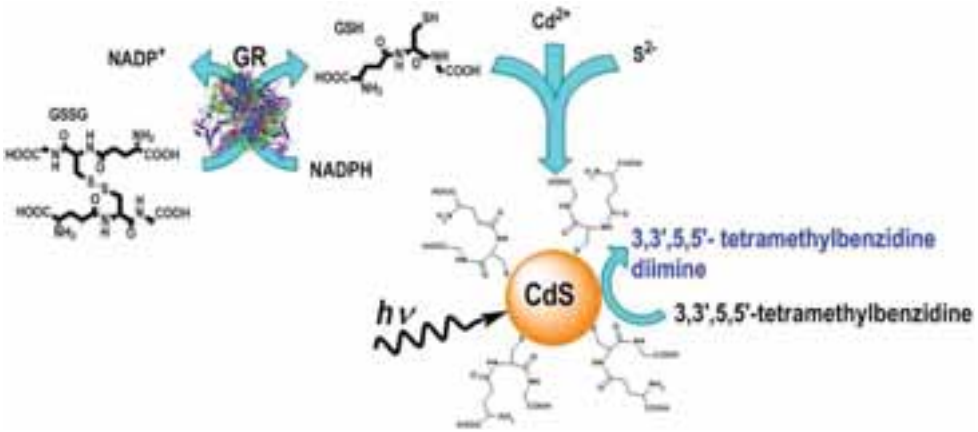

Concentration of Cd^{2+} and S^{2-} ions was optimized using as selection criteria the ratio between responses obtained in the presence and absence of GSH (Figure 2.14). Figure 2.15A presents the effect of increasing concentration of GSH on the absorbance spectra, registered upon photocatalytical oxidation of TMB catalyzed by CdS NPs which were formed due to stabilization with GSH. According to the plot (Figure 2.15B) representing the value of absorbance peak at 650 nm versus concentration of GSH the linear relation is evident up to 60 µM of GSH. This dynamic range is twice as higher than that of the assay based only on measurement of fluorescence arising from newly formed CdS QDs.[29] TEM confirmed the presence of spheroidal monodispersed CdS NPs in the samples (Figure 2.16A) with the diameter of 2 ± 0.3 (Figure 2.16B). TEM images prove that TMB doesn't prevent formation of CdS NPs *in situ*.

Figure 2.14. (A) Calibration curve of Cd^{2+} a) GSH 0.1mM and Na_2S 1 mM , b) GSH 0 mM and Na2S 1 mM; (B) Calibration curve of Na2S a) GSH 0.1 mM and Cd 0.125 mM; b) GSH 0 mM and Cd 0.125 mM.

Figure 2.15. (A) UV-vis absorption spectra of the system containing Na_2S (0.125 mM), $Cd(NO_3)_2$ (0.125 mM), TMB (1.2 mM) and different concentrations of GSH: a) 100 µM, b) 50 µM; c) 37.5 µM; d) 25 µM; e) 12.5 µM; f) 5 µM; g) 2.5 µM; h) 0 µM. (B) Calibration curve of GSH at λ_{abs} = 650 nm.

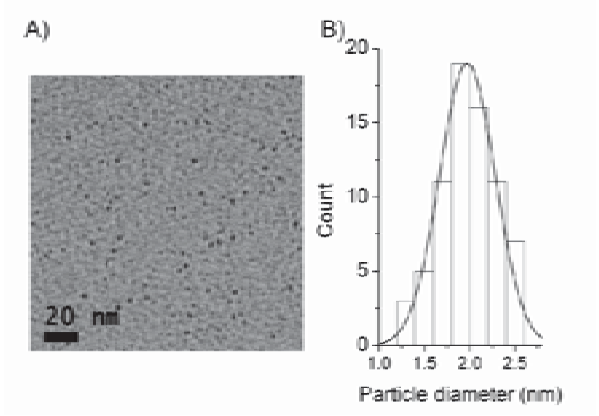

Figure 2.16. (A) TEM image of CdS QDs after TMB oxidation. (B) Size distribution of the GSH-stabilized CdS QDs.

This result allowed us to develop the new enzymatic chromogenic assay for detection of GSSG as one can see in Scheme 2.3. The enzyme GR catalyzes reduction of GSSG with NADPH to yield two molecules of GSH. The latter molecules attach to the surface of growing CdS NPs via the thiol functional group, leaving hydrophilic carboxylic and amino groups exposed to aqueous environment. Such stabilization favors *in situ* growth of semiconductor NPs, which catalyze photocatalytical oxidation of TMB to the colored product 3,3',5,5'-tetramethylbenzidine diimine. The response of this bio-analytical system to varying concentrations of GSSG was studied (Figure 2.17A). In accordance with the calibration plot (Figure 2.17B) the IUPAC detection limit was found to be 0.1 µM. This value is at least one order of magnitude lower than that of the fluorogenic assay (3 µM) relying on quantification of fluorescence originating from CdS QDs.[29] A linear response range for detection of GSSG variate from 0 µM to 4 µM, with a dynamic range up to 14 µM and it showed the same or even better value compare with other reported methods.[29, 30]

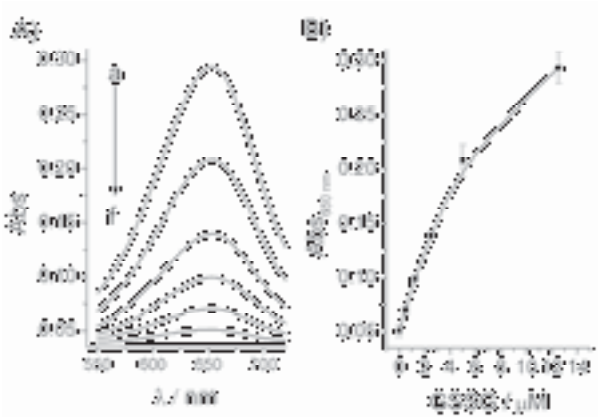

Figure 2.17. (A) UV-vis absorption spectra of the system containing GR (100 pM), NADPH (17.5 µM), Na_2S (0.125 mM), $Cd(NO_3)_2$ (0.125 mM), TMB (1.2 mM) and different concentrations of GSSG: a) 12.5 µM, b) 5 µM; c) 2.5 µM; d) 1.25 µM; e) 0.5 µM; f) 0 µM. (B) Calibration curve of GSSG at λabs = 650 nm.

We also employed the standard addition method for detection of total glutathione (tGSH) in 15% human plasma (Figure 2.18). According to the all dilutions of the samples the found concentration of tGSH was 4.2 ± 1.1 µM. It lies within the range of usual physiological concentrations reported for human plasma.[31, 32]

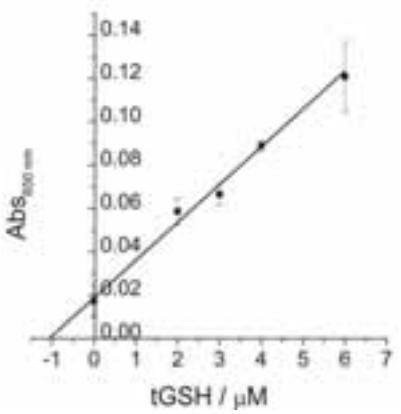

Figure 2.18. UV-vis absorption spectra of total glutathione in human plasma with the method of standard addition. The system containing GR (100 pM), NADPH (17.5 μM), Na_2S (0.125 mM), $Cd(NO_3)_2$ (0.125 mM), TMB (1.2 mM).

We also determined GR activity in our assay. Figure 2.19 shows emission spectra of GR activity in the present of glutathione, NADPH, $Cd(NO_3)_2$ and Na_2S. On the basis of this figure the detection limit of GR activity was calculated 1.44 pM. Our method showed lower detection limit than that of the recently published most sensitive enzymatic fluorogenic assay for glutathione reductase (5 pM).[29]

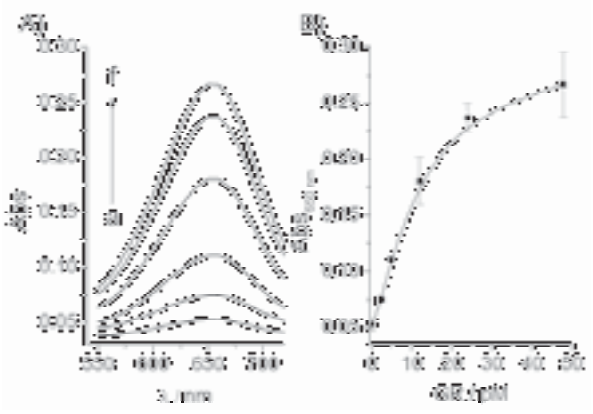

Figure 2.19. (A) UV-vis absorption spectra of the system containing NADPH (17.5 μM), GSSG (13 μM), Na_2S (0.125 mM), $Cd(NO_3)_2$ (0.125 mM), TMB (1.2 mM) and different concentrations of GR: a) 0 pM, b) 2.4 pM; c) 4.8 pM; d) 12 pM; e) 24 pM; f) 48 pM. (B) Calibration curve of GR at λabs = 650 nm.

2.4. Conclusions

In summary, we demonstrated that photocatalytical CdS NPs acting as catalysts powered by UV light can be produced *in situ* under mild conditions in aqueous medium suitable for operation of enzymes. These NPs use energy of photons from a standard UV light and do not require hydrogen peroxide for oxidation of commercially available chromogenic enzymatic substrates TMB. The stability of the present photocatalytical system under ambient laboratory light allows to apply it for development of sensitive bioanalytical chromogenic assays taking advantage of enzymatic formation of QDs. The detection limits and dynamic range demonstrated by two developed chromogenic assays were comparable with or better than those of corresponding fluorogenic, electrochemical and other assays. We proved that photocatalytical TMB oxidation can be applied for sensitive detection of enzymaticaly formed semiconducted nanoparticles by using UV spectroscopy instead of fluorometry.

2.5. References

[1] E. Katz, I. Willner, Integrated nanoparticle-biomolecule hybrid systems: synthesis, properties, and applications, Angewandte Chemie, 43 (2004) 6042-6108.

[2] Y. Xiao, V. Pavlov, S. Levine, T. Niazov, G. Markovitch, I. Willner, Catalytic growth of Au nanoparticles by NAD(P)H cofactors: optical sensors for NAD(P)+-dependent biocatalyzed transformations, Angewandte Chemie, 43 (2004) 4519-4522.

[3] A. Virel, L. Saa, V. Pavlov, Modulated growth of nanoparticles. Application for sensing nerve gases, Analytical chemistry, 81 (2009) 268-272.

[4] Y.T. Tseng, H.Y. Chang, C.C. Huang, A mass spectrometry-based immunosensor for bacteria using antibody-conjugated gold nanoparticles, Chemical communications, 48 (2012) 8712-8714.

[5] V. Pavlov, Y. Xiao, B. Shlyahovsky, I. Willner, Aptamer-functionalized Au nanoparticles for the amplified optical detection of thrombin, Journal of the American Chemical Society, 126 (2004) 11768-11769.

[6] P. Guo, Y. Shu, D. Binzel, M. Cinier, Synthesis, conjugation, and labeling of multifunctional pRNA nanoparticles for specific delivery of siRNA, drugs, and other therapeutics to target cells, Methods in molecular biology, N.J, 928 (2012) 197-219.

[7] S. Pandey, G.K. Goswami, K.K. Nanda, Green synthesis of polysaccharide/gold nanoparticle nanocomposite: an efficient ammonia sensor, Carbohydrate polymers, 94 (2013) 229-234.

[8] W.J. Parak, L. Manna, F.C. Simmel, D. Gerion, P. Alivisatos, Quantum Dots, Nanoparticles, Wiley-VCH Verlag GmbH & Co. KGaA2005, pp. 4-49.

[9] C.-A.J. Lin, T. Liedl, R.A. Sperling, M.T. Fernandez-Arguelles, J.M. Costa-Fernandez, R. Pereiro, A. Sanz-Medel, W.H. Chang, W.J. Parak, Bioanalytics and biolabeling with semiconductor nanoparticles (quantum dots), Journal of Materials Chemistry, 17 (2007) 1343-1346.

[10] B. Sun, W. Xie, G. Yi, D. Chen, Y. Zhou, J. Cheng, Microminiaturized immunoassays using quantum dots as fluorescent label by laser confocal scanning fluorescence detection, Journal of immunological methods, 249 (2001) 85-89.

[11] C.Y. Zhang, H.C. Yeh, M.T. Kuroki, T.H. Wang, Single-quantum-dot-based DNA nanosensor, Nature materials, 4 (2005) 826-831.

[12] B. Shlyahovsky, E. Katz, Y. Xiao, V. Pavlov, I. Willner, Optical and electrochemical detection of NADH and of NAD+-dependent biocatalyzed processes by the catalytic deposition of copper on gold nanoparticles, Small, 1 (2005) 213-216.

[13] Y. Xiao, V. Pavlov, B. Shlyahovsky, I. Willner, An Os(II)--bisbipyridine--4-picolinic acid complex mediates the biocatalytic growth of au nanoparticles: optical detection of glucose and acetylcholine esterase inhibition, Chemistry, 11 (2005) 2698-2704.

[14] P. Fanjul-Bolado, D. Hernandez-Santos, M.B. Gonzalez-Garcia, A. Costa-Garcia, Alkaline phosphatase-catalyzed silver deposition for electrochemical detection, Analytical chemistry, 79 (2007) 5272-5277.

[15] V. Pavlov, Y. Xiao, I. Willner, Inhibition of the acetycholine esterase-stimulated growth of Au nanoparticles: nanotechnology-based sensing of nerve gases, Nano letters, 5 (2005) 649-653.

[16] N. Malashikhina, G. Garai-Ibabe, V. Pavlov, Unconventional application of conventional enzymatic substrate: first fluorogenic immunoassay based on enzymatic formation of quantum dots, Analytical chemistry, 85 (2013) 6866-6870.

[17] P.V. Kamat, Photochemistry on nonreactive and reactive (semiconductor) surfaces, Chemical Reviews, 93 (1993) 267-300.

[18] L. Nguyen, R. Kho, W. Bae, R.K. Mehra, Glutathione as a matrix for the synthesis of CdS nanocrystallites, Chemosphere, 38 (1999) 155-173.

[19] J. Lea, A.A. Adesina, Oxidative degradation of 4-nitrophenol in UV-illuminated titania suspension, Journal of Chemical Technology & Biotechnology, 76 (2001) 803-810.

[20] C.L. Torres-Martinez, R. Kho, O.I. Mian, R.K. Mehra, Efficient Photocatalytic Degradation of Environmental Pollutants with Mass-Produced ZnS Nanocrystals, Journal of colloid and interface science, 240 (2001) 525-532.

[21] P.D. Josephy, T. Eling, R.P. Mason, The horseradish peroxidase-catalyzed oxidation of 3,5,3',5'-tetramethylbenzidine. Free radical and charge-transfer complex intermediates, The Journal of biological chemistry, 257 (1982) 3669-3675.

[22] L. Saa, V. Pavlov, Enzymatic growth of quantum dots: applications to probe glucose oxidase and horseradish peroxidase and sense glucose, Small, 8 (2012) 3449-3455.

[23] A.D. McNaught, A. Wilkinson, IUPAC Compendium of Chemical Terminology., Gold Book, Oxford, UK, 1997.

[24] M. Zayats, R. Baron, I. Popov, I. Willner, Biocatalytic growth of Au nanoparticles: from mechanistic aspects to biosensors design, Nano letters, 5 (2005) 21-25.

[25] F. Wang, X. Liu, C.H. Lu, I. Willner, Cysteine-mediated aggregation of Au nanoparticles: the development of a H2O2 sensor and oxidase-based biosensors, ACS nano, 7 7278-7286.

[26] D.A. Hepburn, I.J. Deary, B.M. Frier, A.W. Patrick, J.D. Quinn, B.M. Fisher, Symptoms of acute insulin-induced hypoglycemia in humans with and without IDDM. Factor-analysis approach, Diabetes care, 14 (1991) 949-957.

[27] A.J. Sommerfield, I.J. Deary, B.M. Frier, Acute hyperglycemia alters mood state and impairs cognitive performance in people with type 2 diabetes, Diabetes care, 27 (2004) 2335-2340.

[28] R.M. Lopez Galera, J.C. Juarez Gimenez, J.B. Montoro Ronsano, R.M. Segura Cardona, M.A. Arbos Via, C. Altisent Roca, J.M. Tusell Puigbert, Glutathione and cysteine in HIV-infected hemophiliacs, Clinica chimica acta; international journal of clinical chemistry, 254 (1996) 63-72.

[29] G. Garai-Ibabe, L. Saa, V. Pavlov, Enzymatic product-mediated stabilization of CdS quantum dots produced *in situ*: application for detection of reduced glutathione, NADPH, and glutathione reductase activity, Analytical chemistry, 85 (2013) 5542-5546.
[30] H.B. Noh, P. Chandra, J.O. Moon, Y.B. Shim, In vivo detection of glutathione disulfide and oxidative stress monitoring using a biosensor, Biomaterials, 33 2600-2607.
[31] H. Ono, A. Sakamoto, N. Sakura, Plasma total glutathione concentrations in healthy pediatric and adult subjects, Clinica chimica acta; international journal of clinical chemistry, 312 (2001) 227-229.
[32] S. Nelly, A. Nino, K. Tamar, K. Iagor, T. Alexander, Plasma Antioxidant Activity as a Marker for a Favourable Outcome in Acute Ischemic Stroke, 2012.

3

Biocatalytic etching of semiconductor cadmium sulfide nanoparticles as a new platform for optical detection of analytes

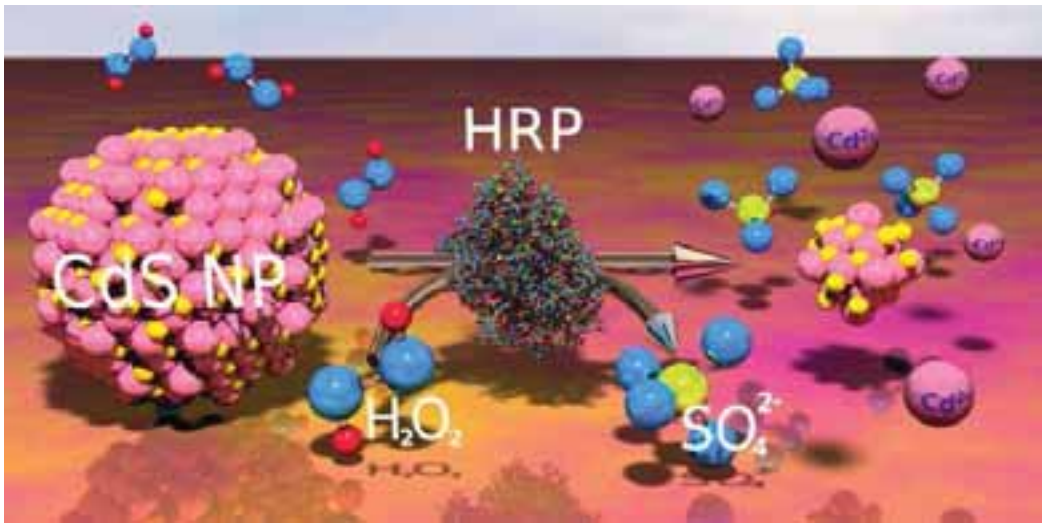

We report for the first time enzymatic etching of cadmium sulfide nanoparticles (CdS NPs). Fluorescence of semiconductor CdS NPs is modulated irreversibly by the enzymatic reaction catalyzed with horseradish peroxidase (HRP). We observed blue-shifts of corresponding fluorescence peak for CdS NPs and decrease in the intensity of the fluorescence signal.

The work presented in this chapter was previously published: Ruta Grinyte, Laura Saa, Gaizka Garai-Ibabe, Valeri Pavlov; Chem. Commun., 2015, 51, 17152-17155.

3.1. Introduction

In bioanalysis detection of analytes of interest is performed using specific interactions of biological recognition elements.[1] A recognition event should be transduced into some weak measurable signal which requires frequently amplification.[2]

Metallic nanoparticles (NPs)[3] and semiconductor nanoparticles (SNPs) can be very conveniently employed for signal transduction by physical methods. Their chemical and physical properties are defined by three dimensional structures of NPs, therefore very slight changes in shape and size lead to drastic variation in absorption and emission spectra. Usually, pre-synthesized semiconductor NPs are tethered to an analyte through recognition elements report a recognition event as labels *via* optical[4], electrochemical[5] or acoustic signal detection.[6] In another biosensing strategy semiconductor cadmium sulfide NPs are employed as light harvesting elements in electrochemical biosensors.[7]

Another strategy pioneered by our group is the enzymatic growth of semiconductor quantum dots (QDs). It was demonstrated that S^{2-} ions, thiolated products or orthophosphate generated through enzymatic reactions interact with exogenously added Cd^{2+} to yield CdS QDs. Assays using enzymatic generation of QDs can be broken down to two major groups. The first group employs enzymatic reactions which lead to formation of H_2S.[8-10] The second group of QDs-generating fluorogenic enzymatic assays developed by us relies on modulating the growth of CdS QDs with the products of biocatalytic transformation through inhibition or enhancement of crystallization rate.[11-14]

In those assays enzymes were used to generate components forming CdS QDs but the opposite process of enzymatic etching of semiconductor NPs has never been achieved. Etching technology is considered to be a particularly important process to resize semiconductor NPs and to tune their luminescence properties. However, very harsh conditions and dangerous oxidizing agents are usually required for oxidation of semiconductor materials.[15, 16] Previously we reported enzymatic etching of gold NPs where free radicals produced by the enzyme horseradish peroxidase (HRP) etch gold NPs in the presence of Br^- anions and H_2O_2.[17] Etching of gold nanorods triggered

by different analytes recently became a very promising platform for optical detection of a number of targets including H_2O_2, Cu^{2+}, Pb^{2+}, Fe^{3+}, Cr(VI), Co^{2+}, CN^-, I^- Cl^-, NO_2^- and glucose.[17-27]

HRP is available and inexpensive enzyme extensively used in biology and biotechnology for its unique characteristics.[28, 29] This enzyme can catalyze the oxidation of various chromogenic substrates such as 3,3´,5,5´-tetramethylbenzidine (TMB) 2,3-dimethoxyphenol, guaiacol, 5-amino- 2,3-dihydro-1,4-phthalazinedione (luminol), 2,2´-azino-bis(3-ethylbenzothiazoline-6-sulfonate) (ABTS), and even oxidation of species having high standard redox potential such as gold atoms of NPs.

As far as we know oxidation of semiconductor CdS NPs catalyzed by redox enzymes such as HRP has never been reported. Here we demonstrate that HRP also is able to catalyze the etching of semiconductor NPs.

3.2. Materials and methods

3.2.1. Materials

Sodium sulfide (Na_2S) and cadmium sulfate $CdSO_4$, cadmium nitrate $Cd(NO_3)_2$, horseradish peroxidase type VI and other chemicals were supplied by Sigma-Aldrich. Polyvinyl chloride microspheres with amine functional group (beadBALL-Amine) where purchase from Chemicell (Germany). All assays were performed in black flat-well (330 µL) NUNC 96 wells microtiter plates, and the fluorescence spectra were recorded with a Varioskan Flash fluorimeter (Thermo Scientific). Microscopy Studies were done by transmission electron microscopy (TEM) and Axio Observer Microscope (Zeiss). For detection of sulfate ions Capillary electrophoresis (CE) with UV/Vis diode-array detector (Agilent CE) and DU® 800 Spectrophotometer (Beckman Coulter) were used.

3.2.2. Methods

3.2.2.1. Cadmium sulfide NPs synthesis

To prepare 1000 µL of CdS NPs solution 20 µL of 10mM Na_2S was mixed with 75 µL of 100 mM Cd^{2+} ions in citrate buffer (3.5 mM, pH 5.0). The mixtures were incubated for 5 min at room temperature and used immediately.

3.2.2.2. HRP assay

For determination of peroxide, varying concentrations of H_2O_2 were added to a solution containing 100 µL of previously prepared CdS NPs, NaBr 8 mM, HRP 2.5 µM and citrate buffer 3.5 mM pH 5.0, in a final volume of 125 µL. The emission spectra of the resulting mixtures were recorded after 15 min λ_{ex}=300. For determination of HRP varying concentrations of HRP were added to a solution containing 100 µL previously prepared CdS NPs, NaBr 8 mM, H_2O_2 0.2 mM and citrate buffer 3.5 mM pH 5.0, in a final volume of 125 µL. The emission spectra of the resulting mixtures were recorded after 15 min at λ_{ex}=300.

3.2.2.3. Sample preparation for sulfate ions detection with CE

Sample 1: To prepare 1000 µL of CdS NPs solution 20 µL of 10 mM Na_2S was mixed with 75 µL of 100 mM $Cd(NO_3)_2$ in citrate buffer (3.5 mM, pH 5.0). The mixture was incubated for 5 min at room temperature. Sample 2: NaBr 8 mM, HRP 2.5 µM and H_2O_2 0.2 mM were added to the solution containing 100 µL previously prepared CdS NPs in citrate buffer 3.5 mM pH 5.0. Sample was incubate 15 min. After all samples were centrifuged using an Amicon Ultra filter with a 3000 molecular weight cutoff. 1 mL of filtrate was used.

3.2.2.4. Sample preparation for sulfate ions detection by a spectrometric method in which sulfate is precipitated as barium sulphate

The samples were prepared like described before. After 1 mL of the sample was mixed with 20 µL of 3.7 % HCl. 47.5 mL of 0.1M $BaCl_2$ and 2.5 mL of Tween 20 were mixed and 100 µL of this solution were added to the samples. The solutions were agitated for 10 min. The absorbance spectra of the resulting suspensions were recorded after 15 min.

3.2.2.5. Preparation of polyvinyl chloride microspheres/CdS NPs composites

40 µL of polyvinyl chloride microsphere-amine (25 mg/mL) were added to 260 µL citrate buffer (3.5 mM, pH 5.0) and centrifuge at 500 x g for 1 min. Supernatant was discarded and 200 µL of previously prepared CdS NPs where added to the beads. After 1 h incubation the beads were washed with 200 µL of citrate buffer 3.5 mM pH 5.0 and

resuspended in the same volume of buffer for the further experiments. For monitoring photoluminescence of etching of CdS NPs with Axio Observer Microscope in real time, 400 times diluted solution was used.

3.2.2.6. HRP assay with polyvinyl chloride microspheres/CdS NPs composites

For determination of etching on polyvinyl chloride microsphere-amine/CdS NPs composites previously mentioned conditions were used. The emission spectra of the resulting mixtures were recorded after 5 min at λ_{ex}=300.

3.2.2.7. Quantification of H_2O_2 in water

Tap water samples (samples were collected in CICbiomagune, San Sebastian, Spain) were spiked with different concentrations of H_2O_2. Next, prepared polyvinyl chloride microspheres/CdS NPs composites were mixed with water samples and with optimal concentration of HRP and NaBr.

For detection H_2O_2 in rain water collected in San Sebastian, Spain, the sample was diluted by 5 times. For quantification of H_2O_2 in rain water standard addition method was used. According to this method, the same amount of the water sample was split into separate eppendorfs. Varying standard amounts of H_2O_2 were injected into the samples with rain water. The results were plotted with the concentration standard added in the x-axis and the obtained absorbance readings in the y-axis of calibration line. The linear regression was carried out to calculate the position of the recalculated calibration line, which showed the concentration of hydrogen peroxide in samples of rain water.

3.3. Results and Discussion

3.3.1. Enzymatic etching of CdS NPS

In the present chapter, we report a facile, fast and straightforward enzymatic etching process of CdS NPs by HRP in the presence of H_2O_2. We prepared CdS NPS by rapid procedure used by us in previous works.[10] A certain amount of sulfide ions was mixed with 37 fold excess of cadmium ions at room temperature in low acidic citrate buffer. After 5 min incubation stable fluorescent CdS NPs were obtained. The obtained

CdS NPs were subjected to the action of different concentrations of H_2O_2 in the presence of fixed quantity of HRP. It was found out that the treatment of CdS NPs with varying concentrations of H_2O_2 in the presence of fixed amount of HRP and sodium bromide leads to the decrease in the intensity of emission peaks corresponding to semiconductor CdS NPs (Figure 3.1). The loss of fluorescence shows that amount of CdS NPs present in the reaction mixture is diminishing in the course of enzymatic oxidation. It is important to note that in the absence of HRP no significant changes in the emission spectra of CdS NPs were noticed in concentration range of H_2O_2 up to 0.2 mM. So the decrease in the fluorescence was not caused by possible quenching effect of H_2O_2. At the same time the position of peaks was shifted from 489 to 479 (Figure 3.1B, inset). As it has been described in the literature[30] the blue shift of emission peaks reveals that the particles were etched and the size decrease is directly related with the concentration of H_2O_2. Both calibration curves shown in Figure 3.1B demonstrated linearity from 0 to 0.05 mM and saturation starting from 0.2 mM of H_2O_2 concentration. The decrease in the fluorescence and shift of the fluorescence peak were directly related with quantity of the enzymatic substrate, H_2O_2, in the reaction mixture.

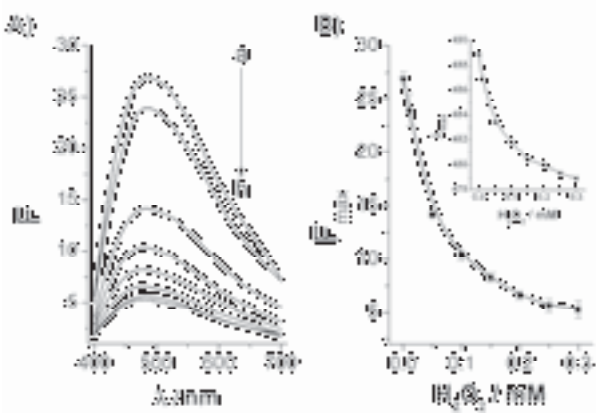

Figure 3.1. (A) Fluorescence emission spectra of the system containing CdS NPs, HRP (2.5 μM), NaBr (8 mM) and different concentrations of H_2O_2: a) 0 mM; b) 0.01 mM; c) 0.05 mM; d) 0.1 mM; e) 0.15 mM; f) 0.2 mM; g) 0.25 mM; h) 0.3 mM; (B) Calibration curve of H_2O_2 obtained using maximum fluorescence intensity of the peak, Fmax. Inset: the position of emission peaks at different concentrations of H_2O_2.

According to the shape of both calibration curves oxidation of CdS NPs with H_2O_2 catalysed by HRP follows the classical Michaelis-Menten kinetic model describing the initial bimolecular reaction between enzyme and the substrate. The experimental data

were fitted by non linear regression method according to the Michaelis-Menten equation $\Delta F = \Delta F_{max} [H_2O_2] / (K_M + [H_2O_2])$, K_M is the apparent Michaelis-Menten constant equal to 57.2 ± 5.2 μM. The value of K_M for H_2O_2 measured using TMB as the substrate under the same experimental conditions was 1300 μM. This difference in apparent Michaelis-Menten constants indicates that oxidation of CdS NPs proceeds through dissociation: $CdS \leftrightarrows Cd^{2+} + S^2$. In accordance with the calibration curve (Figure 3.1B) the limit of H_2O_2 detection was calculated to be 8 μM by UPAC definition.[31] This detection limit is 5 times lower than that reported for detection of H_2O_2 using the enzymatic growth of CdS NPs.[10]

In order to elucidate further the mechanism of enzymatic oxidation of CdS NPs the effect of varying concentrations of HRP on the observed florescence intensity was studied. The reaction was carried out at the constant concentration of hydrogen peroxide equal to 0.2 mM in the presence of sodium bromide.

Figure 3.2 shows the evolution of emission spectra of CdS NPs during the etching process in the presence of increasing concentrations of HRP. We observed that decrease in the fluorescence signal and blue shifts of emission peaks (Figure 3.2B, inset) are directly related with the increase in the concentration of HRP. Given the fact that in the presence of 2.5 μM HRP without H_2O_2 no effect on the florescence of CdS NPs was detected (as one can see in Figure 3.1) the fluorescence loss is caused by the biocatalytic reaction.

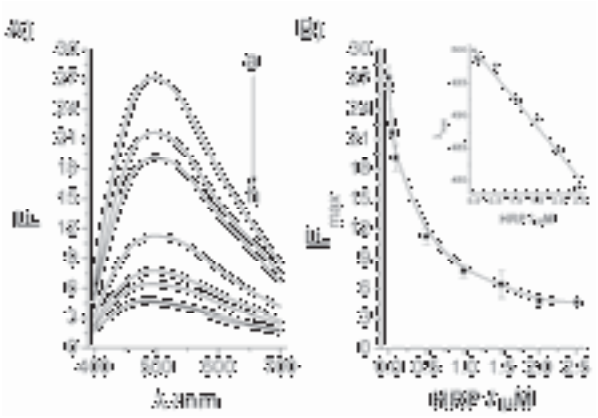

Figure 3.2. (A) Fluorescence emission spectra of the system containing CdS NPs, H_2O_2 (0.2 mM), NaBr (8mM) and different concentrations of HRP: a) 0 μM; b) 0.05 μM; c) 0.1 μM; d) 0.5 μM; e) 1 μM; f) 1.5 μM; g) 2 μM; h) 2.5 μM;. (B) Calibration curve of HRP obtained using maximum fluorescence intensity of the peak, F_{max}. Inset: the position of emission peaks at different concentrations of HRP.

Statistical analysis from transmission electron microscopy (TEM) images was used to analyze the diameter of the CdS NPs before and after biocatalytic oxidation. As demonstrated in Figure 3.3A and B the particle diameter and concentration of CdS NPs decreased due to etching. Furthermore, size distribution plots revealed that before etching the particles had the medium diameter around 2.8 nm (Figure 3.3C). However, upon addition of H_2O_2 the medium diameter of CdS NPs reduced by almost 2 times (Figure 3.3D).

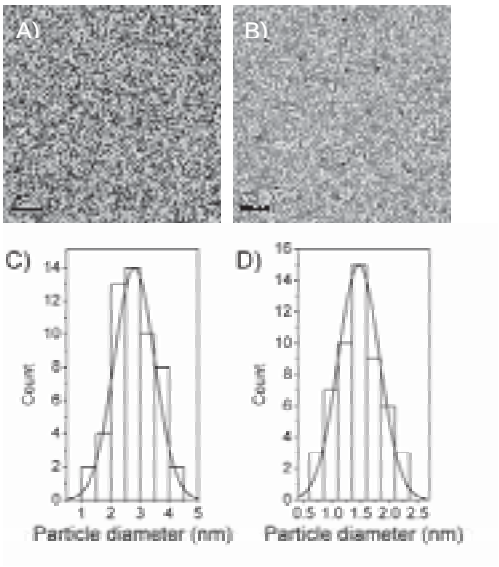

Figure 3.3. TEM images of CdS NPs (A) before (B) after etching; Size distribution of CdS NPs (C) before (D) after etching.

Since the etching reaction did not proceed in the absence of sodium bromide some additional experiments were performed. The influence of varying bromide concentrations on the emission spectrum of CdS NPs was studied. In the absence of H_2O_2 and HRP the fluorescence intensity was not significantly changed up to 8 mM of NaBr and then linearly decreased (Figure 3.4 curve a). We also examined the effect of bromide concentration on the process of enzymatic etching (Figure 3.4 curve b). At fixed concentration of HRP and H_2O_2 the increase in the bromide concentration resulted in rapid acceleration of etching rate up to 8 mM of NaBr. This optimized bromide concentration (8 mM) was used in the previous experiments of enzymatic etching.

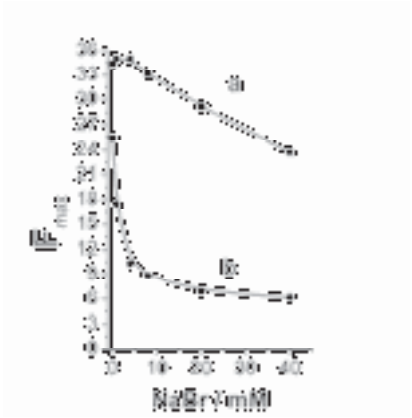

Figure 3.4. Effect of different concentrations of NaBr on peak fluorescence intensity, F_{max}, in the system composed of (a) CdS NPs only (b) CdS NPs, H_2O_2 (0.1 mM), HRP (2 μM).

Other halides such as chloride, iodide and fluoride did not influence the etching rate (Figure 3.5). This observation corroborates well with the previously published finding that Cd^{2+} is able to form $[CdBr_4]^{2-}$ complex with Br^- ions.[32] The formation of $[CdBr_4]^{2-}$ favours oxidation of CdS nanoparticles through sequestering free Cd^{2+} cations produced in the course of enzymatic reaction. The driving force of the etching process is biocatalytic oxidation of S^{2-} yielding SO_4^{2-} ions according to the Equation 1 and 2:

$$CdS \leftrightarrows Cd^{2+} + S^{2-} \qquad (1)$$

$$S^{2-} + 4H_2O_2 \rightarrow SO_4^{2-} + 4H_2O \qquad (2)$$

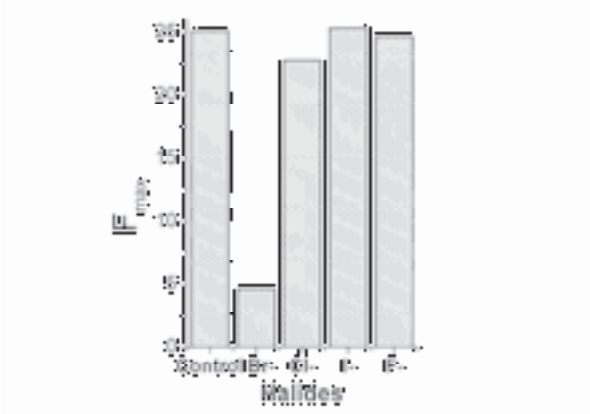

Figure 3.5. Effect of different concentrations halides on peak fluorescence intensity, F_{max}, in the system composed of CdS NPs, H_2O_2 (0.25 mM), HRP (2.5 μM) and 8 mM of halides.

The formation of sulfate ions was confirmed by two independent methods. We employed capillary electrophoresis (CE) (Figure 3.6) to determine sulfate ions in the

filtrate of CdS NPs before and after etching at optimum concentrations of HRP, H_2O_2 and sodium bromide. Sulfate ions were detected only in the filtered reaction mixture obtained after biocatalytic oxidation. No sulfate ions were discovered in the filtered reaction mixture which was not subjected to enzymatic reaction.

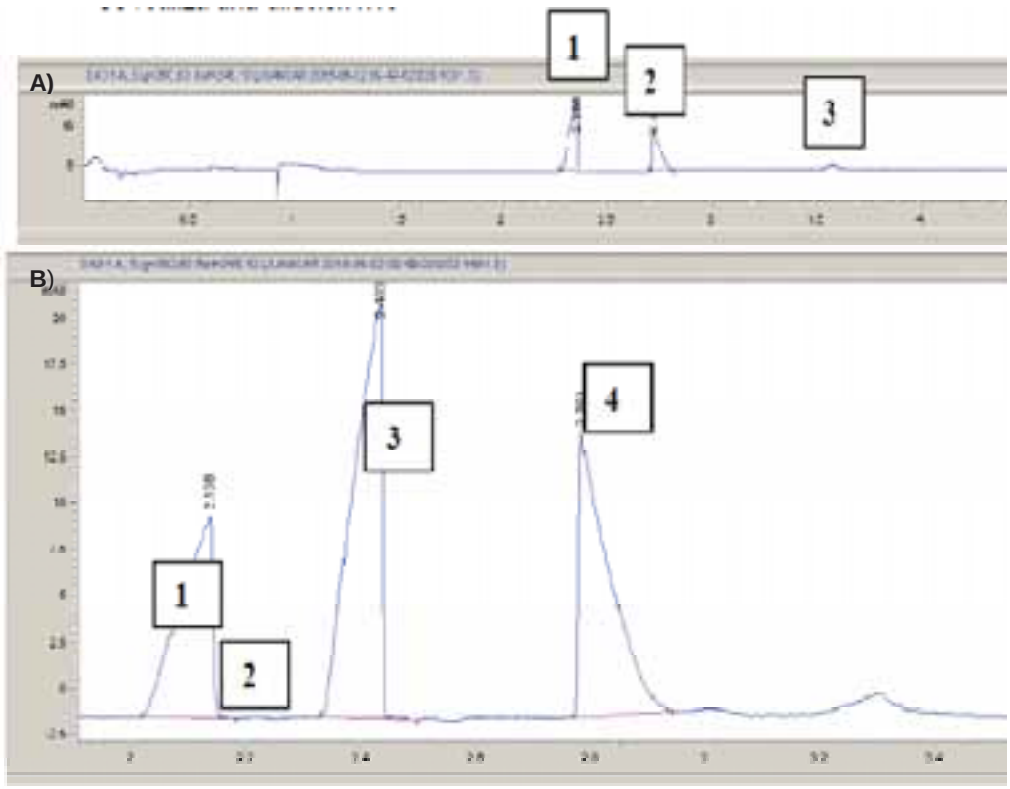

Figure 3.6. CE results. (A) Sample 1 (dissolution 10X). peak 1. NO_3^-, peak 2 citrate ion, peak 3 unknown but not SO_4^{2-} Conclusion no SO_4^{2-} ions were detected; (B) Sample 2 (dissolution 5X). 1. peak 1 Br^-, peak 2 SO_4^{2-}, peak 3 NO_3^-, peak 4 citrate ion. Conclusion 2.4±0.3 mg L^{-1} ions were detected.

Another independent method was based on the classical specific analytical reaction between SO_4^{2-} and Ba^{2+} ions resulting in insoluble $BaSO_4$ particles determined by UV-vis spectroscopy Figure 3.7. This classical analytical assay also confirmed presence of SO_4^{2-} only in the filtrate of reaction mixtures composed of CdS NPs, HRP, H_2O_2 and Br^-.

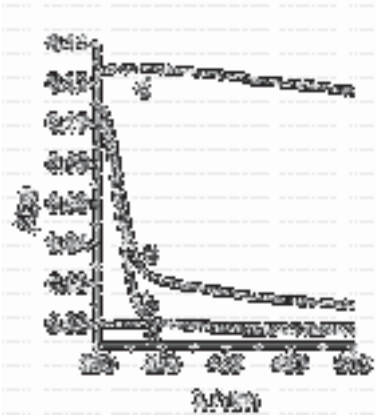

Figure 3.7. Absorbance spectra of SO_4^{2-} a) blank; b) before etching; c) after etching, d) only SO_4^{2-} in citrate buffer.

In the light of the above mentioned experiments we propose the following scheme describing biocatalytic oxidation of CdS NPs with H_2O_2 and HRP (Scheme 3.1). HRP catalyzes oxidation of S^{2-} ions in CdS NPs by H_2O_2 resulting in the formation of sulfate anions and Cd^{2+} cations.

Scheme 3.1. Enzymatic etcing of CdS NPs.

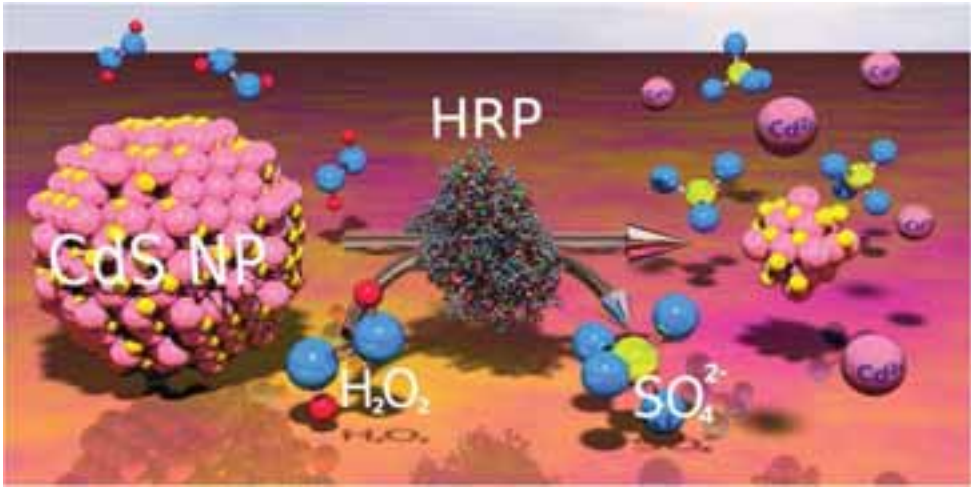

3.3.2. Enzymatic etching of CdS NPS immobilized on the surface of polyvinyl chloride-amine microspheres

In order to check out how the etching process can be influenced by immobilization of CdS NPs on a substrate this semiconductor NPs were immobilized on the surface of

polyvinyl chloride-amine microspheres. Immobilization was performed by adsorption of negatively charged CdS NPs, stabilized with citrate, on the beads bearing positively charged amino groups. Modified beads were washed with citrate buffer. Microspheres carrying CdS NPs were employed as substrates in the enzymatic etching reaction. The same etching phenomenon was observed as in the above-mentioned experiments with free CdS NPs (Figure 3.8). The apparent Michaelis-Menten constant for H_2O_2 calculated from the curve in Figure 3.8B was 21.6 ± 3.1 µM (two times less than that calculated for free CdS NPs).

This difference can be explained by steric hindrance partially preventing dissociation of immobilized CdS NPs into S^{2-} and Cd^{2+} ions. In accordance with the calibration curve (Figure 3.8B) for H_2O_2 the IUPAC detection limit was found to be 7 µM and this value is almost the same than in the experiments with free CdS NPs. The position of the peak was shifted from 500 to 470 (Figure 3.8. inset) indicating the evident decrease in size of immobilized CdS NPs caused by etching.

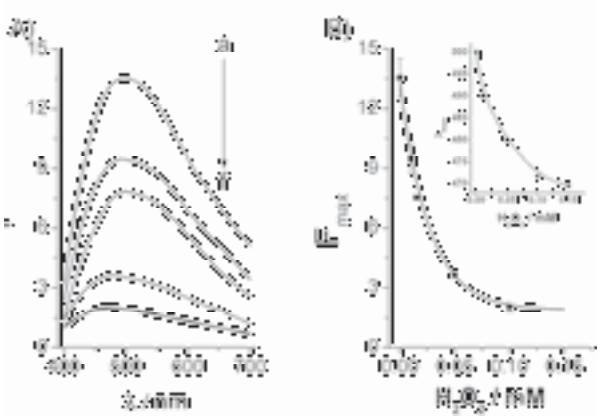

Figure 3.8. (A) Fluorescence emission spectra of the system containing polyvinyl chloride microsphere-amine/CdS NPs composites, HRP (2.5 µM), NaBr (8 mM) and different concentrations of H_2O_2: a) 0 mM; b) 0.01 mM; c) 0.015 mM; d) 0.05 mM; e) 0.1 mM; f) 0.15 mM. (B) Calibration curve of H_2O_2 obtained using maximum fluorescence intensity of the peak, Fmax. Inset: the position of emission peaks at different concentrations of H_2O_2.

In addition, Figure 3.9 shows the fluorescence spectra of polyvinyl chloride-amine microspheres/CdS NPs composites after etching in the presence of fixed amount of NaBr, H_2O_2 and different concentrations of HRP. In this case, we observed that increase in amounts of enzyme was correlated with decrease in emission peak intensity (Figure 3.9B). As in the experiments with CdS NPs only, the same etching

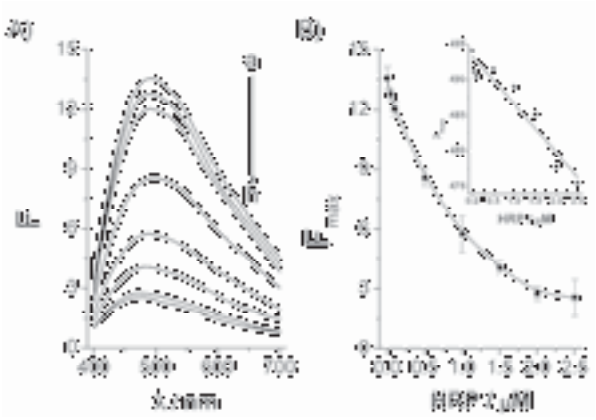

Figure 3.9. (A) Fluorescence emission spectra of the system containing polyvinyl chloride microsphere-amine/CdS NPs composites H_2O_2 (0.2 mM), NaBr (8 mM) and different concentrations of HRP: a) 0 µM; b) 0.05 µM; c) 0.1 µM; d) 0.5 µM; e) 1 µM; f) 1.5 µM; g) 2 µM; h) 2.5 µM;. (B) Calibration curve of HRP obtained using maximum fluorescence intensity of the peak, F_{max}. Inset: the position of emission peaks at different concentrations of HRP.

process was monitored after biocatalytic reaction: the peak was shifted and its intensity decreased. In conclusion, CdS immobilized microspheres could be used as nanosensors in the assay for HRP activity as described in Scheme 3.2.

Scheme 3.2. Enzymatic etching of CdS NPs immobilized on the surface of polyvinyl chloride microsphere-amine.

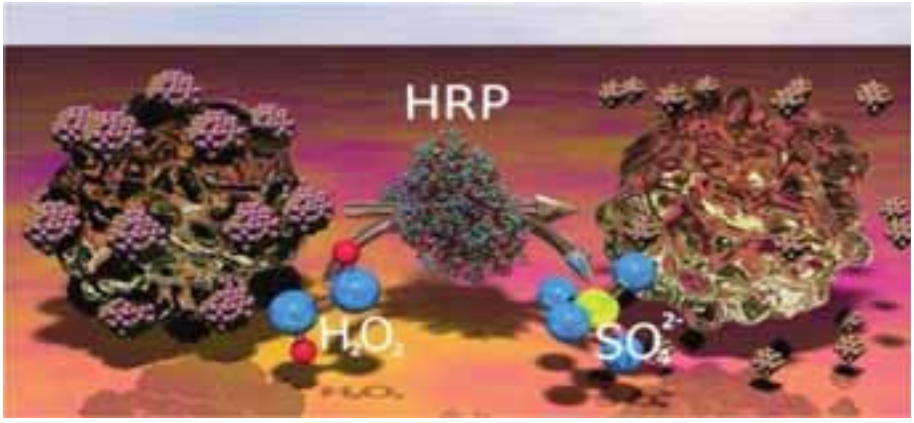

TEM image confirms the presence of CdS NPs on the surface of microspheres (Figure 3.10). As one can see in Figure 3.10C, no traces of CdS NPs were detected on the surface of the beads after biocatalytical etching. It means that during biocatalytic oxidation reaction CdS NPs were etched and lost the link with microspheres or dissolved completely.

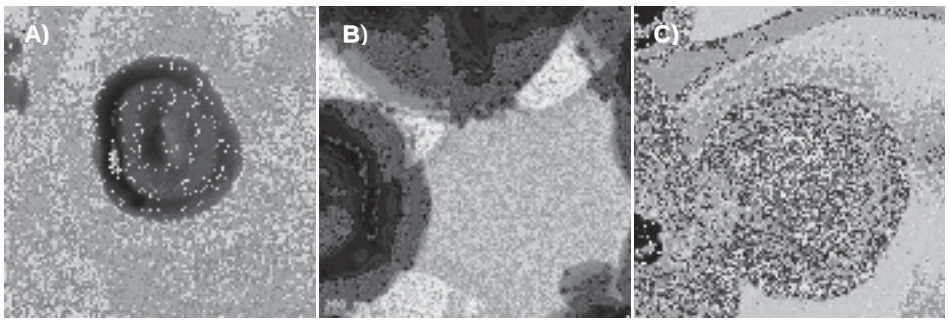

Figure 3.10. TEM images of polyvinyl chloride microsphere-amine (A) microspheres only; (B) polyvinyl chloride microsphere-amine/CdS NPs composites before etching; (C) polyvinyl chloride microsphere-amine/CdS NPs composites after etching.

TEM images of polyvinyl chloride-amine microspheres/CdS NPs composites show dense distribution of CdS NPs on the surface of microspheres, as a result, it was possible to detect fluorescence of the immobilized QDs. For fluorescence imaging analysis wide field fluorescence microscope was used. For the first time the changes in fluorescence in real time during the etching process were monitored by microscope (Figure 3.11). As shown in Figure 3.11, fluorescence on the surface of microspheres was completely lost after 15 min. Figure 3.11B shows that in the absence of HRP no significant changes in fluorescence intensity were observed.

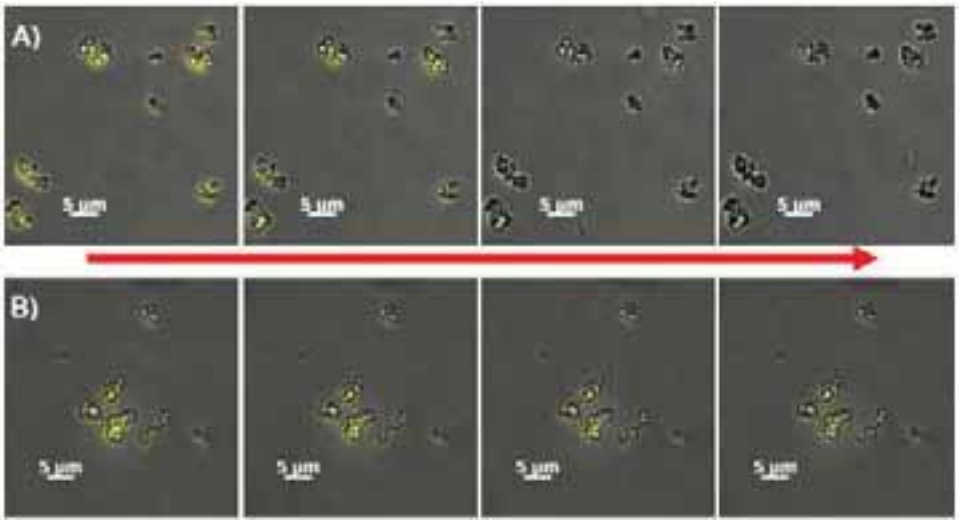

Figure 3.11. Fluorescence microscope images during the etching process (A) polyvinyl chloride microsphere-amine/CdS NPs composites in the presence of NaBr, HRP, H_2O_2 (B) without HRP. The process was recorded during 15 min and pictures were obtained every 5 min.

Polyvinyl chloride microsphere-amine/CdS NPs composites were applied to detection of H_2O_2 (which is used as pre-oxidant in municipal water treatment) in tap

drinking water spiked with H_2O_2. The recovery of this system (Table 4.1) was close to 100% which indicates that enzymatic etching is suitable for detection of hydrogen peroxide in real samples. The latest comparable methods for detection of H_2O_2 using Prussian blue on polyaniline coated halloysite nanotubes or nanoporous Ag@BSA composite microspheres[33, 34] have similar detection limit, reproducibility and selectivity but the preparation of microsphere-amine/CdS NPs composites is much simpler. The proposed method was also used to assay hydrogen peroxide in rain water as described in supplementary information. Taking into consideration all dilutions of the samples, the found concentration of H_2O_2 in rain water was 0.0261 ± 0.0011 mM (Figure 3.12) and it lies within the range of conventional HRP-ABTS enzymatic assay 0.0274 ± 0.0052 mM but our assay showed better reproducibility with the standard deviation lower by about 5 times.

Table 3.1. Results of the analyses of H_2O_2 in drinking tap water

Water sample	Added, mM	Found, mM	RSD	Recovery
Drinking tap water	0	not found		
	0.0075	0.00743	4.60%	99.0 %
	0.01	0.01082	3.20%	108.2 %
	0.015	0.01447	2.90%	96.5 %

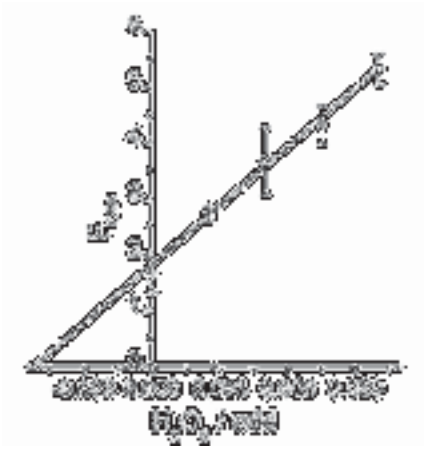

Figure 3.12. Quantification of H_2O_2 in rain water with the method of standard addition. The system containing: polyvinyl chloride microsphere-amine/CdS NPs composites, HRP (2.5 μM), NaBr (8 mM).

3.4. Conclusion

In summary, the present approach describes a facile, mild and inexpensive enzymatic etching method for resizing of CdS NPs. It was found out that the biocatalytic process involving bromide, HRP and H_2O_2 decreased the size of semiconductor CdS NPs. Thus, this phenomenon can be applied to resizing of semiconductor CdS NPs under mild physiological conditions and rapid and sensitive detection of H_2O_2 and HRP. It was proven that also CdS NPs immobilized on polyvinyl chloride microspheres can be etched biocatalytically. We introduce a new platform for optical detection of analytes based on etching of semiconductor NPs. Given the fact that etching of gold NPs became the basis of various analytical assays for metal ions, glucose, H_2O_2 etc. [17-27] we believe that phenomenon discover by us will find broad applications in analytical chemistry. This finding opens new path for enzymatic modification and modulation of biosensors based on semiconductor NPs.

3.5. References

[1] A. Ivask, T. Green, B. Polyak, A. Mor, A. Kahru, M. Virta, R. Marks, Fibre-optic bacterial biosensors and their application for the analysis of bioavailable Hg and As in soils and sediments from Aznalcollar mining area in Spain, Biosensors & bioelectronics, 22 (2007) 1396-1402.

[2] K. Jia, M.Y. Khaywah, Y. Li, J.L. Bijeon, P.M. Adam, R. Deturche, B. Guelorget, M. Francois, G. Louarn, R.E. Ionescu, Strong improvements of localized surface plasmon resonance sensitivity by using Au/Ag bimetallic nanostructures modified with polydopamine films, ACS applied materials & interfaces, 6 219-227.

[3] S. Wu, P. Liang, H. Yu, X. Xu, Y. Liu, X. Lou, Y. Xiao, Amplified single base-pair mismatch detection via aggregation of exonuclease-sheared gold nanoparticles, Analytical chemistry, 86 3461-3467.

[4] E. Morales-Narvaez, H. Monton, A. Fomicheva, A. Merkoci, Signal enhancement in antibody microarrays using quantum dots nanocrystals: application to potential Alzheimer's disease biomarker screening, Analytical chemistry, 84 6821-6827.

[5] M. Medina-Sanchez, S. Miserere, E. Morales-Narvaez, A. Merkoci, On-chip magneto-immunoassay for Alzheimer's biomarker electrochemical detection by using quantum dots as labels, Biosensors & bioelectronics, 54 279-284.

[6] E. Katz, I. Willner, Integrated nanoparticle-biomolecule hybrid systems: synthesis, properties, and applications, Angewandte Chemie, 43 (2004) 6042-6108.

[7] E. Katz, M. Zayats, I. Willner, F. Lisdat, Controlling the direction of photocurrents by means of CdS nanoparticles and cytochrome c-mediated biocatalytic cascades, Chemical communications, (2006) 1395-1397.

[8] L. Saa, A. Virel, J. Sanchez-Lopez, V. Pavlov, Analytical applications of enzymatic growth of quantum dots, Chemistry, 16 (2010) 6187-6192.

[9] L. Saa, J.M. Mato, V. Pavlov, Assays for methionine gamma-lyase and S-adenosyl-L-homocysteine hydrolase based on enzymatic formation of CdS quantum dots *in situ*, Analytical chemistry, 84 (2012) 8961-8965.

[10] L. Saa, V. Pavlov, Enzymatic growth of quantum dots: applications to probe glucose oxidase and horseradish peroxidase and sense glucose, Small, 8 (2012) 3449-3455.

[11] G. Garai-Ibabe, L. Saa, V. Pavlov, Enzymatic product-mediated stabilization of CdS quantum dots produced *in situ*: application for detection of reduced glutathione, NADPH, and glutathione reductase activity, Analytical chemistry, 85 (2013) 5542-5546.

[12] G. Garai-Ibabe, L. Saa, V. Pavlov, Thiocholine mediated stabilization of *in situ* produced CdS quantum dots: application for the detection of acetylcholinesterase activity and inhibitors, The Analyst, 139 (2014) 280-284.

[13] N. Malashikhina, G. Garai-Ibabe, V. Pavlov, Unconventional application of conventional enzymatic substrate: first fluorogenic immunoassay based on enzymatic formation of quantum dots, Analytical chemistry, 85 (2013) 6866-6870.

[14] G. Garai-Ibabe, M. Moller, V. Pavlov, Ultrasensitive assay for detection of serum paraoxonase by modulating the growth of fluorescent semiconductor nanoparticles, Analytical chemistry, 84 (2012) 8033-8037.

[15] H. Matsumoto, T. Sakata, H. Mori, H. Yoneyama, Preparation of Monodisperse CdS Nanocrystals by Size Selective Photocorrosion, The Journal of Physical Chemistry, 100 (1996) 13781-13785.

[16] Y. Wang, Z. Tang, M.A. Correa-Duarte, I. Pastoriza-Santos, M. Giersig, N.A. Kotov, L.M. Liz-Marzan, Mechanism of Strong Luminescence Photoactivation of Citrate-Stabilized Water-Soluble Nanoparticles with CdSe Cores, The Journal of Physical Chemistry B, 108 (2004) 15461-15469.

[17] L. Saa, M. Coronado-Puchau, V. Pavlov, L.M. Liz-Marzan, Enzymatic etching of gold nanorods by horseradish peroxidase and application to blood glucose detection, Nanoscale, 6 (2014) 7405-7409.

[18] Y. Xia, J. Ye, K. Tan, J. Wang, G. Yang, Colorimetric visualization of glucose at the submicromole level in serum by a homogenous silver nanoprism-glucose oxidase system, Analytical chemistry, 85 (2013) 6241-6247.

[19] R. Liu, Z. Chen, S. Wang, C. Qu, L. Chen, Z. Wang, Colorimetric sensing of copper(II) based on catalytic etching of gold nanoparticles, Talanta, 112 (2013) 37-42.

[20] F.-M. Li, J.-M. Liu, X.-X. Wang, L.-P. Lin, W.-L. Cai, X. Lin, Y.-N. Zeng, Z.-M. Li, S.-Q. Lin, Non-aggregation based label free colorimetric sensor for the detection of Cr (VI) based on selective etching of gold nanorods, Sensors and Actuators B: Chemical, 155 (2011) 817-822.

[21] J.-M. Liu, L. Jiao, M.-L. Cui, L.-P. Lin, X.-X. Wang, Z.-Y. Zheng, L.-H. Zhang, S.-L. Jiang, A highly sensitive non-aggregation colorimetric sensor for the determination of Iâˆ’ based on its catalytic effect on Fe^{3+} etching gold nanorods, Sensors and Actuators B: Chemical, 188 (2013) 644-650.

[22] Z. Chen, Z. Zhang, C. Qu, D. Pan, L. Chen, Highly sensitive label-free colorimetric sensing of nitrite based on etching of gold nanorods, The Analyst, 137 (2012) 5197-5200.

[23] R. Zou, X. Guo, J. Yang, D. Li, F. Peng, L. Zhang, H. Wang, H. Yu, Selective etching of gold nanorods by ferric chloride at room temperature, CrystEngComm, 11 (2009) 2797-2803.

[24] Y.-Y. Chen, H.-T. Chang, Y.-C. Shiang, Y.-L. Hung, C.-K. Chiang, C.-C. Huang, Colorimetric Assay for Lead Ions Based on the Leaching of Gold Nanoparticles, Analytical chemistry, 81 (2009) 9433-9439.

[25] L. Shang, L. Jin, S. Dong, Sensitive turn-on fluorescent detection of cyanide based on the dissolution of fluorophore functionalized gold nanoparticles, Chemical Communications, (2009) 3077-3079.

[26] S.K. Tripathy, J.Y. Woo, C.S. Han, Highly selective colorimetric detection of hydrochloric acid using unlabeled gold nanoparticles and an oxidizing agent, Analytical chemistry, 83 (2011) 9206-9212.

[27] Z. Zhang, Z. Chen, D. Pan, L. Chen, Fenton-like reaction-mediated etching of gold nanorods for visual detection of $Co^{(2+)}$, Langmuir, 31 (2015) 643-650.

[28] A.M. Azevedo, V.C. Martins, D.M. Prazeres, V. Vojinovic, J.M. Cabral, L.P. Fonseca, Horseradish peroxidase: a valuable tool in biotechnology, Biotechnology annual review, 9 (2003) 199-247.

[29] N.C. Veitch, Horseradish peroxidase: a modern view of a classic enzyme, Phytochemistry, 65 (2004) 249-259.

[30] J. Liu, X. Yang, K. Wang, D. Wang, P. Zhang, Chemical etching with tetrafluoroborate: a facile method for resizing of CdTe nanocrystals under mild conditions, Chemical communications, (2009) 6080-6082.

[31] A.D. McNaught, A. Wilkinson, IUPAC Compendium of Chemical Terminology. , Gold Book, Oxford, UK, 1997.

[32] R.W. Ramette, Equilibrium constants for cadmium bromide complexes by coulometric determination of cadmium iodate solubility, Analytical chemistry, 55 (1983) 1232-1236.

[33] Q. Sheng, D. Zhang, Q. Wu, J. Zheng, H. Tang, Electrodeposition of Prussian blue nanoparticles on polyaniline coated halloysite nanotubes for nonenzymatic hydrogen peroxide sensing, Analytical Methods, 7 (2015) 6896-6903.

[34] Q. Liu, T. Zhang, L. Yu, N. Jia, D.-P. Yang, 3D nanoporous Ag@BSA composite microspheres as hydrogen peroxide sensors, The Analyst, 138 (2013) 5559-5562.

4

Microbead QD-ELISA: microbead ELISA using biocatalytic formation of quantum dots for ultra high sensitive optical and electrochemical detection

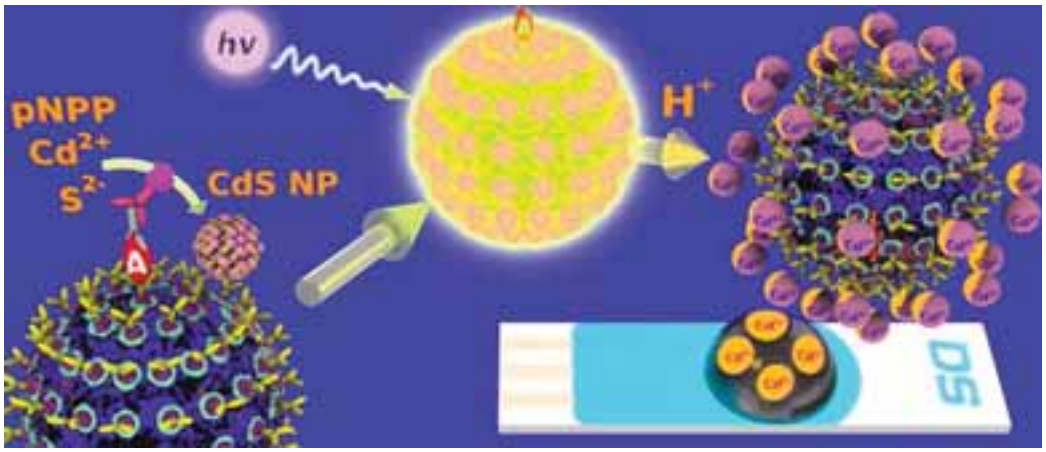

In this study we present the immunoassay in which the target analyte superoxide dismutase (SOD2) mediates immobilization of alkaline phosphatase antibody conjugate on the surface of polyvinyl chloride microbeads. The enzymatic hydrolysis of para-nitrophenylphosphate by alkaline phosphatase triggered rapid formation on the surface of microbeads of phosphate-stabilized cadmium sulfide semiconductor nanoparticles (SNPs) which were detected by fluorescence spectroscopy, microscopy and square-wave voltammetry (SWV). Moreover, our proposed electrochemical assay for SOD2 based on SWV detection Cd^{2+} ions originating from immobilized CdS SNPs showed lower detection limit by two orders of magnitude in comparison with other previously published assays for superoxide dismutase. The electrochemical assay was validated with HepG2 (Human hepatocellular carcinoma) cell lysate containing SOD2.

The work presented in this chapter was previously published: : Ruta Grinyte, Javier Barroso, Laura Saa, , Valeri Pavlov; ACS Appl Mater Interfaces. 2016 Oct DOI:10.1021/acsami.6b08362.

4.1. Introduction

Biochemical assays use specific chemical interaction to detect target analytes by different recognition elements such as antibodies (in immunoassays),[1] DNA (deoxyribonucleic acid) aptamers,[2, 3] or nanostructured imprinted polymer films.[4, 5] Immunoassays have been broadly applied to a variety of platforms, including microtiter plate based immunoassays, lateral flow immunochromatographic assays and bead-based immunoassays. The enzyme-linked immunosorbent assay (ELISA) relying on enzymes like horseradish peroxidase (HRP) or alkaline phosphatase (ALP) for signal amplification is probably the most ubiquitous bioanalysis method used in clinical diagnostics for diagnosis of infectious diseases, food allergen detection and plant pathogens.[6-9]

Microparticles are commonly used as a solid support for the immobilization of recognition elements in immunoreactions[10] in order to capture and separate target molecules and thus are also used in conjunction with ELISA. The bead-based ELISA originates from sandwich ELISA and substitutes the flat plastic surface supports with magnetic, polymeric beads or microspheres. Due to the mobility of the particles, bead-based ELISA can be applied in more detection systems.[11-14] Traditionally, the detection of the enzyme labels was performed by optical assays based on chromogenic and fluorogenic organic substrates, which change absorption or emission spectra in the course of enzymatic reactions. However, most of the organic dyes currently in use for bead-based ELISA are not very resistant against decomposition under the action of light in the presence of oxygen, hydrogen peroxide and water in the assay mixture resulting in bleaching. Metal nanoparticles (NPs) demonstrate much higher stability, and due to their high extinction coefficients they are increasingly finding application in bioanalysis, for instance by triggering the formation of detectable metal NPs by an enzymatic reaction chain involving glucose oxidase (GOx), ALP or alcohol dehydrogenase (AlcDH).[15-19] However, metal NPs produced by the enzymes are not fluorescent and rarely demonstrate photocatalytic activities, and therefore their use in bioapplications is limited. In contrast, semiconductor NPs show the intrinsic capacity to become photoexcited and subsequently emit fluorescent light in the relaxation process. Quantum effects govern this behavior, and therefore these particles are

referred to in the literature as quantum dots (QDs). The wavelength and intensity of the emitted light is defined by the chemical composition and the shape of the QDs, and also by its environment, which makes them a very interesting target for a wider application in bioassays.[20]

Our group has pioneered the enzymatic *in situ* growth[21-25] and etching [26] of fluorescent semiconductor CdS QDs, and on this base developed fluorogenic enzymatic assays. Those assays were much more cost efficient, lower production time and demonstrated lower detection limits and better sensitivities than the standard assays based on organic substrates.[20] The general methodology can now be readily applied to any bioassay using enzymes for signal amplification. We applied this technique to a traditional optical ELISA test where biocatalytic growth of fluorescent CdS QDs was used for the detection of an analyte captured on the surface of polystyrene microplates.[27]

While the exploitation of the optical properties of QDs is usually a key parameter in the design of such ultra sensitive assays, there is still little knowledge about the practical exploitation of a pure electrochemical (without the need of any light source and optical detector) quantification of enzymatically generated QDs. Usually, the metal ions (Cd^{2+}, Pb^{2+}, Zn^{2+}) of semiconductor NPs possess different oxidation potentials yielding well-resolved voltammetric signals with a nicely low detection limit, [28-32] and works by Bard et al. showed that in particular CdS QDs exhibit the requested inherent electrochemical properties which are necessary for an electrochemical detection.[33, 34]

In recent years, several voltammetric techniques such as linear sweep, differential pulse voltammetry (DPV) and square-wave voltammetry (SWV) have been the most widely employed electrochemical methods for characterization and quantification of QDs.[35, 36] SWV became the most employed methodology due to its high selectivity and sensitivity.[28-32] The inexpensive, commercially available, disposable screen-printed electrodes (SPEs) with their versatility, miniaturization and ease of handling[37, 38] significantly diminish assay times and volume samples, being therefore increasingly used.

To the best of our knowledge the electrochemical detection of biocatalytically generated QDs has neither been reported nor applied to bioanalysis. On the other

hand, the enzymatic formation and deposition of QDs on microbeads with analytical applications has never been reported. *In situ* deposition of CdS QDs by the amplifying enzyme ALP potentially can yield very sensitive electrochemical assays due to the fact that one enzyme can generate several CdS QDs. In this study, we developed a methodology for the direct detection of enzymatically generated CdS QDs captured on microbeads which subsequently were subjected to an acid attack. The released cadmium ions were monitored by SWV using SPEs.

If the exploitation of an electrochemical quantification of QDs in an enzymatically amplified bioassay would turn out to be less expensive than fluorometry, then we could offer a quite universal bioanalytical platform using the enzymatic growth of QDs It would finally be applicable to an extremely wide range of detection systems, spanning from optical laboratory equipment to perspective low power requiring microfluidic systems (in which even the final washing step can be automated) and thus fast point of care (POC) analysis systems.

We applied the developed electrochemical Microbead QD-ELISA to the detection of the important biomarker superoxide dismutase 2 (SOD2) and compared the assay performance with that of the relevant fluorogenic and chromogenic affinity bioassays. SOD2 is an antioxidant enzyme which catalyzes the dismutation of superoxide anion into molecular oxygen and hydrogen peroxide. This enzyme protects cells against reactive free radicals by neutralizing superoxide anions produced under oxidative conditions.[39] Numerous studies have demonstrated over-expression of SOD2 in various types of cancer cells like breast cancer, pancreatic adenocarcinoma, papilloma, prostate carcinoma and other cancer cells.[40-43] Measurement of the SOD2 concentration in cells is essential for monitoring the clinical course of the disease and distinguishing between the different stages of tumors. In this study, we applied our system to analysis of SOD2 in Human hepatocellular carcinoma (HepG2) cells lysate.

4.2. Materials and methods

4.2.1. Materials

Bovine serum albumin (BSA), antimouse Immunoglobulin G (IgG)-(whole molecule)-ALP, sodium sulfide (Na_2S), cadmium nitrate $Cd(NO_3)_2$, 4-nitrophenyl

phosphate disodium salt (pNPP) and other chemicals were supplied by Sigma-Aldrich. Human SOD2 full length protein, anti-SOD2 antibody-biotin (developed in rabbit), anti-SOD2 antibody (developed in mouse), HepG2 whole cell lysate were purchased from Abcam. 1 μm diameter polyvinyl chloride microbeads decorated with streptavidin (beadBALL-Streptavidin®) were purchased from Chemicell (Germany). Screen-printed electrodes (SPEs) were purchased from DropSens (Spain). Disposable customized devices based on a single-working carbon electrode, carbon counter electrode and Ag/AgCl reference electrode were specially designed to work with microvolumes of a sample. The stability of the Ag/AgCl reference electrode was confirmed by performing cyclic voltammetry with $K_3[Fe(CN)_6]$. A boxed connector (DropSens) was employed as interface between SPEs and potentiostat.

4.2.2. Methods

4.2.2.1. Preparation of polyvinyl chloride microspheres/antiSOD2 composites

100 μL of polyvinyl chloride microbeads-streptavidin (10 mg mL^{-1}) were added into a clean 0.5 mL microcentrifuge tube and centrifuged at 500 x g for 1 min. The supernatant was discarded, and 100 μL of Tris-buffered saline, pH 8.0 (TBS) buffer were added to the beads. The beads were spun down and resuspended into 50 μL of buffer, and 50 μL of anti-SOD2 antibody-biotin (0.1 mg mL^{-1}) were added to the solution. The concentration of SOD2 antibody-biotin equal to 0.1 mg mL^{-1} was suggested by the standard protocol of Chemicell for immobilization of biotinylated antibodies. After 15 min incubation the beads were washed 3 times with 100 μL of TBS and resuspended in 100 μL of buffer. To prevent nonspecific binding of proteins microbeads were blocked by incubation with 5 % (w/v) BSA in TBS, overnight at 4 ^{o}C. Then beads were washed three times with TBS/0.05 % (v/v) Tween20® (TBST) and resuspended in the same buffer to a final volume of 100 μL.

4.2.2.2. Detection of SOD2 protein by fluorogenic and chromogenic methods

20 μL of prepared beads were incubated for 1 hour in samples of different concentration of SOD2 protein in TBS, final volume 100 μL. The microbeads were washed 3 times with 200 μL TBST. The mixture of microbeads, anti-SOD2 antibody

(1:10) and antimouse-ALP (1:100) in TBS was agitated in the microcentrifuge tube for 1 h at room temperature (RT). The beads were then washed three times with TBST and once with Tris buffer (50 mM Tris-HCl buffer and 1 mM $MgCl_2$, pH 8.8). Then, 90 µL of ALP substrate (0.56 mM pNPP in 50 mM Tris-HCl buffer and 1 mM $MgCl_2$, pH 8.8) was added to each sample and incubated for 30 min at RT. Afterwards, 5 µL of 1 mM Na_2S and 5 µL of 50 mM $Cd(NO_3)_2$ were added. After incubation of 30 min the beads were washed once with 100 µL Tris buffer (50 mM Tris-HCl buffer and 1 mM $MgCl_2$, pH 8.8) and placed to a black 96-well NUNC® microtiter plate. The fluorescence emission spectra of the resulting suspension were recorded at λ_{ex} = 320 nm. For ALP substrate detection by the standard chromogenic method, the supernatant obtained after washing was transferred into transparent flat-well NUNC® 96-well microtiter plates. The absorbance at λ = 410 nm was measured. Furthermore, the fluorescence spectra for the detection of spiked SOD2 (3 µg mL^{-1}) in real samples (HepG2 whole cell lysate) was measured.

4.2.2.3. Release of free cadmium ions from adsorbed CdS NPs

100 µL aliquots of microbeads samples bearing enzymatically produced CdS NPs obtained in the above mentioned experiment were placed into Amicon® Ultra-0.5 centrifugal filters (3000 NMWL) and washed 3 times with Tris-HCl buffer (10mM, pH 8.8). Finally, the recovered mixtures were transferred into new filters and 200 µL of 0.2 M HCl was added to release Cd^{2+} cations from the captured CdS NPs. After centrifugation, the cadmium solutions were transferred to the pretreated SPEs.

4.2.2.4. Electrochemical detection

Before SWV measurements SPEs were pretreated electrochemically by cyclic voltammetry (CV) for 20 cycles at a potential range of 0 – 1 V in Tris-HCl buffer (10 mM, pH 8.8). Subsequently, a 40 µL drop of collected solutions was placed on the SPEs and electrochemical SWV measurements were conducted by electrodepositing cadmium at -1.2 V for 2 minutes and stripping from -1.2 to -0.6 V. The square wave parameters mainly included 2 mV step potential, 25 mV amplitude and 25 Hz frequency.

In order to follow the the quality of the washing of CdS NPs adsorbed on microbeads from exogenous Cd^{2+} ions, the collected waste solution was measured by SWV after each washing step (Figure 4.1.).

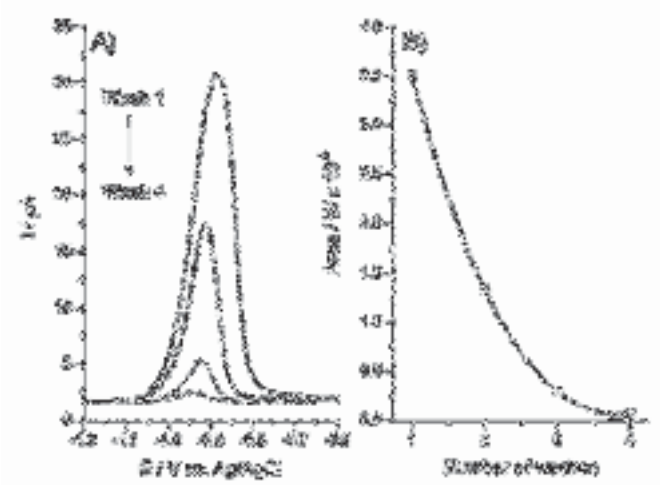

Figure 4.1. (A) Square wave voltammograms obtained from successive washings of waste solutions. (B) Decreasing curve of Cd concentrations.

All electrochemical data was recorded on the Autolab Electrochemical Workstation (Model: PGSTAT302N, Metrohm Autolab, The Netherlands) equipped with NOVA 1.10 software. All experiments were performed at room temperature. Unless mentioned otherwise, all experimental results presented here are averaged from three independent measurements (n = 3).

4.3. Results and Discussion

4.3.1. Preparation of microbeads

Scheme 4.1. outlines the model assay for detection of SOD2 by enzymatic generation of CdS QDs. The stages of modification of polyvinyl chloride microbeads with antiSOD2 are shown in Scheme 4.1A. Briefly, streptavidin coated microbeads were mixed with polyclonal biotin labeled capture antibodies specific to SOD2 protein. To avoid nonspecific adsorption of interfering species on the surface of the beads 5% (w/v) BSA was used to block the surface. The stages of the bioassay for SOD2 are presented in Scheme 4.1B. It describes microbead-based ELISA for detection of SOD2 protein. Previously prepared blocked polyvinyl chloride microbeads bearing capture antiSOD2 were incubated in sample solutions containing different concentrations of

SOD2 protein. Next, detecting anti-SOD2 antibody from mouse was specifically bound to SOD2 protein on the microbead surface. Secondary ALP-conjugated antimouse IgG was added to label the Fc region of immobilized mouse anti-SOD2 detecting antibody. The microbeads were washed to remove the unbound secondary antibody-enzyme conjugates.

Scheme 4.1. The Principle of Microbead-Based ELISA. (A) Procedure of Microbeads Bearing Anti-SOD2 and BSA; (B) Immobilization of ALP Mediated by the Analyte; (C) The Biocatalytic Signal Amplification Cascade for Detection of Analyte.

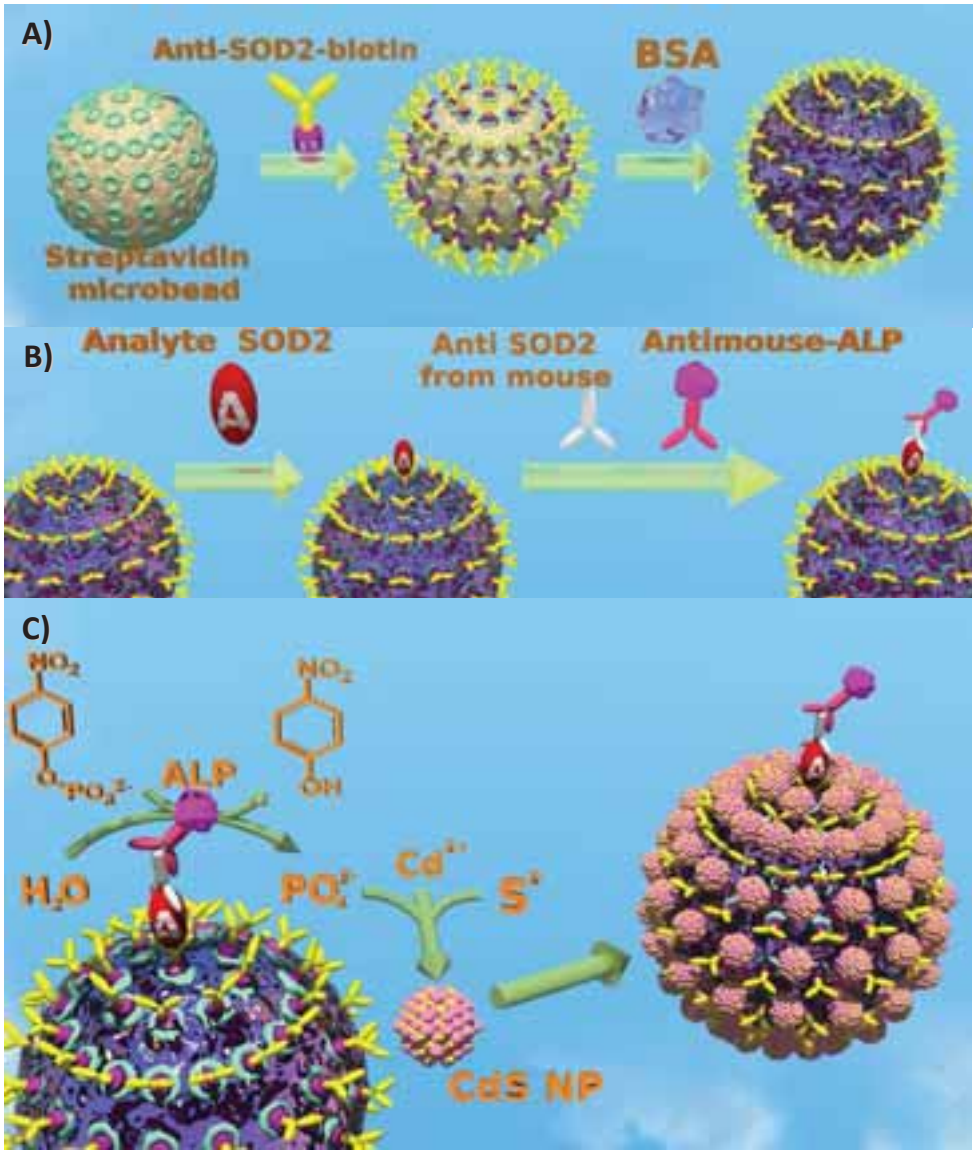

In the past we demonstrated that orthophosphate ions (PO_4^{3-}) produced by ALP stabilize CdS NPs produced from Na_2S and $Cd(NO_3)_2$ *in situ*.[27] Scheme 4.1C outlines the biocatalytic signal amplification cascade for detection of analyte SOD2 by the enzymatic production of CdS QDs *in situ*. As demonstrated in Scheme 4.1C, ALP captured on the microbeads due to the recognition event hydrolyzes para-nitrophenylphosphate (pNPP) to para-nitrophenol and orthophosphate ions which stabilize CdS NPs produced *in situ* by the interaction of Cd^{2+} with S^{2-} ions. The optimum concentrations of $Cd(NO_3)_2$ was 2.5 mM and Na_2S was 0.05 mM as shown in Figure 4.2. For optimization of $Cd(NO_3)_2$ concentration ALP-conjugated antimouse IgG was tethered to the surface of microbeads bearing SOD2 as described on experimental session. The concentration of SOD2 equal to 1 μg/ml was used for immobilization of ALP-conjugated antimouse IgG. CdS NPs were formed and deposited on the surface of micriobeads in the presence of varying concentration of $Cd(NO_3)_2$ and fixed concentration of 0.5mM of the Na_2S. The fluorescence of the beads prepared with and without SOD2 was measured. The ratio of fluorescence intensity peaks registered in the presence and in the absence of SOD2 is shown in Figure 4.2A. For optimization of Na_2S concentration the deposition of CdS NPs was performed in the presence of different concentrations of Na_2S and fixed concentration of 2.5mM $Cd(NO_3)_2$. The ration of the fluorescence intensity peaks registered in the presence and in the absence of SOD2 is shown in Figure 4.2B.

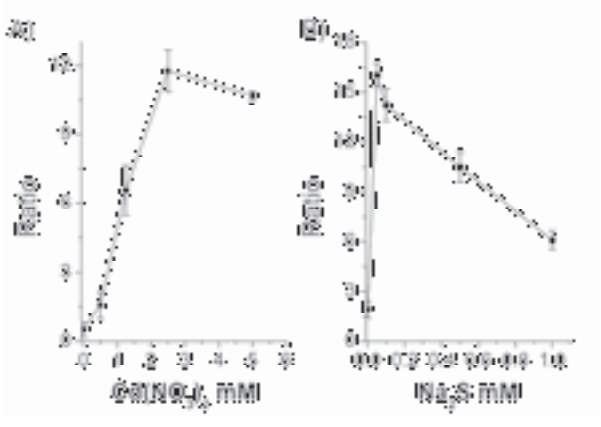

Figure 4.2. The ratio of fluorescence intensity peaks registered in the presence and in the absence of SOD2 containing (A) different concentration of $Cd(NO_3)_2$; (B) containing different concentration of Na_2S.

ALP demonstrates the highest specific activity at basic pH in the presence of Mg^{2+} cations. On the other hand CdS NPs capped by negative PO_4^{-3} anions are more stable at

basic pH which shifts the following three equilibriums to the right increasing the total stabilizing negative charge on QDs:

$H_3PO_4 \leftrightarrow H_2PO_4^- + H^+$

$H_2PO_4^- \leftrightarrow HPO_4^{-2} + H^+$

$HPO_4^{-2} \leftrightarrow PO_4^{-3} + H^+$

Therefore we used 50 mM Tris-HCl buffer containing 1 mM $MgCl_2$ with pH 8.8 for the enzymatic growth of CdS QDs. The resulting CdS NPs bind to the surface of microbeads, as confirmed by the experimental characterization of the microbeads.

4.3.2. Characterization of microbeads

In order to confirm the presence of the generated CdS NPs on the surface of the microbeads a wide field fluorescence microscope and a transmission electron microscopy (TEM) equipped with an Energy Dispersive X-Ray Spectrometer (EDX) were used. Fluorescence imaging analysis confirms the presence of CdS NPs on the surface of microspheres (Figure 4.3.). In the absence of SOD2 no fluorescence was detected (Figure 4.3.). In the images obtained in the presence of 111.5 ng mL^{-1} SOD2, high fluorescence intensity was observed due to the adsorption of enzymatically generated CdS NPs on the surface of microbeads.

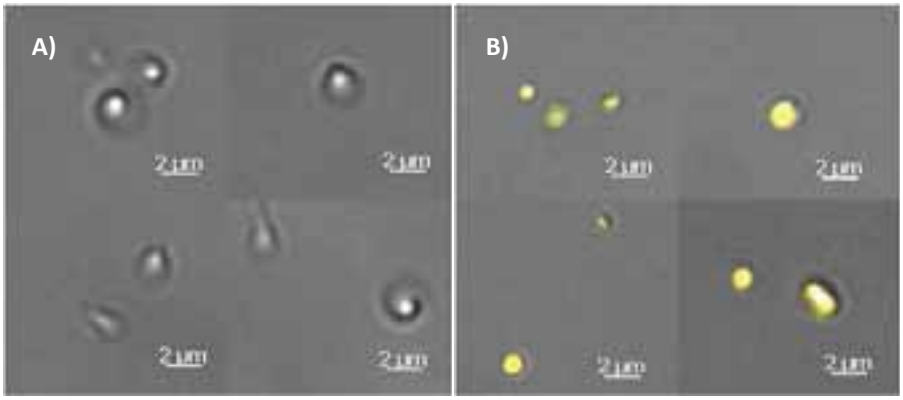

Figure 4.3. Fluorescence microscope images obtained (four different pictures in different areas of each sample were taken): (A) in the absence of SOD2 protein; (B) in the presence of SOD2 protein.

EDX spectra have been acquired in a transmission electron microscope (TEM) in scanning mode (STEM). Detected Cd was found to be colocalized with the microbeads for SOD2 treated samples (Figure 4.4.). In the absence of SOD2 protein in the assay no

Cd was detected. The present, low EDX signal was proven to be in this case noise only, and thus no image is shown for this sample (the EDX data analysis is presented in the appendix chapter 4).

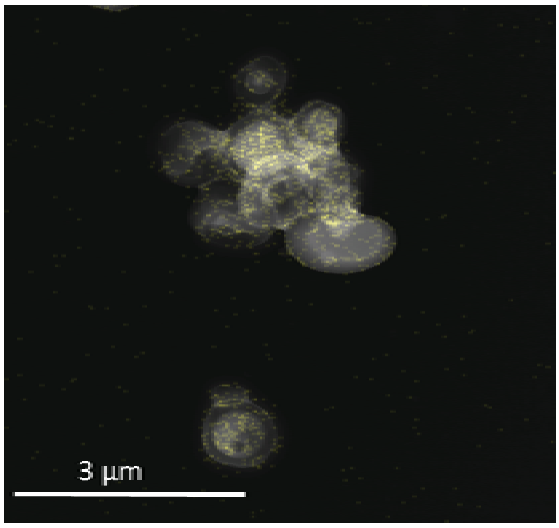

Figure 4.4. Overlay of detected Cd signal to the corresponding STEM image (20.000 magnification). The excitation occurred where the organic matrix is localized.

4.3.3. Optical detection methods

Three different analytical methods: fluorogenic, chromogenic and electrochemical, were used to follow the readout signal. Scheme 4.2. represents the fluorogenic test, where CdS QDs immobilized on the surface of microbeads emit fluorescence under excitation with 320 nm light. Figure 4.5A represents fluorescence emission spectra of CdS QDs corresponding to different concentrations of SOD2 (from 0 to 111.6 ng mL^{-1})

Scheme 4.2. Fluorogenic detection method

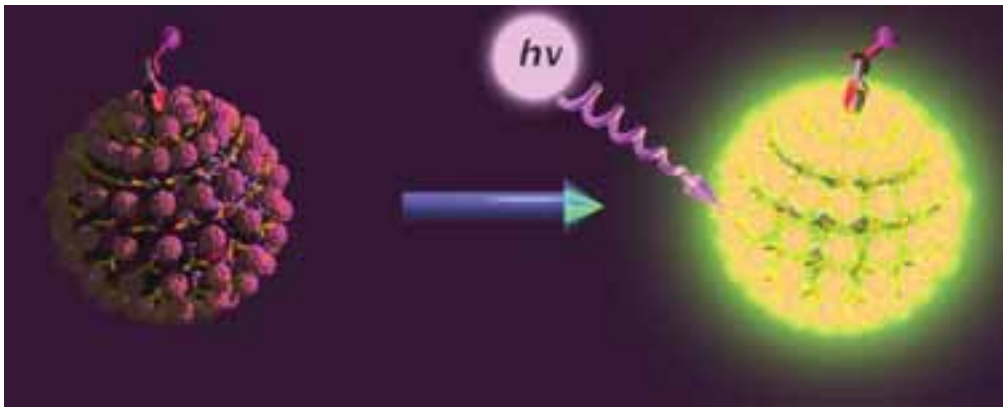

in buffer solutions. The increase in the amount of adsorbed SOD2 protein leads to a rising fluorescence intensity. The received calibration curve in Figure 4.5B demonstrates that the intensity of the emission peaks increases with the concentration of the SOD2 protein. The response to varying SOD2 concentrations shows linearity from 0 to 11 ng mL^{-1} and saturation starting from 80 ng mL^{-1} SOD2 concentration. According to the calibration curve the limit of SOD2 detection was found to be 0.52 ng mL^{-1} (2.31 x 10^{-11} M).

Furthermore, we compared the performance of the fluorogenic method with that of the standard immunoassay based on the enzymatic hydrolysis of chromogenic substrate pNPP, followed by UV−Vis spectroscopy (Figure 4.5C). A linear response range for detection of SOD2 by this method was between 0 ng mL^{-1} and 11 ng mL^{-1} and it shows the same value compared with the fluorogenic one. However, the lowest concentration of SOD2 that could be detected by this chromogenic system was found to be 1.307 ng mL^{-1} (5.82 x 10^{-11} M), which is 2.5 times worse than that of the fluorogenic assay.

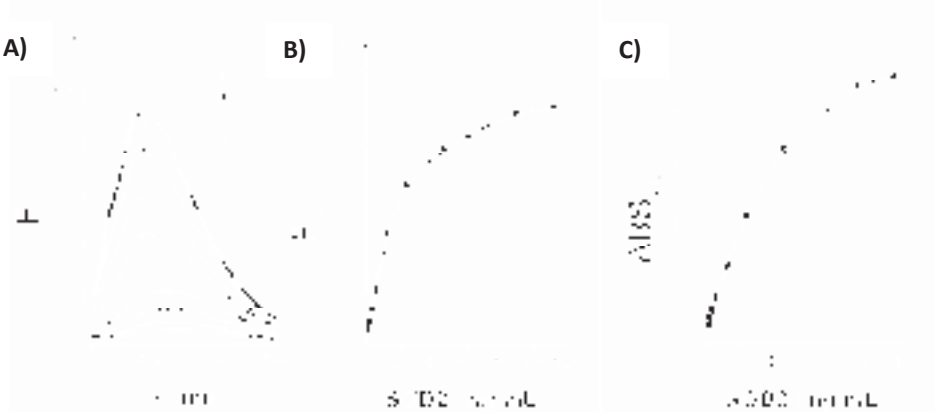

Figure 4.5. (A) Fluorescence emission spectra of the system containing: $Cd(NO_3)_2$ (2.5 mM), Na_2S (0.05 mM), pNPP (0.5 mM) and various concentrations of SOD2: (a) 0 ng mL^{-1}; (b) 1.1 ng mL^{-1}; (c) 2.23 ng mL^{-1}; (d) 4.46 ng mL^{-1}; (e) 11.16 ng mL^{-1}; (f) 22.3 ng mL^{-1}; (g) 44.6 ng mL^{-1}; (h) 89 ng mL^{-1}; and (i) 111.6 ng mL^{-1}. (B) Calibration curve of SOD2 obtained using maximum fluorescence intensity of the peak, F_{max}. (C) Calibration curve of SOD2 obtained using λ_{abs} = 410

4.3.4. Electrochemical detection of SOD2

Under the optimized operating conditions (step potential, amplitude and frequency), a series of different concentrations of enzymatically generated CdS NPs corresponding to SOD2 concentrations from 0 to 111.6 ng mL^{-1} was measured. Before performing the electrochemical studies, free exogenous cadmium ions which were not

immobilized as CdS NPs on the surface of microbeads were washed off by ultrafiltration. Finally, the microbeads bearing CdS NPs were recovered and treated with hydrochloride acid to now dissolve the cadmium from the NPs as it is depicted in Scheme 4.3. Like this we exclusively made available for the electrochemical detection only the cadmium which before formed QDs.

Scheme 4.3. Electrochemical Detection Method Using Screen Printed Electrodes

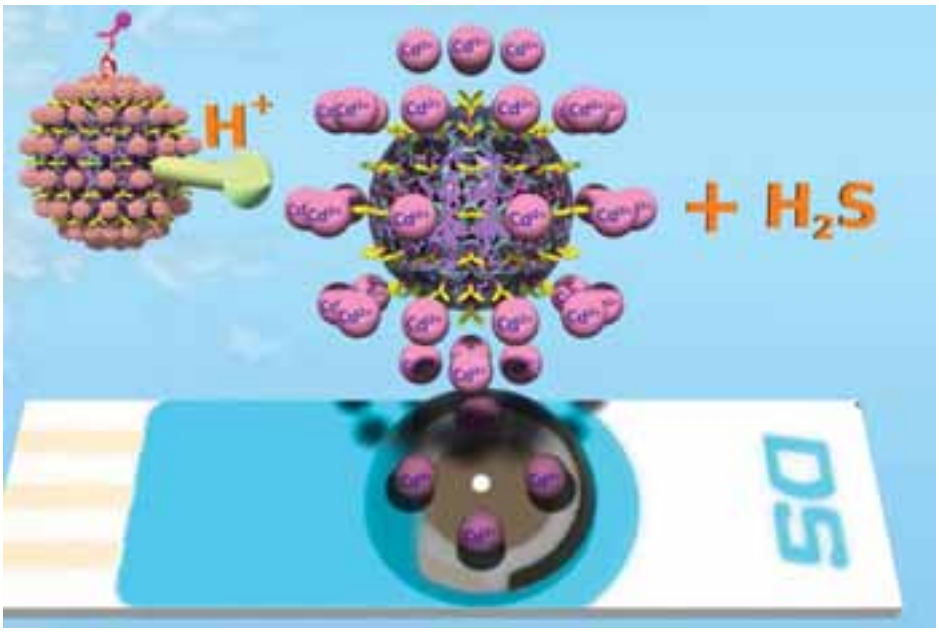

The mechanism of Cd^{2+} ions detection consists of several steps: accumulation, reduction and stripping stages as described below:

$$CdS\ NPs + 2HCl \xrightarrow{acid\ attack} Cd^{2+}\ (dis) + 2Cl^{-} + H_2S \uparrow$$

$$Cd^{2+}\ (dis) + 2e^{-} \xrightarrow{deposition\ (-1.2\ V\ vs.\ Ag/AgCl)} Cd(SPE)$$

$$Cd(SPE) \xrightarrow{SWV\ (-0.9\ V\ vs.\ Ag/AgCl)} Cd^{2+}\ (dis) + 2e^{-}$$

Firstly, the dissolved Cd^{2+} ions were reduced at -1.2 V *vs.* Ag/AgCl and electrochemically deposited on the surface of working electrode of disposable SPE. Subsequently, the deposited cadmium was electrochemically oxidized at -0.90 V *vs.* Ag/AgCl. The electrochemical signal increased during selective electrodeposition of

cadmium ions corresponding to the increasing amounts of SOD2. Well-defined stripping peaks with maximum currents increasing in proportion to the concentration of SOD2 were observed at -0.90 V *vs.* Ag/AgCl as shown in stripping curves of Figure 4.6A. The square-wave voltammograms demonstrated four times wider linearity (up to 45 ng mL^{-1} Figure 4.6B) in comparison with that of the fluorogenic assay. It was confirmed that all the dissolved Cd^{2+} ions were deposited on the surface of the SPE (Figure A4.2, appendix chapter 4). Fluorescence quenching phenomenon is usually observed upon aggregation of CdS NPs as has been reported in the literature.[44, 45] So, enzymatically generated CdS NPs partially lose fluorescence upon aggregation on microbeads, resulting in narrower linear range demonstrated by the fluorogenic assay. We explained the wider linearity of the electrochemical method by the fact that the electrochemical SWV readout signal depends only on the total amount of Cd^{2+} ions captured on microbeads in CdS and is not affected by the quenching due to quantum interaction between neighboring QDs. The lowest amount of SOD2 that could be detected by electrochemical method was found to be 0.44 ng mL^{-1} (1.96×10^{-11} M). The average relative standard deviation (RSD) calculated from the SOD2 calibration (obtained using at least three independent measurements) was 6.75%. The previously published various assays for superoxide dismutase demonstrated much worse detection limits than our electrochemistry detection immunoassay.

The electrochemical oxygen probe showed a detection limit of 1.5×10^{-9} M,[46] and two assays using surface plasma resonance (SPR) had detection limits of 1×10^{-9} M [47] and 0.9×10^{-6} M.[48] The chromogenic ELISA employing HRP-antibody conjugate and 3,3',5,5'-tetramethylbenzidine gave a detection limit of 1.2×10^{-6} M and requires at least 6 h.[48] The most recent electrochemical method for detection of superoxide dismutase using affinity interaction has detection limit of 0.5 nM.[49] Thus, our fluorogenic and electrochemical assays requiring between 4 and 6 h of total incubation and washing time improve upon these published detection limits by three orders of magnitude. This remarkable decrease in the detection limit will allow for smaller samples needed from patients.

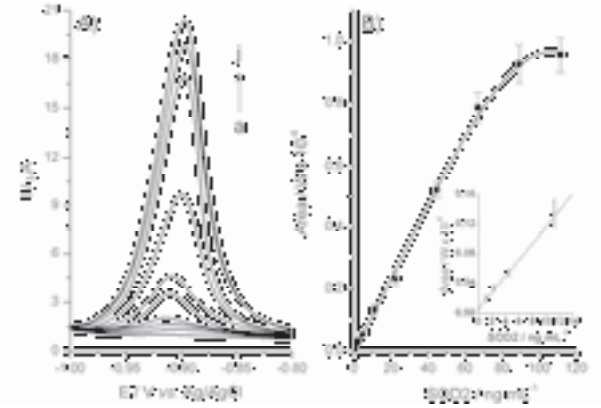

Figure 4.6. (A) Square wave voltammograms obtained for the SOD2 detection at different concentrations of (a) 0 ng mL^{-1}, (b) 1.12 ng mL^{-1}, (c) 2.23 ng mL^{-1}, (d) 4.46 ng mL^{-1}, (e) 11.15 ng mL^{-1}, (f) 22.30 ng mL^{-1}, (g) 44.60 ng mL^{-1}, (h) 66.90 ng mL^{-1}, (i) 89.20 ng mL^{-1} and (j) 111.50 ng mL^{-1}. (B) Calibration curve of SOD2 obtained using integrated area under peaks. Inset: Part of the calibration plot at low concentrations.

Finally, the detection of tumor markers in real samples is really of importance and gives information of the disease stage. For that reason, we also evaluated our assay for detection of SOD2 in HepG2 cell lysate samples. We validated the developed electrochemical method by running assays employing HepG2 cell lysate samples containing different known concentrations (spiked concentration: 0, 11.15, 22.30 and 44.60 ng mL^{-1}) of SOD2, which demonstrated the voltammetric curves depicted in Figure 4.7A. The calibration plot including the error bars for three different measurements (RSD = 7%) is also shown in Figure 4.7B. The similar calibration curves for SOD2 detection in buffer (dashed line) and cell lysate (dark line) demonstrate the suitability of the method for use in real samples.

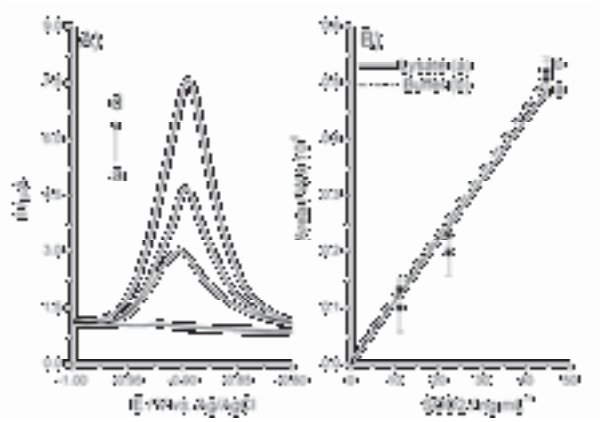

Figure 4.7. (A) Square wave voltammograms obtained using HepG2 cell lysate samples containing various SOD2 amounts: (a) 0 ng mL^{-1}, (b) 11.15 ng mL^{-1}, (c) 22.30 ng mL^{-1} and (d) 44.60 ng mL^{-1}. (B) Calibration curve of SOD2 in lysate (dark line) and buffer (dashed line) obtained using integrated area under peaks.

4.4. Conclusion

We developed a bead-based immunoassay for the detection of tumor biomarkers such as SOD2 employing enzymatic *in situ* generation and immobilization of CdS QDs onto microspheres. We have demonstrated that electrochemical and fluorogenic detection employing enzymatically generated CdS NPs yield new immunoassays with better detection limits in comparison with those of the previously published methods at least by three orders of magnitude. The electrochemical detection immunoassay did not suffer from signal loss due to aggregation of CdS NPs on microbeads and showed four times wider linear range than that of the fluorogenic immunoassay. Our methodology allows for the detection of SOD2 in lysates from HepG2 cells.

Enzymatic formation of QDs *in situ* enables employment of various physical methods such as fluorescence spectroscopy and electrochemistry to follow the readout signals and significantly improves the detection limit of immunoassays.

Thus, Microbead QD-ELISA, developed by us, can be applied with ultra high sensitivity in both detection systems, optical and electrochemical. While the optical characteristics of QDs made them well known, their electrochemical characteristics are not of any less power in Microbead QD-ELISA especially because of the wider linear response.

4.5. References

[1] B. Shlyahovsky, V. Pavlov, L. Kaganovsky, I. Willner, Biocatalytic Evolution of a Biocatalyst Marker: Towards the Ultrasensitive Detection of Immunocomplexes and DNA Analysis, Angewandte Chemie International Edition, 45 (2006) 4815-4819.

[2] V. Pavlov, Y. Xiao, B. Shlyahovsky, I. Willner, Aptamer-Functionalized Au Nanoparticles for the Amplified Optical Detection of Thrombin, Journal of the American Chemical Society, 126 (2004) 11768-11769.

[3] G. Garai-Ibabe, R. Grinyte, E.I. Golub, A. Canaan, M.L. de la Chapelle, R.S. Marks, V. Pavlov, Label free and amplified detection of cancer marker EBNA-1 by DNA probe based biosensors, Biosensors and Bioelectronics, 30 (2011) 272-275.

[4] L. Elmlund, C. Kack, T. Aastrup, I. Nicholls, Study of the Interaction of Trastuzumab and SKOV3 Epithelial Cancer Cells Using a Quartz Crystal Microbalance Sensor, 2015, pp. 5884.

[5] S. Suriyanarayanan, H. Nawaz, N. Ndizeye, I. Nicholls, Hierarchical Thin Film Architectures for Enhanced Sensor Performance: Liquid Crystal-Mediated Electrochemical Synthesis of Nanostructured Imprinted Polymer Films for the Selective Recognition of Bupivacaine, 2014, pp. 90.

[6] S. Sakamoto, J. Sakoda, O. Morinaga, P. Waraporn, R. Tsuchihashi, S. Morimoto, J. Kinjo, H. Tanaka, Development of an Enzyme Linked Immunosorbent Assay for Direct Determination of Anticancer Drug Vitamin K3 in Serum, Journal of Health Science, 54 (2008) 508-511.

[7] W. Phrompittayarat, W. Putalun, H. Tanaka, S. Wittaya-Areekul, K. Jetiyanon, K. Ingkaninan, An enzyme-linked immunosorbant assay using polyclonal antibodies against bacopaside I, Analytica chimica acta, 584 (2007) 1-6.

[8] S. Sakamoto, W. Putalun, R. Tsuchihashi, S. Morimoto, J. Kinjo, H. Tanaka, Development of an enzyme-linked immunosorbent assay (ELISA) using highly-specific monoclonal antibodies against plumbagin, Analytica chimica acta, 607 (2008) 100-105.

[9] J.D. Thacker, E.S. Casale, C.M. Tucker, Immunoassays (ELISA) for Rapid, Quantitative Analysis in the Food-Processing Industry, Journal of Agricultural and Food Chemistry, 44 (1996) 2680-2685.

[10] M. Medina-Sánchez, S. Miserere, E. Morales-Narváez, A. Merkoçi, On-chip magneto-immunoassay for Alzheimer's biomarker electrochemical detection by using quantum dots as labels, Biosensors and Bioelectronics, 54 (2014) 279-284.

[11] T.Y.J. Ho, C.-C. Chan, K. Chan, Y.C. Wang, J.-T. Lin, C.-M. Chang, C.-S. Chen, Development of a novel bead-based 96-well filtration plate competitive immunoassay for the detection of Gentamycin, Biosensors and Bioelectronics, 49 (2013) 126-132.

[12] D. Jiang, P. Zhu, H. Jiang, J. Ji, X. Sun, W. Gu, G. Zhang, Fluorescent magnetic bead-based mast cell biosensor for electrochemical detection of allergens in foodstuffs, Biosensors and Bioelectronics, 70 (2015) 482-490.

[13] H. Zhang, L. Liu, X. Fu, Z. Zhu, Microfluidic beads-based immunosensor for sensitive detection of cancer biomarker proteins using multienzyme-nanoparticle amplification and quantum dotslabels, Biosensors and Bioelectronics, 42 (2013) 23-30.

[14] H.C. Tekin, M.A.M. Gijs, Ultrasensitive protein detection: a case for microfluidic magnetic bead-based assays, Lab on a chip, 13 (2013) 4711-4739.

[15] E. Katz, I. Willner, Integrated Nanoparticle–Biomolecule Hybrid Systems: Synthesis, Properties, and Applications, Angewandte Chemie International Edition, 43 (2004) 6042-6108.

[16] L.M. Liz-Marzán, Nanometals: Formation and color, Materials Today, 7 (2004) 26-31.

[17] R.A. Sperling, P. Rivera Gil, F. Zhang, M. Zanella, W.J. Parak, Biological applications of gold nanoparticles, Chemical Society Reviews, 37 (2008) 1896-1908.

[18] Y. Xiao, V. Pavlov, S. Levine, T. Niazov, G. Markovitch, I. Willner, Catalytic Growth of Au Nanoparticles by NAD(P)H Cofactors: Optical Sensors for NAD(P)+-Dependent Biocatalyzed Transformations, Angewandte Chemie International Edition, 43 (2004) 4519-4522.

[19] B. Shlyahovsky, E. Katz, Y. Xiao, V. Pavlov, I. Willner, Optical and Electrochemical Detection of NADH and of NAD+-Dependent Biocatalyzed Processes by the Catalytic Deposition of Copper on Gold Nanoparticles, Small, 1 (2005) 213-216.

[20] V. Pavlov, Enzymatic Growth of Metal and Semiconductor Nanoparticles in Bioanalysis, Particle & Particle Systems Characterization, 31 (2013) 36-45.

[21] L. Saa, A. Virel, J. Sanchez-Lopez, V. Pavlov, Analytical applications of enzymatic growth of quantum dots, Chemistry, 16 (2010) 6187-6192.

[22] L. Saa, J.M. Mato, V. Pavlov, Assays for methionine gamma-lyase and S-adenosyl-L-homocysteine hydrolase based on enzymatic formation of CdS quantum dots *in situ*, Analytical chemistry, 84 (2012) 8961-8965.

[23] L. Saa, V. Pavlov, Enzymatic growth of quantum dots: applications to probe glucose oxidase and horseradish peroxidase and sense glucose, Small, 8 (2012) 3449-3455.

[24] G. Garai-Ibabe, L. Saa, V. Pavlov, Enzymatic product-mediated stabilization of CdS quantum dots produced *in situ*: application for detection of reduced glutathione, NADPH, and glutathione reductase activity, Analytical chemistry, 85 (2013) 5542-5546.

[25] G. Garai-Ibabe, L. Saa, V. Pavlov, Thiocholine mediated stabilization of *in situ* produced CdS quantum dots: application for the detection of acetylcholinesterase activity and inhibitors, The Analyst, 139 (2014) 280-284.

[26] R. Grinyte, L. Saa, G. Garai-Ibabe, V. Pavlov, Biocatalytic etching of semiconductor cadmium sulfide nanoparticles as a new platform for the optical detection of analytes, Chemical Communications, 51 (2015) 17152-17155.

[27] N. Malashikhina, G. Garai-Ibabe, V. Pavlov, Unconventional application of conventional enzymatic substrate: first fluorogenic immunoassay based on enzymatic formation of quantum dots, Analytical chemistry, 85 (2013) 6866-6870.

[28] X.-Y. Dong, X.-N. Mi, W.-W. Zhao, J.-J. Xu, H.-Y. Chen, CdS Nanoparticles functionalized colloidal carbon particles: Preparation, characterization and application for electrochemical detection of thrombin, Biosensors and Bioelectronics, 26 (2011) 3654-3659.

[29] A. Sharma, V.K. Rao, D.V. Kamboj, R. Gaur, S. Upadhyay, M. Shaik, Relative efficiency of zinc sulfide (ZnS) quantum dots (QDs) based electrochemical and fluorescence immunoassay for the detection of Staphylococcal enterotoxin B (SEB), Biotechnology Reports, 6 (2015) 129-136.

[30] F.-Y. Kong, B.-Y. Xu, J.-J. Xu, H.-Y. Chen, Simultaneous electrochemical immunoassay using CdS/DNA and PbS/DNA nanochains as labels, Biosensors and Bioelectronics, 39 (2013) 177-182.

[31] A. Sharma, V.K. Rao, D.V. Kamboj, S. Upadhyay, M. Shaik, A.R. Shrivastava, R. Jain, Sensitive detection of staphylococcal enterotoxin B (SEB) using quantum dots by various methods with special emphasis on an electrochemical immunoassay approach, RSC Advances, 4 (2014) 34089-34095.

[32] H. Monton, C. Parolo, A. Aranda-Ramos, A. Merkoci, C. Nogues, Annexin-V/quantum dot probes for multimodal apoptosis monitoring in living cells: improving bioanalysis using electrochemistry, Nanoscale, 7 (2015) 4097-4104.

[33] S.K. Haram, B.M. Quinn, A.J. Bard, Electrochemistry of CdS Nanoparticles: A Correlation between Optical and Electrochemical Band Gaps, Journal of the American Chemical Society, 123 (2001) 8860-8861.

[34] Y. Bae, N. Myung, A.J. Bard, Electrochemistry and Electrogenerated Chemiluminescence of CdTe Nanoparticles, Nano letters, 4 (2004) 1153-1161.

[35] A. Chen, B. Shah, Electrochemical sensing and biosensing based on square wave voltammetry, Analytical Methods, 5 (2013) 2158-2173.

[36] H. Huang, J.-J. Zhu, The electrochemical applications of quantum dots, The Analyst, 138 (2013) 5855-5865.

[37] A. Arben Merkoçi and Luiz Humberto Marcolino-Junior and Sergio Marín and Orlando Fatibello-Filho and Salvador, Detection of cadmium sulphide nanoparticles by using screen-printed electrodes and a handheld device, Nanotechnology, 18 (2007) 035502.

[38] V. Escamilla-Gómez, D. Hernández-Santos, M.B. González-García, J.M. Pingarrón-Carrazón, A. Costa-García, Simultaneous detection of free and total prostate specific antigen on a screen-printed electrochemical dual sensor, Biosensors and Bioelectronics, 24 (2009) 2678-2683.

[39] J.M. McCord, I. Fridovich, Superoxide dismutase. An enzymic function for erythrocuprein (hemocuprein), The Journal of biological chemistry, 244 (1969) 6049-6055.

[40] C.J. Weydert, T.A. Waugh, J.M. Ritchie, K.S. Iyer, J.L. Smith, L. Li, D.R. Spitz, L.W. Oberley, Overexpression of manganese or copper-zinc superoxide dismutase inhibits breast cancer growth, Free radical biology & medicine, 41 (2006) 226-237.

[41] N. Li, T.D. Oberley, L.W. Oberley, W. Zhong, Overexpression of manganese superoxide dismutase in DU145 human prostate carcinoma cells has multiple effects on cell phenotype, The Prostate, 35 (1998) 221-233.

[42] Y. Zhao, Y. Xue, T.D. Oberley, K.K. Kiningham, S.M. Lin, H.C. Yen, H. Majima, J. Hines, D. St Clair, Overexpression of manganese superoxide dismutase suppresses tumor formation by modulation of activator protein-1 signaling in a multistage skin carcinogenesis model, Cancer research, 61 (2001) 6082-6088.

[43] J.J. Cullen, C. Weydert, M.M. Hinkhouse, J. Ritchie, F.E. Domann, D. Spitz, L.W. Oberley, The role of manganese superoxide dismutase in the growth of pancreatic adenocarcinoma, Cancer research, 63 (2003) 1297-1303.

[44] M. Noh, T. Kim, H. Lee, C.-K. Kim, S.-W. Joo, K. Lee, Fluorescence quenching caused by aggregation of water-soluble CdSe quantum dots, Colloids and Surfaces A: Physicochemical and Engineering Aspects, 359 (2010) 39-44.

[45] T. Kang, K. Um, J. Park, H. Chang, D.C. Lee, C.-K. Kim, K. Lee, Minimizing the fluorescence quenching caused by uncontrolled aggregation of CdSe/CdS core/shell

quantum dots for biosensor applications, Sensors and Actuators B: Chemical, 222 (2016) 871-878.
[46] D. Moscone, M. Mascini, Determination of superoxide dismutase activity with an electrochemical oxygen probe, Analytica chimica acta, 211 (1988) 195-204.
[47] D. Ivansson, K. Bayer, C.-F. Mandenius, Quantitation of intracellular recombinant human superoxide dismutase using surface plasmon resonance, Analytica chimica acta, 456 (2002) 193-200.
[48] I. Vostiar, J. Tkac, C.-F. Mandenius, Intracellular monitoring of superoxide dismutase expression in an Escherichia coli fed-batch cultivation using on-line disruption with at-line surface plasmon resonance detection, Analytical Biochemistry, 342 (2005) 152-159.
[49] P. Santharaman, M. Das, S.K. Singh, N.K. Sethy, K. Bhargava, J.C. Claussen, C. Karunakaran, Label-free electrochemical immunosensor for the rapid and sensitive detection of the oxidative stress marker superoxide dismutase 1 at the point-of-care, Sensors and Actuators B: Chemical, 236 (2016) 546-553.

5

Modulation of growth of cysteine-capped cadmium sulfide quantum dots with enzymatically produced hydrogen peroxide

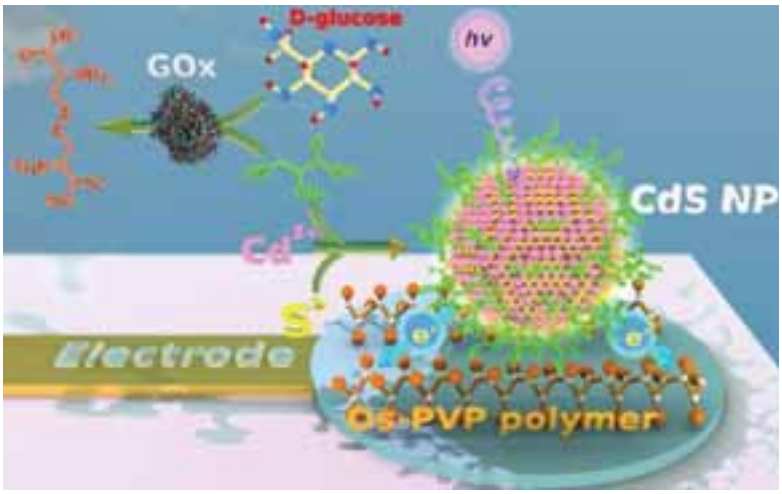

We demonstrate that oxidation of cysteine (CSH) by hydrogen peroxide (H_2O_2) causes the decrease in the rate of the formation of CSH-capped CdS QDs from Cd^{2+} and S^{2-} ions. For the first time, we combined the oxidation of CSH with biocatalytic oxidation of D-glucose catalyzed by glucose oxidase (GOx) leading to the buildup of hydrogen peroxide in the reaction mixture. Enzymatically modulated growth of CdS QDs in situ was monitored by two techniques: fluorescence spectroscopy and photoelectrochemical (PEC) analysis. This system allowed quantification of GOx and glucose in human serum.

The work presented in this chapter was previously published: Ruta Grinyte, Javier Barroso, Laura Saa, Valeri Pavlov; Nano Research., 2016 Nov DOI:10.1007/s12274-016-1378-1.

5.1. Introduction

The unstoppable development of nanotechnology during the last decades has allowed for the fabrication of new materials and design of novel biosensing methods. One of the valuable tools employed in biosensing are inorganic nanoparticles (NPs). NPs of noble metals like gold and silver exhibit high extinction coefficients due to surface plasma resonance [1]. The optical properties of metal NPs depend on their shape and size [2]. Traditionally metal NPs were used in bioanalysis as labels in affinity assays [3-5]; enhancers of raman scattering [6-9]; quenchers of fluorescence[10, 11] and scaffolds for assembling of biorecognition elements [12, 13]. Metal NPs can be produced *in situ* with biocatalytic processes catalyzed by different enzymes, for instance, glucose oxidase (GOx), alkaline phosphatase (ALP), and alcohol dehydrogenase (AlcDH) [14-16]. Metal NPs generated *in situ* by enzymes usually are not fluorescence and hardly demonstrate photocatalitic activities. This feature limits their employment in bioassays.

NPs composed of semiconductor materials demonstrate quantum effects and can be photoexcited emitting photons during the relaxation process. Therefore, those particles are referred to in the literature as quantum dots (QDs). They find broad application in nanotechnology, diagnostics and therapy [1, 17-20]. The energy of the emitted photons and consequently the intensity and the wavelength of the observed fluorescence depend on the nature and the shape of QDs, the environment and capping agents (stabilizers).

Cysteine (CSH), which carries thiol functional group for binding at CdS interface and hydrophilic amino and carboxylic groups, is an efficient stabilizer of CdS NPs [21, 22]. On the other hand, CSH can be easily oxidized to form a dimer containing disulfide bridge between two CSHs, known as cystine (CSSC). Oxidation of CSH with hydrogen peroxide (H_2O_2) in aqueous buffers can be described by the two-step nucleophilic reaction model [23-25]. This process is initiated by rate-determining nucleophilic attack of thiolate anion (CS^-) on unionized H_2O_2 to generate sulfenic acid (CSOH) as an intermediate product (Equation 1). The latter interacts with CS^- ions to yield CSSC as shown in equation 2.

$$CS^- + H_2O_2 \rightarrow CSOH + HO^- \quad (1)$$

$$CSOH + CS^- \rightarrow CSSC + HO^- \quad (2)$$

For the first time, we combined this reaction with biocatalytic oxidation of D-glucose (glucose) catalyzed by GOx leading to the buildup of H_2O_2 in the reaction mixture. GOx is the protein composed of two identical 80 kDa subunits containing two bound FAD coenzymes. Chemical, pharmaceutical, food, beverage, clinical chemistry, biotechnology and other industries broadly employ GOx [26]. The determination of GOx enzymatic activity is quite important in industry. The standard assay for GOx activity relies on the reaction mixture containing the additional enzyme horseradish peroxidase (HRP) that is used for detection of H_2O_2 produced by GOx (enzymatic assay of GOx from Sigma-Aldrich).

In the present work we demonstrate that the oxidation of the stabilizing agent CSH by H_2O_2 produced by GOx causes the decrease in the rate of the formation of CSH-capped CdS QDs from Cd^{2+} and S^{2-} ions. This process allows relating the enzymatic activity of GOx and glucose concentration with amount of CdS QDs produced *in situ* which defines the emission spectrum of the assay mixture followed by the fluorescence spectroscopy, the extremely sensitive laboratory technique for detection of the fluorescence readout signal.

We also used the powerful alternative to fluorometry, the photoelectrochemical (PEC) analysis [27, 28]. PEC sensors are becoming a promising low cost approach for the detection of light responsive chemical and biochemical molecules [29-31]. The process of PEC detection converts luminous energy into electrochemical energy at the surface of the electrode, generating electrical readout signal. The photocurrent intensity is defined by the characteristics of excitation light, applied potential and the rate of the electron transfer between the electron surface and QDs. A number of electrocatalysts have been applied to facilitate the electron transfer to the electrode surface in PEC analysis, such as microporous carbon including carbon nanotubes and grapheme [32], small organic molecules like methyl viologen immobilized on polymeric nafion matrix [33], semiconductor metal oxides like TiO_2 [34]. Usually electrocatalysts were immobilized on expensive gold and indium tin oxide (ITO) electrodes using

anchoring thiol and silane groups [35]. Screen-printed carbon electrodes (SPCE) are significantly cheaper but their modification with electrocatalysts is quite difficult due to the absence of anchoring functional groups on the surface of the carbon material of the working electrode. In the present work we employ the complex of poly(vinylpyridine) with Os(bipyridine)$_2$Cl$_2$ (Os-PVP complex) as the electrocatalyst to facilitate the electron exchange. Previously, the redox polymer of this structure was applied to wire redox enzymes, for instance, glucose-6-phosphate dehydrogenase [36] and HRP [37].

In this article we present a new strategy for detection of enzymatic activities using the fluorescent spectroscopy and PEC. We offer a quite universal bioanalytical platform relying on the enzymatically modulated growth of CdS QDs *in situ* followed by two techniques which finally will be applicable to the range of detection systems spanning from optical laboratory equipment to low power mobile fast point of care (POC) analytical systems.

5.2. Materials and methods

5.2.1. Materials

Sodium sulfide (Na_2S), cadmium nitrate $Cd(NO_3)_2$, glucose oxidase type VII from Aspergillus niger and other chemicals were purchased from Sigma Aldrich. Anhydrous ß-D-glucose and hydrogen peroxide (30% v/v) were purchased from Panreac.

5.2.2. Methods

5.2.2.1. Characterisation

Spectroscopy. Transmission electron miscroscopy (TEM) images were collected with a JEOL JEM 2100F operating at 120 kV.

Optical methods. Fluorescence measurements were performed on a Varioskan Flash microplate reader (Thermo Scientific) using black microwell plates at room temperature. The system was controlled by SkanIt Software 2.4.3. RE for Varioskan Flash.

Photoelectrochemistry. All electrochemical experiments were conducted in the Autolab Electrochemical Workstation (Model: PGSTAT302N, Metrohm Autolab, The Netherlands) equipped with NOVA 1.10 software. Disposable screen-printed carbon electrodes (SCPEs) were purchased from DropSens (model DRP-110, 4 mm diameter). Electrical contact to workstation was done with a special boxed connector supplied by DropSens. The illumination source was a compact UV illuminator (UVP, Analytik Jena AG). All PECs were performed at room temperature. All the potentials reported in our work were against Ag/AgCl. Unless mentioned otherwise, all experimental results presented here are averaged from three independent measurements (n = 3).

5.2.2.2. CdS QD-mediated determination of H_2O_2

Different concentrations of H_2O_2 were incubated with 0.075 mM of CSH in citrate-phosphate buffer (pH 7.5) for 40 min at room temperature. After that, Na_2S (10 µL , 1 mM) and $Cd(NO_3)_2$ (2.5 µL , 50 mM) were added to the samples (87.5 µL). The emission spectra of the resulting suspensions were recorded after 5 min at λ_{exc} = 300 nm.

5.2.2.3. GOx assay

Varying amounts of glucose were incubated with different amounts of GOx in citrate-phosphate buffer (pH 7.5) for 40 min at room temperature, in the presence of CSH (0.075 mM). After that, Na_2S (10 µL, 1 mM) and $Cd(NO_3)_2$ (2.5 µL, 50 mM) were added to the samples (87.5 µL). The emission spectra of the resulting CdS QDs were recorded after 5 min at λ_{exc} = 300 nm.

Quantification of glucose in human serum. Quantification of glucose in human serum was performed by the standard edition method. Samples of pooled human serum (Sigma-Aldrich) were spiked with known different concentrations of glucose and the glucose concentration of the mixtures was determined. The dilution factor of plasma in the assay was 1:100.

5.2.2.4. Photoelectrochemical detection

SPCEs were initially pretreated electrochemically by cyclic voltammetry (CV) at a potential range of 0 – 0.8 V in citrate-phosphate buffer (pH 7.5). Subsequently, a 40 µL

drop of Os-PVP complex (1.375 mg mL^{-1}) was placed on the SPEs and deposited by CV scanning (2 cycles, 50 mV s^{-1}). Later, SPCEs were rinsed out with ultrapure water and dried under argon atmosphere. Finally, a 40 µL of samples were dropped on the SPCE and PEC measurements were carried out with UV illuminator at 365 nm and a controlled potential of 0.3 V. The dependence of photocurrent on time was measured at 5 minutes during 10 seconds. 1-thioglycerol (TG) was added to the samples to amplify the signal.

5.3. Results and Discussion

5.3.1. CdS QD-mediated determination of H_2O_2 and optimization of the system

The ability of CSH to stabilize CdS QDs was studied. Cadmium nitrate ($Cd(NO_3)_2$) was interacted with sodium sulfide (Na_2S), in citrate phosphate buffer (pH 7.5) in the presence of CSH or CSSC, which is the oxidized form of CSH. The formation of fluorescent CdS QDs was followed by fluorescence spectroscopy. As one can see in Figure 5.1 reaction mixture containing CSH, Cd^{2+} and S^{2-} ions demonstrated high emission peak (curve a). No significant fluorescence was observed in the presence of CSSC (curve b) or without any CSH and CSSC (curve c). This finding proves that CSSC does not stabilize fluorescent QDs so efficiently as CSH (Figure 5.1, curve b).

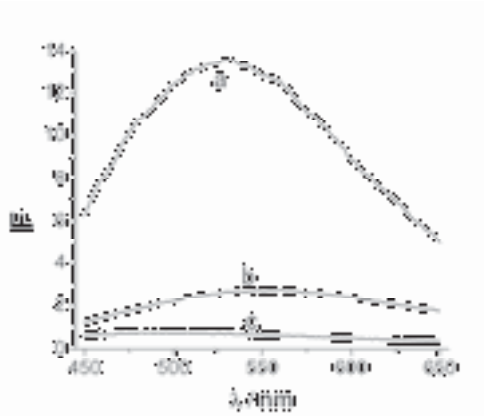

Figure 5.1. Fluorescence emission spectra of the system containing (a) CSH (0.5 mM), Na_2S (0.1 mM), $Cd(NO_3)_2$ (1.25 mM); (b) CSSC (0.5 mM), Na_2S (0.1 mM), $Cd(NO_3)_2$ (1.25 mM); (c) only Na_2S (0.1 mM) and $Cd(NO_3)_2$ (1.25 mM)

In order to increase the yield of CSH-stabilized CdS NPs the effect of CSH concentration on fluorescence spectrum of the reaction mixtures containing Cd^{2+} and S^{2-} ions was investigated. According to Figure 5.2 optimum concentration of CSH was 0.075 mM, which was used in all subsequent experiments.

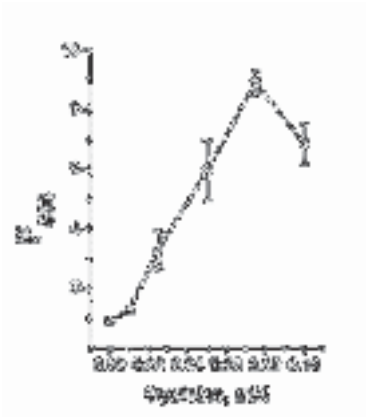

Figure 5.2 Effect of cysteine concentration on fluorescence intensity in the reaction mixture composed of Na_2S 0.1 mM and $Cd(NO_3)_2$ 1.25 mM. Incubation time 5 min, λ_{exc} = 300 nm.

Thus, CSH is able to stabilize CdS NPs formed *in situ* from S^{2-} and Cd^{2+} ions in aqueous solutions within the incubation time of 5 min at room temperature (Scheme 5.1). The previously published procedures for the synthesis of CSH-stabilized CdS QDs required much longer incubation times (over 1 hour) and very harsh experimental conditions like high temperatures (over 80 ^{o}C) [22] or irradiation with γ-rays [21]. The process of CdS QDs formation under physiological conditions, optimized by us, was very rapid and compatible with natural biochemical pathways leading to oxidation of CSH for modulation of QDs' growth.

Scheme 5.1. Modulation of CdS QDs growth with cysteine.

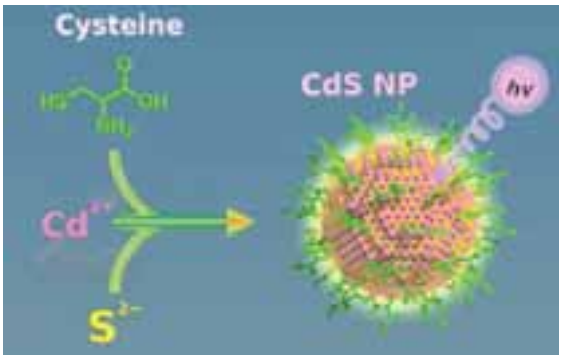

It was found out that the treatment of CSH with varying concentrations of H_2O_2 leads to the decrease in the rate of formation of CdS NPs due to oxidation of CSH into CSSC. As one can see in Figure 5.3, the decrease in the fluorescence signal was directly related to the quantity of the H_2O_2 in the reaction mixture. Calibration curve shown in Figure 5.4 inset demonstrated linearity from 0.0 to 0.045 mM and saturation starting from 0.15 mM H_2O_2 concentration. In accordance with the calibration curve the limit of H_2O_2 detection (LOD) was calculated to be 12.6 µM by UPAC definition [38]. This LOD is 4 times lower than that of the reported most relevant fluorogenic assay for detection of H_2O_2 using the enzymatic growth of CdS NPs [39]. It is important to note that after addition of H_2O_2 (0.1 mM) to the pre-prepared CdS NPs stabilized with CSH no changes in the emission spectra of CdS NPs were noticed (Figure A5.1, curve b in the appendix chapter 5). So, the decrease in the fluorescence was not caused by the possible quenching effect of H_2O_2.

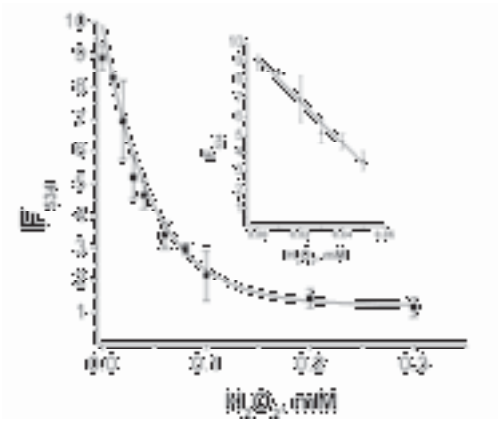

Figure 5.3. Calibration curve of H_2O_2 obtained using the intensity if the emission peak at 534 nm (F_{534}) The system containing of CSH (0.075 mM), Na_2S (0.1 mM) and $Cd(NO_3)_2$ (1.25 mM), and different concentrations of H_2O_2: a) 0 mM; b) 0.01 mM; c) 0.02 mM; d) 0.03 mM; e) 0.04 mM; f) 0.06 mM; g) 0.08 mM; h) 0.1 mM; i) 0.2 mM; j) 0.3 mM. Inset: linear part of the calibration plot.

Transmission electron microscopy (TEM) was applied to confirm the existence of CSH stabilized CdS QDs in the reaction mixture at three different concentration of H_2O_2 (Figure 5.4). Analysis of the TEM images of CdS QDs revealed that the medium diameter of the produced NPs was 2.03 ± 0.32 nm in the absence of H_2O_2. When the concentration of H_2O_2 was 0.03 nm the observed CdS QDs exhibited the medium

diameter of 1.29 ± 0.26 nm. In the presence of saturating concentration of H_2O_2 equal to 0.3 mM the absence of CdS QDs were confirmed by TEM.

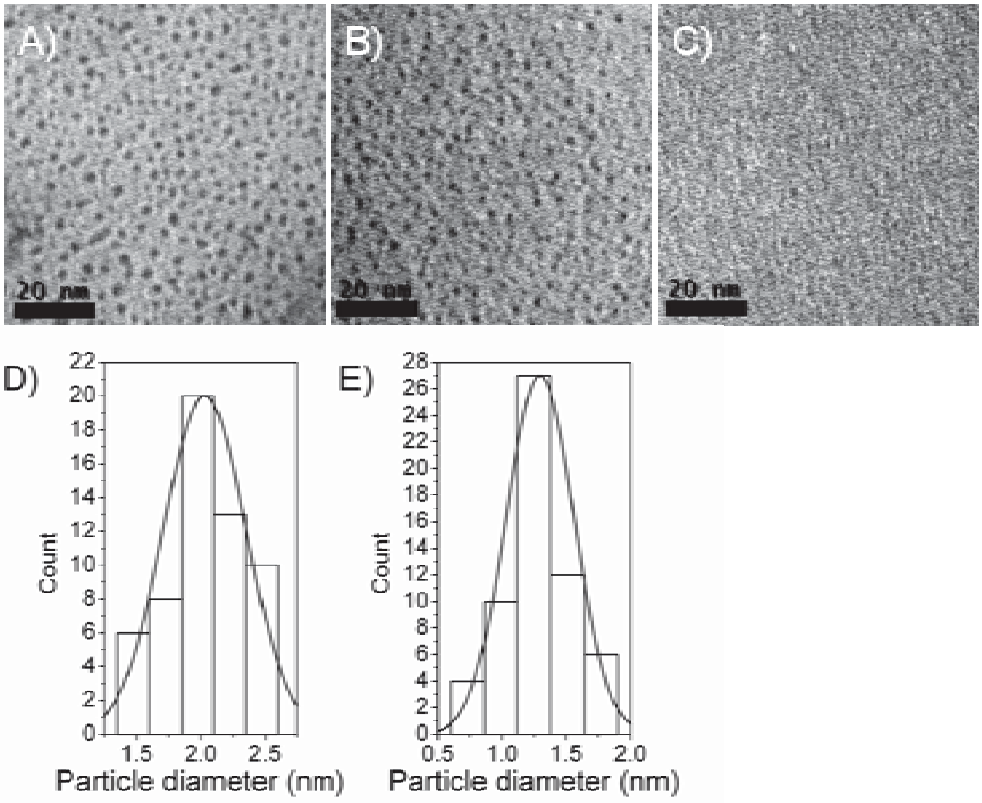

Figure 5.4. TEM images of cysteine stabilized CdS QDs in the presence of (A) 0 mM of H_2O_2 (B) 0.03 mM of H_2O_2 (C) 0.3 mM of H_2O_2; Size distribution of cysteine stabilized CdS QDs in the presence of (D) 0 mM of H_2O_2 (E) 0.03 mM of H_2O_2.

5.3.2. Glucose oxidase assay

The above mentioned fluorogenic method for H_2O_2 detection can be readily combined with enzymatic reactions resulting in the formation of H_2O_2, for example oxidation of enzymatic substrates by oxidases. The operation principle of the fluorogenic assay for evaluation of enzymatic activity of GOx is represented in Scheme 5.2.

Oxidation of glucose with oxygen catalyzed by GOx ends up in the final products D-glucono 1,5-lactone and H_2O_2. Enzymatically produced H_2O_2 is able to oxidize CSH preventing stabilization and rapid formation of CdS QDs. Figure 5.5 shows the emission spectra of CdS QDs formed in the presence of the fixed 1 mM glucose concentration and different concentrations of GOx. As one can see in Figure 5.5, the increase in the

Scheme 5.2. Fluorometric assay for glucose oxidase activity.

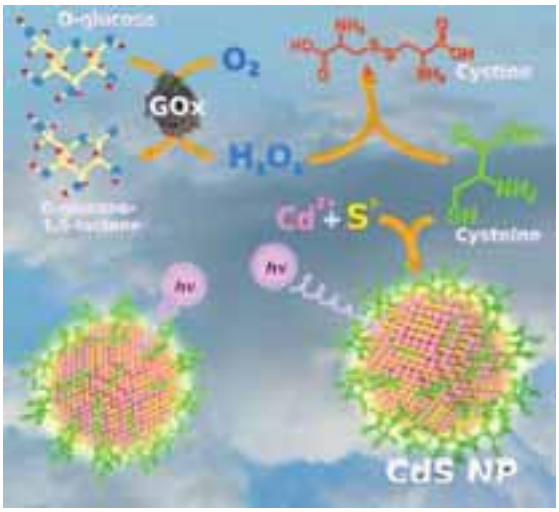

amount of GOx leads to the decrease in the fluorescence signal as expected for this biocatalytic reaction. We calculated that the LOD of the system was 0.1 µg of GOx per mL. This assay showed 5 times better sensitivity that that of the previous published CdS-based fluorogenic assay for GOx [39]. Moreover, this fluorogenic GOx assay is much more sensitive than the colorimetric test for GOx based on CdS NPs [40].

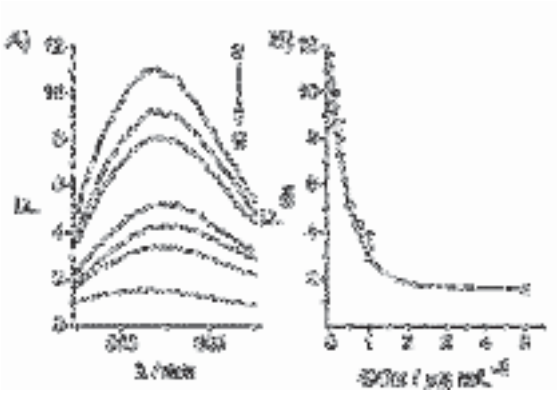

Figure 5.5. (A) Fluorescence emission spectra of the system containing glucose (1 mM), CSH (0.075 mM), Na_2S (0.1 mM) and $Cd(NO_3)_2$ (1.25 mM) and different concentrations of GOx: a) 0 µg mL^{-1}; b) 0.1 µg mL^{-1}; c) 0.25 µg mL^{-1}; d) 0.5 µg mL^{-1}; e) 0.75 µg mL^{-1}; f) 1 µg mL^{-1}; g) 5 µg mL^{-1}; (B) Calibration curve of GOx obtained using, F_{534}.

We also studied the influence of varying glucose concentrations on the response of our flourogenic assay. Figure 5.6 shows emission spectra of assay mixtures containing increasing concentrations of glucose and fixed amounts of GOx, CSH, $Cd(NO_3)_2$ and Na_2S. On the basis of the calibration curve in Figure 5.6B the LOD of

glucose was calculated to be 0.1 mM by UPAC definition [38]. According to the calibration curve (Figure 5.6B) the response to the increasing amounts of glucose was linear within the range from 0 mM to 0.3 mM. Given the fact that the normal level of glucose in human serum published by World Health Organization is < 6.1 mM [41] our assay is even applicable to quantification of glucose in medical laboratories. Therefore, we applied our assay to detection of glucose in human serum employing the standard addition method. In this method several serum sample of the same volume were distributed between different 0.5 mL tubes. The standard known varying amounts of glucose were injected into the samples with human serum. The fluorescence of the samples was measured. The experimental data were plotted with the concentration standards showed in the x-axis and the obtained fluorescence signals in the y-axis of the plot.

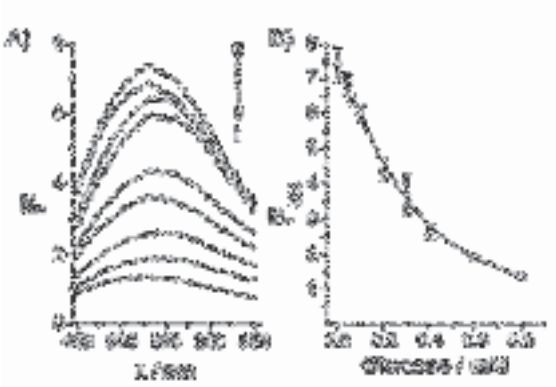

Figure 5.6. (A) Fluorescence emission spectra of the system containing GOx (5 μg mL^{-1}), CSH (0.075 mM), Na_2S (0.1 mM) and $Cd(NO_3)_2$ (1.25 mM) and different concentrations of glucose: a) 0 mM; b) 0.04 mM; c) 0.06 mM; d) 0.1 mM; e) 0.2 mM; f) 0.3 mM; g) 0.4 mM; h) 0.6 mM; i) 0.8 mM; (B) Calibration curve of glucose obtained using, F_{534}.

The linear regression analysis was performed to calculate the position of the intercept of the calibration line with x-axis, which showed the concentration of glucose in human serum samples (Figure 5.7). Taking into consideration all dilutions of the samples, the found concentration of glucose was 6.01 mM. It lies within the limits of normal level of glucose in human serum [41].

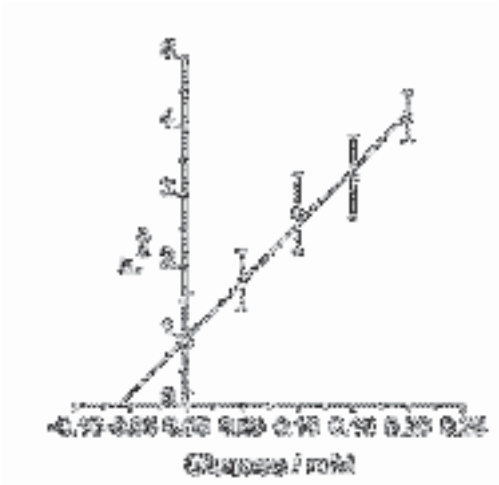

Figure 5.7. Quantification of glucose in human serum with the method of standard addition. The system contained GOx (5 μg mL^{-1}), CSH (0.075 mM), Na_2S (0.1 mM) and $Cd(NO_3)_2$ (1.25 mM) and various known amounts of added glucose standards.

5.3.3. Photoelectrochemical detection of glucose

The developed QDs-based PEC system is depicted in Scheme 5.3. GOx catalyzes oxidation of glucose with oxygen to D-glucono-1,5-lactone and H_2O_2. The former decreases the concentration of CSH modulating the growth of CdS QDs *in situ*. When the assay solution containing produced CdS QDs is placed over the surface of a SPCE and irradiated with UV light, photons are absorbed by CdS QDs and excite electrons from the occupied valence band (VB) to the empty conduction band (CB) forming electron-hole pairs. CB electrons are transferred from surface of CdS QDs to the electroconductive polymer immobilized on the surface of the SPCE when the positive potential is applied to generate anodic photocurrent. This polymeric electrocatalyst is composed of poly(vinylpyridine) complexed with $Os(bipyridine)_2Cl_2$ (Os–PVP polymer depicted in Figure A5.2, appendix chapter 5). Holes from VB of CdS QDs are neutralized by the electron donor 1-thioglycerol (TG) which is oxidized to bis(1-thio-2,3 propanediol) at the surface of QDs.

Scheme 5.3. Electrochemical detection of CdS QDs “wired” by Os-PVP complex to the surface of a SPCE.

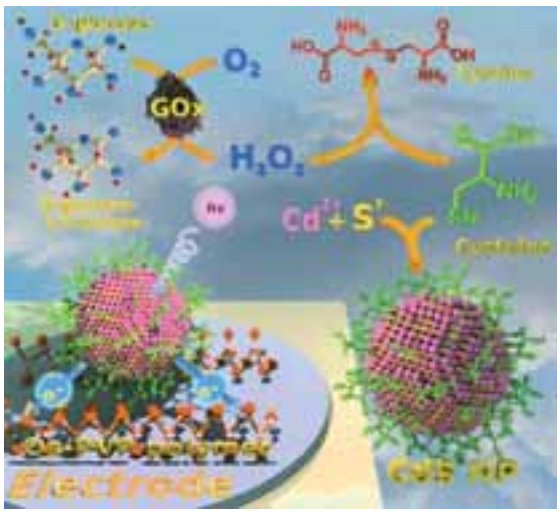

In order to photosensitize the surface of SPCE, Os-PVP complex was deposited by cyclic voltammetry (CV) during two cycles in the range from 0 to 0.6 V. After the electrochemical deposition of Os-PVP complex the electrode was washed with water and CV was performed to evaluate the surface coverage of osmium moieties (Table A5.1, appendix chapter 5). Two redox waves were revealed, confirming that the redox process involves only the central osmium atom (Figure A5.3, appendix chapter 5). Furthermore, the possible interference from Os-PVP complex with the photocurrent background was assessed at different potentials. The effect of applied potential on the anodic photocurrent is shown in Figure 5.4 (A) appendix chapter 5. The working potential of 0.3 V *vs.* Ag/AgCl was selected to avoid nonspecific oxidation of TG at the electrode surface. It should be taken into account that the best ratio of photocurrents registered in the presence and in the absence of CdS QDs (I_{QDs}/I_{Os}) was also achieved at 0.3V *vs.* Ag/AgCl (data not shown)with the signal-to-noise ratio of 3 (S/N = 3).

According to the plot representing the effect of different excitation wavelengths on the fluorescence signal (Figure A5.5 appendix chapter 5), the intensity of the emission peak registered using the excitation wavelength of 365 nm is still higher than 80 % of the maximum emission peak registered using the excitation wavelength of 300 nm. The standard UV illuminator with the maximum output at 365 nm is the most available and inexpensive source of the intense light with the emission peak close to 300 nm therefore it was employed for the photoelectrochemical measurements. All

photocurrent responses are presented with the background subtracted at this potential. To estimate the importance of photosensitizing the electrode surface with Os-PVP polymer the control experiment was performed in which non modified SPCE was used for the detection of anodic photocurrent in the presence of CdS QDs and TG in the assay mixture. No significant photocurrent was observed in the absence of Os-PVP polymer on the electrode surface (Figure 5.6 appendix chapter 5). Thus, Os-PVP polymer is the crucial electrocatalyst mediating the electron transfer of CB electrons from CdS QDs to the SPCE. The photocatalytic oxidation of TG at saturating concentration of 20 mM (Figure A5.7 appendix chapter 5), which still does not favor its nonspecific electrochemical oxidation, provides the electrons transferred to the surface of the photosensitized SPCEs during quantification of CdS QDs. In the absence of CdS QDs, no significant photocurrent was observed (Figure A5.4B curve 2).

The influence of the different amounts of glucose on photocurrent is shown in Figure 5.8. The decrease in photocurrent is directly related to the increase in the concentration of glucose added to the system. The response shows linearity from 0 to 0.2 mM and saturation starting from 0.4 mM glucose concentration. The LOD was found to be 20 µM (3σ). The average relative standard deviation (RSD) calculated from the glucose calibration plot (obtained using at least three independent SPCEs modified by Os-PVP) was 8%.

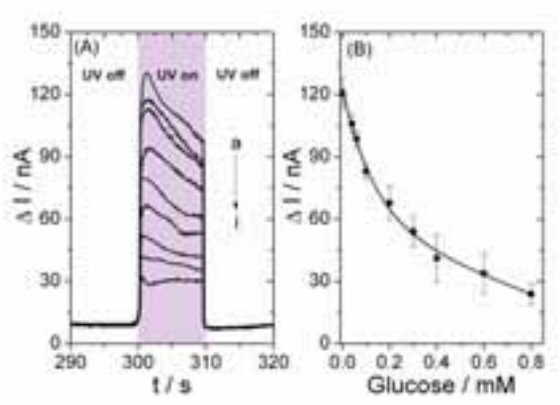

Figure 5.8. (A) Photocurrent responses of CdS QDs in the system containing GOx (5 µg mL^{-1}), CSH (0.075 mM), TG (20 mM), Na_2S (0.1 mM) and $Cd(NO_3)_2$ (1.25 mM) and different concentrations of glucose: a) 0 mM; b) 0.04 mM; c) 0.06 mM; d) 0.1 mM; e) 0.2 mM; f) 0.3 mM; g) 0.4 mM; h) 0.6 mM; i) 0.8 mM; (B) Calibration curve of GOx obtained at 0.3 V (vs. Ag/AgCl) and 365 nm excitation light.

We also evaluated the response of the system varying the concentration of GOx in the reaction mixture in the presence of 1 mM glucose (Figure 5.9). According to the calibration curve the LOD was equal to 0.05 μg mL^{-1} (RSD = 4.6%). The control experiments performed in the presence and absence of GOx and glucose showed no significant variation of photocurrent (data no shown).

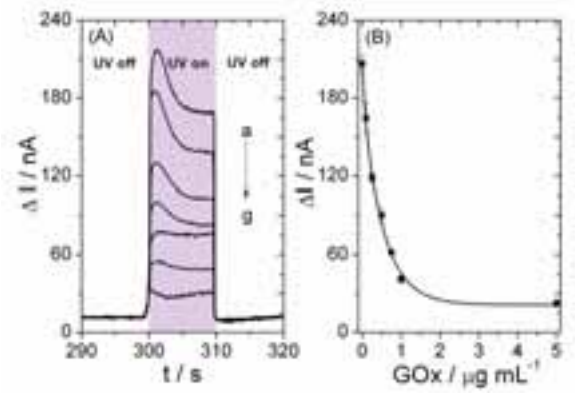

Figure 5.9. (A) Photocurrent responses of the system containing glucose (1 mM), cysteine (0.075 mM), 1-thioglycerol (TG) 20 mM, Na_2S (0.1 mM) and $Cd(NO_3)_2$ (1.25 mM) and different concentrations of GOx: a) 0 μg mL^{-1}; b) 0.1 μg mL^{-1}; c) 0.25 μg mL^{-1}; d) 0.5 μg mL^{-1}; e) 0.75 μg mL^{-1}; f) 1 μg mL^{-1}; g) 5 μg mL^{-1}; (B) Calibration curve of GOx obtained at 0.3 V (vs. Ag/AgCl) and 365 nm excitation light.

Comparing with the performance of the fluorogenic method, the PEC system is 5 times more sensitive. Furthermore, the obtained result is also much better than previously published works based on electrochemical detection of glucose, which show worse LODs [42-44].

The standard chromogenic assay for detection of GOx is based on the method previously described in the literature. [45] The chemical interactions employed in the standard commercially available assays:

$$\beta\text{-D-Glucose} + O_2 + H_2O \xrightarrow{GOx} \text{D-Glucono-1,5 – Lactone} + H_2O_2$$

$$H_2O_2 + \text{o-Dianisidine(reduced)} \xrightarrow{HRP} \text{o-Dianisidine(oxidized)}$$

As one can see, this method requires the additional enzyme horseradish peroxidase and very cancerogenic chromogenic dye o-Dianisidine to detect hydrogen peroxide produced by GOx. The commercially available fluorometric kits for detection of GOx (Sigma Aldrich, AbCam) employ fluorogenic substrate of peroxidase 10-acetil-3,7-dihidroxifenoxacina, (AmplexRed®, AbRed®) instead of o-Dianisidine to follow the

formation of hydrogen peroxide and require expensive fluorimeters. The dependence of GOx assay on the second enzyme makes the assay prone to errors due to inevitable deactivation of peroxidase even if the components of kits are stored at low temperature. The photoelectrochemical assay for detection of GOx activity developed by us does require neither expensive fluorogenic dyes nor fluorimeters nor the second enzyme.

Finally, the developed sensor was evaluated by the determination of glucose in human serum samples employing the standard addition method. The real samples were not pretreated. As shown in Figure A5.6B curve 3, electrodes photosensitized with Os-PVP polymer demonstrate a negligible background photocurrent in the presence of human serum samples (around 10 nA) at 0.3V vs. Ag/AgCl. This background current was subtracted from the data of the plot. The known varying amounts of glucose were injected into the samples with human serum. Photocurrents of all samples were measured. The experimental data were plotted with the concentration standards showed in the x-axis and the observed photocurrents in the y-axis of the plot. The intercept of the calibration line with x-axis showing the concentration of glucose in human serum samples was calculated by linear regression (Figure 5.10). The found concentration of glucose was 5.06 mM. As reported previously,[41] the normal concentration of glucose in human blood is around 5-7 mM. Thus, our device displayed an excellent linear range and RSD values within 10%, showing good sensitivity for detecting glucose.

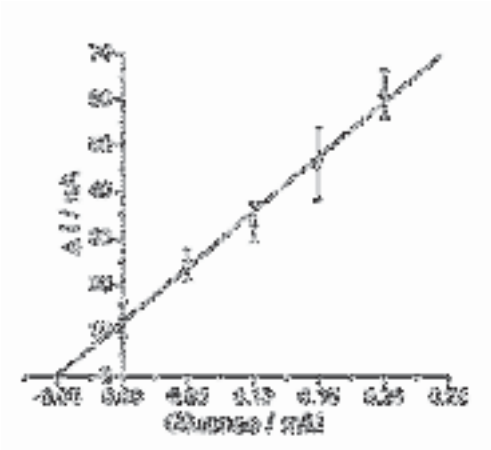

Figure 5.10. PEC quantification of glucose in human serum with the method of standard addition. The system contained GOx (5 μg mL^{-1}), CSH (0.075 mM), TG (20 mM), Na_2S (0.1 mM) and $Cd(NO_3)_2$ (1.25 mM).

5.4. Conclusion

The employment of cysteine (CSH) as a capping agent allows for rapid formation of fluorescent CdS QDs in aqueous solutions at room temperature. Hydrogen peroxide (H_2O_2), produced in the course of enzymatic oxidation of D-glucose by glucose oxidase (GOx), oxidizes CSH to cystine (CSSC) modulating the growth of QDs. This biocatalytic process can be applied to the development of simple sensitive fluorometric and photoelectrochemical (PEC) assays for GOx activity in buffered solutions and D-glucose in real samples of human serum using the photocatalytic activity of the resulting QDs. The biocatalytic processes ending up in formation of H_2O_2 are quite abundant in nature. Therefore, we believe that our two model systems potentially can find broad application to quantify enzymatic activities of many other enzymes generating or consuming H_2O_2.

5.5. References

[1] E. Katz, I. Willner, Integrated Nanoparticle–Biomolecule Hybrid Systems: Synthesis, Properties, and Applications, Angewandte Chemie, 43 (2004) 6042-6108.

[2] L.M. Liz-Marzán, Nanometals: Formation and color, Mater. Today, 7 (2004) 26-31.

[3] H. Li, D. Xu, Silver nanoparticles as labels for applications in bioassays, TrAC, Trends Analytical Chemistry, 61 (2014) 67-73.

[4] K. Omidfar, F. Khorsand, M. Darziani Azizi, New analytical applications of gold nanoparticles as label in antibody based sensors, Biosensors and Bioelectronics, 43 (2013) 336-347.

[5] M. Mehrabi, R. Wilson, Intercalating gold nanoparticles as universal labels for DNA detection, Small, 3 (2007) 1491-1495.

[6] C. David, N. Guillot, H. Shen, T. Toury, M.L. de la Chapelle, SERS detection of biomolecules using lithographed nanoparticles towards a reproducible SERS biosensor, Nanotechnology, 21 (2010) 475501.

[7] K. Jia, P.M. Adam, R.S. Marks, R.E. Ionescu, Fixed Escherichia coli bacterial templates enable the production of sensitive SERS-based gold nanostructures, Sensors and Actuators, B, 211 (2015) 213-219.

[8] R.S. Marks, I. Abdulhalim, Nanomaterials for Water Management: Signal Amplification for Biosensing from Nanostructures, 2015.

[9] K. Jia, J.-L. Bijeon, P.-M. Adam, R.E. Ionescu, Large Scale Fabrication of Gold Nano-Structured Substrates Via High Temperature Annealing and Their Direct Use for the LSPR Detection of Atrazine, Plasmonics, 8 (2013) 143–151.

[10] S. Mayilo, M.A. Kloster, M. Wunderlich, A. Lutich, T.A. Klar, A. Nichtl, K. Korzinger, F.D. Stefani, J. Feldmann, Long-Range Fluorescence Quenching by Gold Nanoparticles in a Sandwich Immunoassay for Cardiac Troponin T, Nano Letters, 9 (2009) 4558-4563.

[11] A. Saidi, M. Mirzaei, S. Zeinali, Using antibody coated gold nanoparticles as fluorescence quenchers for simultaneous determination of aflatoxins (B1, B2) by soft modeling method, Chemometrics and Intelligent Laboratory Systems, 127 (2013) 29-34.

[12] C.A. Mirkin, R.L. Letsinger, R.C. Mucic, J.J. Storhoff, A DNA-based method for rationally assembling nanoparticles into macroscopic materials, Nature, 382 (1996) 607-609.

[13] V. Pavlov, Y. Xiao, B. Shlyahovsky, I. Willner, Aptamer-functionalized Au nanoparticles for the amplified optical detection of thrombin, Journal of American Chemical Society, 126 (2004) 11768-11769.

[14] Y. Xiao, V. Pavlov, B. Shlyahovsky, I. Willner, An Os(II)--bisbipyridine--4-picolinic acid complex mediates the biocatalytic growth of au nanoparticles: optical detection of glucose and acetylcholine esterase inhibition, Chemistry, 11 (2005) 2698-2704.

[15] P. Fanjul-Bolado, D. Hernandez-Santos, M.B. Gonzalez-Garcia, A. Costa-Garcia, Alkaline phosphatase-catalyzed silver deposition for electrochemical detection, Analytical Chemistry, 79 (2007) 5272-5277.

[16] B. Shlyahovsky, E. Katz, Y. Xiao, V. Pavlov, I. Willner, Optical and Electrochemical Detection of NADH and of NAD+-Dependent Biocatalyzed Processes by the Catalytic Deposition of Copper on Gold Nanoparticles, Small, 1 (2005) 213-216.

[17] V. Pavlov, Enzymatic Growth of Metal and Semiconductor Nanoparticles in Bioanalysis, Particle & Particle Systems Characterization, 31 (2013) 36-45.

[18] A. Merkoçi, Biosensing Using Nanomaterials, John Wiley & Sons, Inc.2009.

[19] G. Garai-Ibabe, L. Saa, V. Pavlov, Enzymatic product-mediated stabilization of CdS quantum dots produced *in situ*: application for detection of reduced glutathione, NADPH, and glutathione reductase activity, Analytical Chemistry, 85 (2013) 5542-5546.
[20] L. Saa, J.M. Mato, V. Pavlov, Assays for methionine gamma-lyase and S-adenosyl-L-homocysteine hydrolase based on enzymatic formation of CdS quantum dots *in situ*, Analytical Chemistry, 84 (2012) 8961-8965.
[21] A. Chatterjee, A. Priyam, S.K. Das, A. Saha, Size tunable synthesis of cysteine-capped CdS nanoparticles by gamma-irradiation, Journal of Colloid and Interface Science, 294 (2006) 334-342.
[22] P. Kumar, P. Kumar, L.M. Bharadwaj, A.K. Paul, S.C. Sharma, P. Kush, A. Deep, Aqueous Synthesis of l-Cysteine Stabilized Water-Dispersible CdS:Mn Quantum Dots for Biosensing Applications, BioNanoSci., 3 (2013) 95-101.
[23] D. Luo, S.W. Smith, B.D. Anderson, Kinetics and mechanism of the reaction of cysteine and hydrogen peroxide in aqueous solution, J. Pharm. Sci., 94 (2005) 304-316.
[24] C.C. Winterbourn, D. Metodiewa, Reactivity of biologically important thiol compounds with superoxide and hydrogen peroxide, Free Radical Biology and Medicine, 27 (1999) 322-328.
[25] J.P. Barton, J.E. Packer, R.J. Sims, Kinetics of the reaction of hydrogen peroxide with cysteine and cysteamine, J. Chem. Soc., Perkin Trans. 2, (1973) 1547-1549.
[26] S.B. Bankar, M.V. Bule, R.S. Singhal, L. Ananthanarayan, Glucose oxidase--an overview, Biotechnology Advances, 27 (2009) 489-501.
[27] W.-W. Zhao, J.-J. Xu, H.-Y. Chen, Photoelectrochemical bioanalysis: the state of the art, Chemical Society Reviews, 44 (2015) 729-741.
[28] A. Devadoss, P. Sudhagar, C. Terashima, K. Nakata, A. Fujishima, Photoelectrochemical biosensors: New insights into promising photoelectrodes and signal amplification strategies, Journal of Photochemistry and Photobiology C: Photochemistry Reviews, 24 (2015) 43-63.
[29] Z. Yue, F. Lisdat, W.J. Parak, S.G. Hickey, L. Tu, N. Sabir, D. Dorfs, N.C. Bigall, Quantum-Dot-Based Photoelectrochemical Sensors for Chemical and Biological Detection, ACS Applied Materials and Interfaces, 5 (2013) 2800-2814.
[30] H. Zhou, J. Liu, S. Zhang, Quantum dot-based photoelectric conversion for biosensing applications, TrAC Trends in Analytical Chemistry, 67 (2015) 56-73.

[31] W.-W. Zhao, J. Wang, Y.-C. Zhu, J.-J. Xu, H.-Y. Chen, Quantum Dots: Electrochemiluminescent and Photoelectrochemical Bioanalysis, Analytical Chemistry, 87 (2015) 9520-9531.

[32] A. Walcarius, Electrocatalysis, sensors and biosensors in analytical chemistry based on ordered mesoporous and macroporous carbon-modified electrodes, TrAC, Trends Analytical Chemistry, 38 (2012) 79-97.

[33] Y.-T. Long, C. Kong, D.-W. Li, Y. Li, S. Chowdhury, H. Tian, Ultrasensitive Determination of Cysteine Based on the Photocurrent of Nafion-Functionalized CdS–MV Quantum Dots on an ITO Electrode, Small, 7 (2011) 1624-1628.

[34] W.-W. Zhao, Z.-Y. Ma, D.-Y. Yan, J.-J. Xu, H.-Y. Chen, *In Situ* Enzymatic Ascorbic Acid Production as Electron Donor for CdS Quantum Dots Equipped TiO2 Nanotubes: A General and Efficient Approach for New Photoelectrochemical Immunoassay, Analytical Chemistry, 84 (2012) 10518-10521.

[35] H. Zhou, J. Liu, S. Zhang, Quantum dot-based photoelectric conversion for biosensing applications, TrAC, Trends Analytical Chemistry, 67 (2015) 56-73.

[36] R. Iyer, V. Pavlov, I. Katakis, L.G. Bachas, Amperometric Sensing at High Temperature with a "Wired" Thermostable Glucose-6-phosphate Dehydrogenase from Aquifex aeolicus, Analytical Chemistry, 75 (2003) 3898-3901.

[37] M.S. Vreeke, K.T. Yong, A. Heller, A Thermostable Hydrogen Peroxide Sensor Based on "Wiring" of Soybean Peroxidase, Analytical Chemistry, 67 (1995) 4247-4249.

[38] A.D. McNaught, A. Wilkinson, IUPAC Compendium of Chemical Terminology. , Gold Book, Oxford, UK, 1997.

[39] L. Saa, V. Pavlov, Enzymatic growth of quantum dots: applications to probe glucose oxidase and horseradish peroxidase and sense glucose, Small, 8 (2012) 3449-3455.

[40] R. Grinyte, G. Garai-Ibabe, L. Saa, V. Pavlov, Application of photocatalytic cadmium sulfide nanoparticles to detection of enzymatic activities of glucose oxidase and glutathione reductase using oxidation of 3,3',5,5'-tetramethylbenzidine, Analytica chimica acta, 881 (2015) 131-138.

[41] B.L. Rodriguez, R.D. Abbott, W. Fujimoto, B. Waitzfelder, R. Chen, K. Masaki, I. Schatz, H. Petrovitch, W. Ross, K. Yano, P.L. Blanchette, J.D. Curb, The American Diabetes Association and World Health Organization Classifications for Diabetes, Their

impact on diabetes prevalence and total and cardiovascular disease mortality in elderly Japanese-American men, 2002, pp. 951-955.

[42] W. Li, D. Qian, Q. Wang, Y. Li, N. Bao, H. Gu, C. Yu, Fully-drawn origami paper analytical device for electrochemical detection of glucose, Sensors and Actuators B: Chemical, 231 (2016) 230-238.

[43] L. Li, B. Liang, F. Li, J. Shi, M. Mascini, Q. Lang, A. Liu, Co-immobilization of glucose oxidase and xylose dehydrogenase displayed whole cell on multiwalled carbon nanotube nanocomposite films modified electrode for simultaneous voltammetric detection of d-glucose and d-xylose, Biosensors and Bioelectronics, 42 (2013) 156-162.

[44] J. Tanne, D. Schäfer, W. Khalid, W.J. Parak, F. Lisdat, Light-Controlled Bioelectrochemical Sensor Based on CdSe/ZnS Quantum Dots, Analytical Chemistry, 83 (2011) 7778-7785.

[45] H.U. Bergmeyer, Gawehn, K., Grassl, M., Methods of Enzymatic Analysis, Academic Press, New York, 1974.

6

Modulating growth of CdS nanoparticles with redox process catalyzed by copper ions

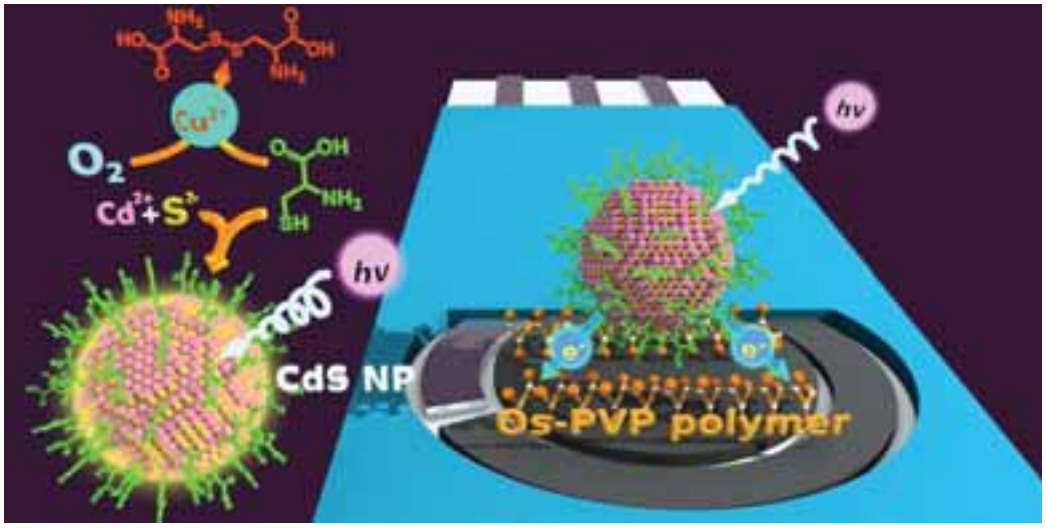

We discovered that copper (Cu^{2+}) ions modulate growth of cysteine-capped CdS quantum dots (QDs) via redox process involving cysteine and oxygen. We applied this new chemical process to sensitive fluorogenic and photoelectrochemical detection of Cu^{2+} ions in real samples of mineral and tap water.

The work presented in this chapter was submitted to: Ruta Grinyte, Javier Barroso, Laura Saa, Valeri Pavlov;Nano Letters.

6.1. Introduction

Nanomaterials based analytical assays are becoming a promising low cost approach for the detection of analytes. Usually, nanomaterials like metal and semiconductor nanoparticles (SNPs) were employed in analytical systems as fluorescent and electrochemical labels tethered to recognition elements such as antibodies and DNA oligomers,[1-3] enhancers of raman scattering,[4, 5] fluorescence quenchers[6, 7] or tracers.[8, 9] Moreover, metal NPs can be generated *in situ* in the course of biocatalytic processes catalyzed by different enzymes.[10-12] Unfortunately, metal NPs produced *in situ* in the above mention biocatalytical assays are not fluorescent thus the sensitivity of those assays is limited by the sensitivity of UV-vis spectroscopy employed to follow the formation of gold and silver NPs. Bioanalytical assays employing formation of semiconductor QDs allow to use much more sensitive fluorescence spectroscopy and photoelectrochemistry to follow the readout signal. Indeed, enzymatic assays based on *in situ* generation[13, 14] and etching[15] of semiconductor QDs are much more sensitive and cost efficient but they still require expensive and unstable enzymes. The employment of biocatalysts requires a very stringent control of their enzymatic activities in order to attain reproducible readout signals. Here, we present a new analytical methodology to overcome this intrinsic shortcoming of biocatalytical assays.

Cysteine (CSH) is an efficient stabilizer of CdS NPs[16, 17] due to the presence of thiol functional group facilitating binding at the CdS surface and hydrophilic amino and carboxylic groups conferring solubility in aqueous solutions. On the other hand, CSH can be oxidized to form a dimer containing disulfide bridge between two CSHs, known as cystine (CSSC) by oxygen in the presence of copper ions. Oxidation of CSH by O_2 catalyzed with Cu^{2+} ions proceeds through the following equation:[18]

$$CSH + O_2 \xrightarrow{Cu^{2+}} CSSC + H_2O_2$$

Cu^{2+} ions are among the heavy meal ions occurring in drinking water. Copper (Cu) plays a critical role in living organisms. Excessive consumption of Cu may increase gastrointestinal distress, even liver or kidney damage or increase the risk of Wilson´s disease.[19, 20] Therefore, it is important to develop a rapid and simple method for

monitoring low concentrations of Cu^{2+} ions in drinking water. A number of analytical techniques have been developed over the years for Cu^{2+} ions analysis, including electrochemical sensors,[21-23] fluorogenic analytical system[24] and others.[25-27] However these systems have high limits of detection (LODs), they are time-consuming and require expensive materials. For the first time, we combine oxidation of CSH catalyzed by Cu^{2+} ions with the formation of QDs *in situ*. We were able to monitor the modulated growth of CSH stabilized QDs with fluorescence and photoelectrochemical (PEC) measurements. The process of PEC detection usually involves transformation of light into other forms of energy like electrochemical energy at the surface of the electrode, creating electrical readout signal. Exploiting the nature of light and electrochemical properties of semiconductor nanoparticles (SNPs), low cost PEC devices can be developed exhibiting high sensitivity and easiness of handling. Therefore, PEC assays finds broader application to analysis,[28] substituting more expensive fluorescence spectroscopy.

We have designed the new very simple and inexpensive PEC analytical system based on disposable screen-printed carbon electrode (SPCE) and a standard laboratory UV lamp. The SPCEs were coated by the complex of poly(vinylpyridine) with Os(bipyridine)$_2$Cl$_2$ (Os-PVP complex), which facilitates electron transfer between the electrode surface and SNPs, thus allowing for ultrafast PEC detection of “wired” CdS NPs. Previously, this Os-PVP complex was used as the electrocatalyst to enhance the electron transfer between the electrode surface and active centers of redox enzymes.[29, 30]

6.2. Materials and methods

6.2.1. Materials

Sodium sulfide (Na_2S), cadmium nitrate $Cd(NO_3)_2$, copper chloride ($CuCl_2$) and other chemicals were supplied by Sigma-Aldrich.

6.2.2. Methods

6.2.2.1. Characterisation

Spectroscopy. Transmission electron miscroscopy (TEM) images were collected with a JEOL JEM 2100F operating at 120 kV.

Optical methods. Fluorescence measurements were performed in a Varioskan Flash microplate reader (Thermo Scientific) using black flat-well (330 µL) NUNC 96 wells microwell plates at room temperature. The system was controlled by SkanIt Software 2.4.3. RE for Varioskan Flash.

Photoelectrochemistry. All electrochemical experiments were conducted on the Autolab Electrochemical Workstation (Model: PGSTAT302N, Metrohm Autolab, The Netherlands) equipped with NOVA 1.10 software. Disposable screen-printed carbon electrodes (SPCEs) were purchased from DropSens (model DRP-110, 4 mm diameter). Electrical contact to workstation was done with a special boxed connector supplied by DropSens. The illumination source was a compact UV Lamp emitting at 365 nm (UVP, Analytik Jena AG). The comercially available UV lamps and UV-illuminators are able to genrate light with the peak intensity at 365 nm by default. They allow to illuminate large areas with the light of high intensity and high homogenity. Of cause, other sources of light like xenon or mercury-xenon lamps cupled to monochromators are available on the market, but they are very expensive, generate dangerous ozon, require a lot of space, specially trained personal, therefore they are not in the comon use in general analytical laboratories. Usage of the standard UV lamp in PEC devices makes analytical assays based on photoelactrochemical measurements much more available and cost eficient. All PECs were performed at room temperature. All the potentials reported in our work were against Ag/AgCl. Unless mentioned otherwise, all experimental results presented here are averaged from three independent measurements (n = 3).

6.2.2.2. CdS QD-mediated determination of Cu^{2+} ions

Different concentrations of Cu^{2+} were incubated with 0.075 mM of cysteine in citrate-phosphate buffer (pH 7.5). After 10 min Na_2S (9 µL, 1 mM) and $Cd(NO_3)_2$ (18 µL,

1 mM) were added to the samples of 73 µL. The emission spectra of the resulting suspensions were recorded after 5 min at λ_{exc} = 300 nm.

6.2.2.3. Quantification of Cu^{2+} ions in real samples (mineral and tap water)

Tap water samples (samples were collected in CICbiomagune, San Sebastian, Spain) and mineral water samples (Insalus, Tolosa, Spain) were spiked with different concentrations of Cu^{2+} (0 µM; 12.5 µM; 25 µM; 37.5 µM). Next, for measurements the samples were diluted by 100 times by standard citrate-phosphate buffer, pH 7.5. The results were plotted with the concentration standard added in the x-axis and the obtained fluorescence readings in the y-axis of calibration line.

6.2.2.4. Photoelectrochemical detection

SPCEs were initially pretreated electrochemically by cyclic voltammetry (CV) at a potential range of 0 – 0.8 V in citrate-phosphate buffer (pH 7.5) for cleansing. Subsequently, a 40 µL drop of Os-PVP complex (1.375 mg mL^{-1}) was placed on the SPCEs and deposited by CV scanning (2 cycles, 50 mV s^{-1}). Later, SPCEs were rinsed out with ultrapure water and dried under argon atmosphere. Finally, a 40 µL of samples were placed on the SPCE and PEC measurements were carried out with UV lamp emitting at 365 nm and the applied potential of 0.31 V. The dependence of photocurrent on time was measured after reaching the steady state (5 minutes). 1-thioglycerol (TG) 20mM was added to the samples.

6.3. Results and Discussion

6.3.1. CdS QD-mediated determination of Cu^{2+} ions

The oxidation of CSH can be easily applied for detection of Cu^{2+} ions. The principle of the QD based determination of Cu^{2+} ions is represented in Scheme 6.1 and can be described as follows. In the absence of Cu^{2+} ions in the reaction mixture CSH interacts with Na_2S and $Cd(NO_3)_2$ to give cysteine-stabilized CdS nanocrystals.

Scheme 6.1 QD based fluorogenic determination of Cu^{2+} ions.

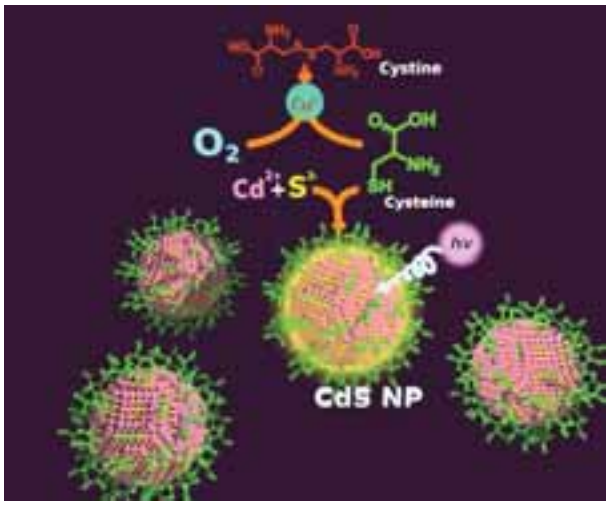

Transmission electron microscopy (TEM) was used to confirm the presence of spheroid CdS QDs in the reaction mixture in the absence of Cu^{2+} ions (see Figure A6.1 in the appendix chapter 6). On the other hand, if Cu^{2+} ions are present in the system, they catalyze oxidation of CSH by O_2 to CSSC reducing the amount of formed QDs and consequentially fluorescence intensity shown by the system. Figure 6.1A represents the effect of varying quantities Cu^{2+} at constant CSH concentration on the fluorescence registered in the system. Upon excitation at 300 nm of those CdS QDs, a characteristic fluorescence emission spectrum is observed with the peak between 450 and 650 nm and a maximum emission at about 540 nm. As one can see in Figure 6.1B the increase in the concentration of Cu^{2+} ions up to 375 nM is linearly related with the decrease in the intensity of fluorescence. According to European Union Drinking Water Directive the Maximum Contaminant Level (MCL) of Cu^{2+} ions in tap water is 2 mg/L (32 µM). So, our assay is suitable for quantification of Cu^{2+} ions in drinking tap water. The lowest Cu^{2+} ions amount that could be detected by this analytical assay was found to be 6.7 nM. In comparison with other analytic methods like colorimetric detections based on aggregation of Au NPs[31] or Ag NPs,[32] fluorogenic detection,[24] electrochemical assay,[21] and others[26, 27] for detection of Cu^{2+} ions, the method proposed by us is more sensitive and does not require neither any complicated procedures nor expensive fluorogenic dyes.

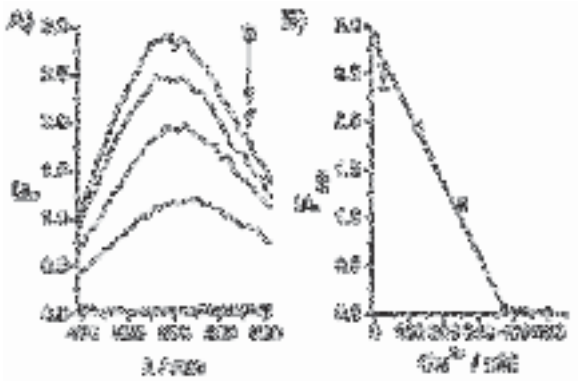

Figure 6.1 (A) Fluorescence emission spectra of the system containing cysteine (0.075 mM), Na_2S (0.09 mM), $Cd(NO_3)_2$ (0.18 mM) and different concentrations of copper: a) 0 nM; b) 25 nM; c) 125 nM; d) 250 nM; e) 375 nM; f) 500 nM; (B) Calibration curve of copper obtained using, F_{540}.

Next, in order to check out the selectivity of the proposed assay we conducted additional experiments with the heavy metal ions (Co^{2+}, Fe^{3+}, Pb^{2+}, Ni^{2+}) usually accompanying Cu^{2+} ions in tap water. We also studied the influence of other ions (Na^+, SO_4^{2-}, Cl^-, I^-, CH_3COO^-) on the response of our system. All components were used at 500 nM concentrations taking into account that this amount of Cu^{2+} ions can oxidize CSH completely under the experimental conditions (according to the calibration plot in Figure 6.1B). The diagram in Figure 6.2 does not show any influence on the readout signal by other ions added to the system. In order to demonstrate that the decrease in the fluorescence intensity in the presence of Cu^{2+} ions is not caused by simple quenching effect, the following control experiment was performed. Cu^{2+} ions (375 nM) were added to cysteine-capped CdS QDs which were pre-formed in the absence of Cu^{2+} ions. The emission peak upon the addition of 375 nM Cu^{2+} ions still retained 88% of the initial emission peak. Taking into consideration that 3 independent measurements of fluorescence peaks were performed with 10% relative standard deviation (RSD) no significant quenching was observed upon addition of Cu.

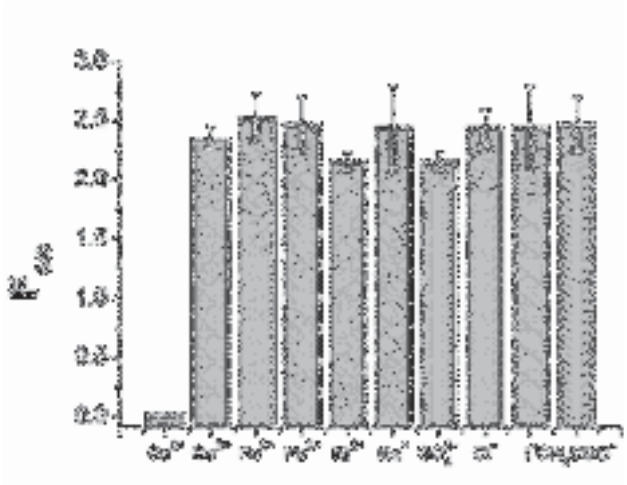

Figure 6.2. Effect of different ions on peak fluorescence intensity, F_{540}, in the system composed of CSH (0.075 mM), Na_2S (0.09 mM), $Cd(NO_3)_2$ (0.18 mM) and 500 nM of ions.

We also checked out the effect of Cu^{2+} ions on *in situ* generation of CdS QDs in the presence of other capping agents, such as reduced glutathione and orthophosphate using the optimum experimental conditions reported elsewhere[14, 33] in the presence of 500 nM of Cu^{2+} ions. According to Figure6.3 CdS QDs capped by reduced glutathione demonstrate higher emission intensity but reduced glutathione-capped QDs obtained in the presence of 500 nM of Cu still retain 60% of the readout signal. It means that Cu^{2+} ions are able to catalyze oxidation of reduced glutathione[34] but this reaction is much slower than the oxidation of CSH. When CdS QDs were formed using another stabilizing agent (orthophosphate), Cu^{2+} ions did not show any effect on fluorescence intensity and consequently formation of QDs confirming that Cu catalyzes only the oxidation of thiolated products and does quench efficiently CdS QDs under our experimental conditions.

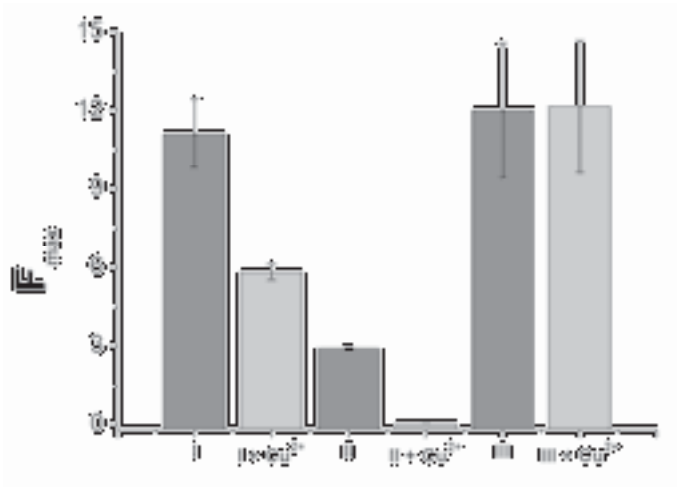

Figure 6.3. Effect of 500 nM of copper ions on formation of QDs capped with different agents: I. CdS NPs stabilized with reduced L-glutathione (reduced L-glutathione 0.075 mM, Na_2S 0.09 mM, $Cd(NO_3)_2$ 0.18 mM, Tris-HCl 10mM, pH 8); II Cysteine stabilized CdS NPs (cysteine (0.075 mM), Na_2S (0.09 mM), $Cd(NO_3)_2$ (0.18 mM)); III Orthophosphate stabilized CdS NPs (Na_3PO_4 0.3 mM, Na_2S 0.3 mM, $Cd(NO_3)_2$ 1.25 mM, Tris-HCl 50mM, pH 9.8).

We also evaluated our assay for detection of Cu^{2+} ions by real samples. As it was mentioned before, the MCL of Cu^{2+} ions in tap water is 32 µM. Keeping this value in mind, we validated the developed fluorogenic method employing mineral water and tap water samples containing different known concentrations of Cu close to MCL value (spiked concentrations of Cu^{2+} were 0 µM; 12.5 µM; 25 µM; 37.5 µM). In order to land on the linear section of the calibration plot the real samples were diluted by 100 times to obtain final Cu concentrations not higher than 375 nM. The received calibration plot including the error bars for three different measurements is shown in Figure 6.4. The calibration curves obtained using mineral water (dotted line) and tap water (dashed line) are very similar to the calibration line demonstrated previously by the system using buffered solutions (dark line). So, we demonstrated that the system is suitable for detection of Cu^{2+} ions in real samples taking into consideration the extreme sensitivity of our assay and MCL values.

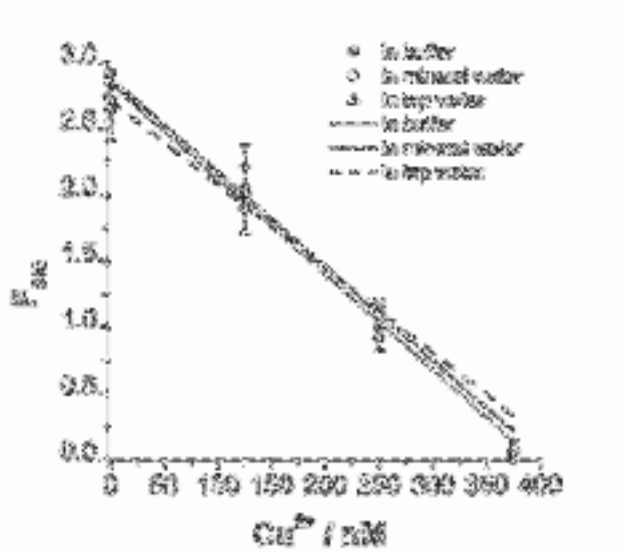

Figure 6.4. Fluorescence quantification of Cu^{2+} ions in buffer (dark line), in mineral water (dotted line) and tap water (dashed line) using peak fluorescence intensity at 540 nm (F_{540}) in the system composed of cysteine (0.075 mM), Na_2S (0.09 mM), $Cd(NO_3)_2$ (0.18 mM).

6.3.2. Photoelectrochemical detection of Cu^{2+} ions

In addition to fluorescence, the other remarkable property of QDs is their capacity to act as photoelectrochemical catalysts. The designed QDs-based PEC system is depicted in Scheme 6.2. The oxidation of CSH promoted by Cu^{2+} ions provokes a decrease in the amount of form QDs and consequently their electrochemical activity. The latter is measured using disposable electrodes coated with Os-PVP complex and a standard laboratory UV lamp for excitation of CdS QDs. Photons emitted by the UV lamp are absorbed by CdS QDs to excite electrons from the occupied valence band (VB) to the empty conduction band (CB) forming electron-hole pairs. Os-PVP complex immobilized on the surface of the SPCE facilitates the electron transfer of excited electrons to the electrode surface. In order to neutralize the holes on the surface of CdS QDs the electron donor, 1-thioglycerol (TG), exhibiting high affinity to CdS,[35] was added to the assay mixture after formation of QDs. During this redox process TG is oxidized to bis(1-thio-2,3 propanediol).

Initial screening was focused on identifying the optimal parameters for the best performance of PEC assay. First of all, the surface of SPCE was photosensitized with Os-PVP complex by cyclic voltammetry (CV) applying varying potential in the range

between 0.0 and 0.6 V vs. Ag/AgCl during two cycles. The surface coverage (Γ / nmol cm^{-2}) of osmium moieties (Table A6.1, appendix chapter 6) was determined by CV, revealing two specific redox waves related to the presence of the central osmium atom (see Figure A6.2, appendix chapter 6). The saturating concentration of TG equal to 20 mM was selected for measurements (see Figure A6.3, appendix chapter 6). The working potential of 0.3V *vs.* Ag/AgCl was selected taking into account the highest ratio (I_{QDs}/I_0) between photocurrents registered in the presence (I_{QDs}) and in the absence (I_0) of CdS QDs (data not shown) with the signal-to-noise ratio greater than 3.

Scheme 6.2. Electrochemical detection of CdS QDs "wired" by Os-PVP complex to the surface of a SPCE.

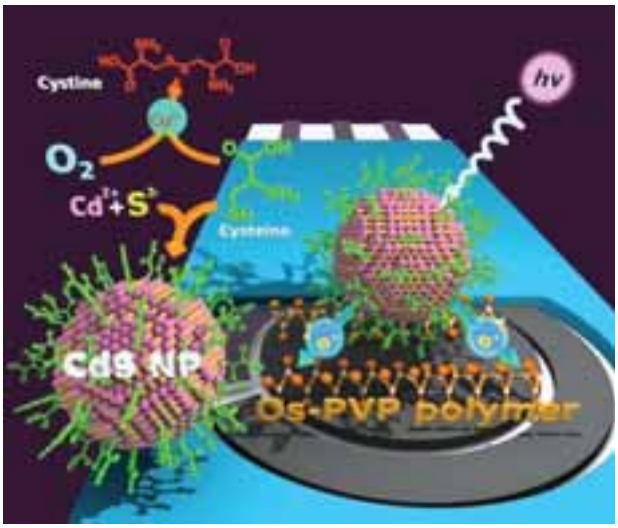

Having identified the optimal reaction conditions, the control experiments were performed using non modified SPCE for the detection of anodic photocurrent in the presence of CdS QDs and TG in the assay mixture. No significant photocurrent was observed in the absence of Os-PVP complex.

As depicted in Figure 6.5A and 6.5B the photocurrent intensities decreased in the presence of Cu^{2+} ions. The response shows linearity from 0 to 350 nM and saturation starting from 500 nM Cu^{2+}concentration. The LOD was found to be 2nM (3σ). The average RSD calculated from the Cu^{2+} calibration plot (obtained using at least three independent SPCEs with Os-PVP) was 6%. In previously published PEC system for detection of Cu the LOD was found to be 10 nM.[36, 37] Compared to the previously published methods, our system demonstrated better sensitivity using the standard UV

lamp emitting at 365 nm as the source of photons (see in the materials and methods, characterisation).

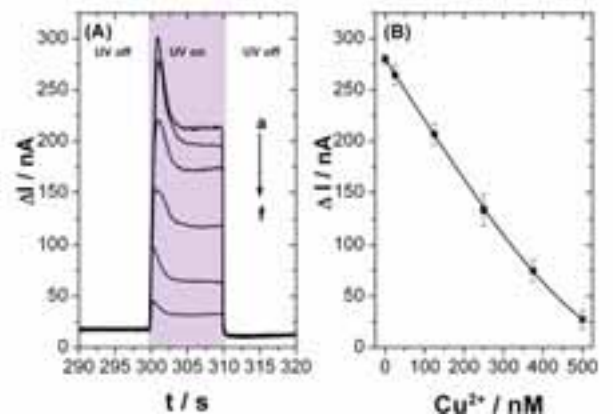

Figure 6.5. (A) Photocurrent responses of CdS QDs in the system containing cysteine (0.075 mM), 1-thioglycerol (0.02 M), Na_2S (0.09 mM), $Cd(NO_3)_2$ (0.18 mM) and different concentrations of copper: a) 0 nM; b) 25 nM; c) 125 nM; d) 250 nM; e) 375 nM; f) 500 nM; (B) Calibration curve of copper obtained at 0.3 V (vs. Ag/AgCl) and 365 nm excitation light.

The PEC assay was validated by determination of Cu^{2+} ions in real water samples: mineral and tap water (Figure 6.6). The photocurrent responses are shown in Figure A6.4, appendix chapter 6. The LODs of Cu determination in mineral and tap water were 2.1 nM (RSD = 9%) and 3 nM (RSD = 7%), respectively. So, we demonstrated the simplicity and validity of developed PEC assay for determination of trace amount of Cu^{2+} ions in real samples.

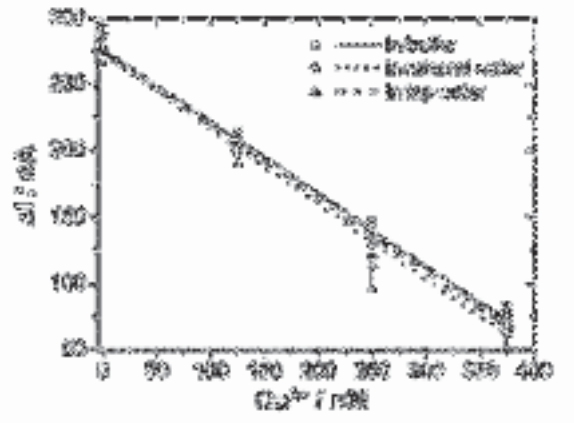

Figure 6.6. Photoelectrochemical quantification of Cu^{2+} ions in buffer (dark line), in mineral water (dotted line) and tap water (dashed line) in the system composed of cysteine (0.075 mM), 1-thioglycerol (0.02 M), Na_2S (0.09 mM), $Cd(NO_3)_2$ (0.18 mM).

6.4. Conclusion

In summary, we have developed assays for Cu^{2+} ions based on the growth of CdS NPs modulated by oxidation of CSH. The sensitivity of our assays covers the European Union standard limit of Cu^{2+} ions in drinking water. Besides, this assay did not suffer from interference with other ions accompanying Cu^{2+}. We believe that the present approach shows high potential for monitoring Cu^{2+} ions in environmental samples. Furthermore, exploiting the photoelectrochemical properties of *in situ* formed QDs opens up new possibilities in the field of nanotechnology exploiting formation of nanoparticles *in situ* modulated by redox reactions.

6.5. References

[1] E. Katz, I. Willner, Integrated Nanoparticle–Biomolecule Hybrid Systems: Synthesis, Properties, and Applications, Angewandte Chemie International Edition, 43 (2004) 6042-6108.

[2] A. de la Escosura-MuÃ±iz, C. Parolo, A. Merkoçi, Immunosensing using nanoparticles, Materials Today, 13 (2010) 24-34.

[3] T. Zhao, R. Liu, X. Ding, J. Zhao, H. Yu, L. Wang, Q. Xu, X. Wang, X. Lou, M. He, Y. Xiao, Nanoprobe-Enhanced, Split Aptamer-Based Electrochemical Sandwich Assay for Ultrasensitive Detection of Small Molecules, Analytical chemistry, 87 (2015) 7712-7719.

[4] C. David, N. Guillot, H. Shen, T. Toury, M.L. de la Chapelle, SERS detection of biomolecules using lithographed nanoparticles towards a reproducible SERS biosensor, Nanotechnology, 21 (2010) 475501.

[5] K. Jia, P.M. Adam, R.S. Marks, R.E. Ionescu, Fixed Escherichia coli bacterial templates enable the production of sensitive SERS-based gold nanostructures, Sensors and Actuators B: Chemical, 211 (2015) 213-219.

[6] U.S. Raikar, V.B. Tangod, B.M. Mastiholi, V.J. Fulari, Fluorescence quenching using plasmonic gold nanoparticles, Optics Communications, 284 (2011) 4761-4765.

[7] A. Samanta, Y. Zhou, S. Zou, H. Yan, Y. Liu, Fluorescence Quenching of Quantum Dots by Gold Nanoparticles: A Potential Long Range Spectroscopic Ruler, Nano letters, 14 (2014) 5052-5057.

[8] A. Clemente, N. Moreno, M.P. Lobera, F. Balas, J. Santamaria, Fluorescently labelled SiO2 nanoparticles as tracers in natural waters: dependence of detection limits on environmental conditions, Environmental Science: Nano, 3 (2016) 631-637.

[9] N. Manabe, A. Hoshino, Y.Q. Liang, T. Goto, N. Kato, K. Yamamoto, Quantum dot as a drug tracer in vivo, IEEE transactions on nanobioscience, 5 (2006) 263-267.

[10] V. Pavlov, Y. Xiao, I. Willner, Inhibition of the acetycholine esterase-stimulated growth of Au nanoparticles: nanotechnology-based sensing of nerve gases, Nano letters, 5 (2005) 649-653.

[11] A. Virel, L. Saa, V. Pavlov, Modulated growth of nanoparticles. Application for sensing nerve gases, Analytical chemistry, 81 (2009) 268-272.

[12] Y. Xiao, V. Pavlov, S. Levine, T. Niazov, G. Markovitch, I. Willner, Catalytic Growth of Au Nanoparticles by NAD(P)H Cofactors: Optical Sensors for NAD(P)+-Dependent Biocatalyzed Transformations, Angewandte Chemie International Edition, 43 (2004) 4519-4522.

[13] G. Garai-Ibabe, M. Moller, V. Pavlov, Ultrasensitive assay for detection of serum paraoxonase by modulating the growth of fluorescent semiconductor nanoparticles, Analytical chemistry, 84 (2012) 8033-8037.

[14] G. Garai-Ibabe, L. Saa, V. Pavlov, Enzymatic product-mediated stabilization of CdS quantum dots produced *in situ*: application for detection of reduced glutathione, NADPH, and glutathione reductase activity, Analytical chemistry, 85 (2013) 5542-5546.

[15] R. Grinyte, L. Saa, G. Garai-Ibabe, V. Pavlov, Biocatalytic etching of semiconductor cadmium sulfide nanoparticles as a new platform for the optical detection of analytes, Chemical Communications, 51 (2015) 17152-17155.

[16] A. Chatterjee, A. Priyam, S.K. Das, A. Saha, Size tunable synthesis of cysteine-capped CdS nanoparticles by gamma-irradiation, Journal of colloid and interface science, 294 (2006) 334-342.

[17] P. Kumar, P. Kumar, L.M. Bharadwaj, A.K. Paul, S.C. Sharma, P. Kush, A. Deep, Aqueous Synthesis of l-Cysteine Stabilized Water-Dispersible CdS:Mn Quantum Dots for Biosensing Applications, 2013, pp. 95-101.

[18] L. Pecci, G. Montefoschi, G. Musci, D. Cavallini, Novel findings on the copper catalysed oxidation of cysteine, 1997, pp. 355-367.

[19] R. Lei, B. Yang, C. Wu, M. Liao, R. Ding, Q. Wang, Mitochondrial dysfunction and oxidative damage in the liver and kidney of rats following exposure to copper nanoparticles for five consecutive days, Toxicology Research, 4 (2015) 351-364.

[20] A. Ala, A.P. Walker, K. Ashkan, J.S. Dooley, M.L. Schilsky, Wilson's disease, Lancet (London, England), 369 (2007) 397-408.

[21] C. Ocana, N. Malashikhina, M. del Valle, V. Pavlov, Label-free selective impedimetric detection of Cu2+ ions using catalytic DNA, The Analyst, 138 (2013) 1995-1999.

[22] M. Etienne, J. Bessiere, A. Walcarius, Voltammetric detection of copper(II) at a carbon paste electrode containing an organically modified silica, Sensors and Actuators B: Chemical, 76 (2001) 531-538.

[23] T. Shtoyko, S. Conklin, A.T. Maghasi, J.N. Richardson, A. Piruska, C.J. Seliskar, W.R. Heineman, Spectroelectrochemical sensing based on attenuated total internal reflectance stripping voltammetry. 3. Determination of cadmium and copper, Analytical chemistry, 76 (2004) 1466-1473.

[24] J. Jo, H.Y. Lee, W. Liu, A.s. Olasz, C.-H. Chen, D. Lee, Reactivity-Based Detection of Copper(II) Ion in Water: Oxidative Cyclization of Azoaromatics as Fluorescence Turn-On Signaling Mechanism, Journal of the American Chemical Society, 134 (2012) 16000-16007.

[25] M.S. Chan, S.D. Huang, Direct determination of cadmium and copper in seawater using a transversely heated graphite furnace atomic absorption spectrometer with Zeeman-effect background corrector, Talanta, 51 (2000) 373-380.

[26] M.R. Awual, M. Ismael, T. Yaita, S.A. El-Safty, H. Shiwaku, Y. Okamoto, S. Suzuki, Trace copper(II) ions detection and removal from water using novel ligand modified composite adsorbent, Chemical Engineering Journal, 222 (2013) 67-76.

[27] R. Wang, W. Wang, H. Ren, J. Chae, Detection of copper ions in drinking water using the competitive adsorption of proteins, Biosensors and bioelectronics, 57 (2014) 179-185.

[28] H. Zhou, J. Liu, S. Zhang, Quantum dot-based photoelectric conversion for biosensing applications, TrAC Trends in Analytical Chemistry, 67 (2015) 56-73.

[29] R. Iyer, V. Pavlov, I. Katakis, L.G. Bachas, Amperometric Sensing at High Temperature with a "Wired" Thermostable Glucose-6-phosphate Dehydrogenase from Aquifex aeolicus, Analytical chemistry, 75 (2003) 3898-3901.
[30] M.S. Vreeke, K.T. Yong, A. Heller, A Thermostable Hydrogen Peroxide Sensor Based on "Wiring" of Soybean Peroxidase, Analytical chemistry, 67 (1995) 4247-4249.
[31] Q. Gao, Y. Zheng, C. Song, L.-Q. Lu, X.-K. Tian, A.-W. Xu, Selective and sensitive colorimetric detection of copper ions based on anti-aggregation of the glutathione-induced aggregated gold nanoparticles and its application for determining sulfide anions, RSC Advances, 3 (2013) 21424-21430.
[32] Y. Ye, Y. Guo, Y. Yue, H. Huang, L. Zhao, Y. Gao, Y. Zhang, Colorimetric sensing of copper ions based on the anti-aggregation of unmodified silver nanoparticles in the presence of 1,4-dithiothreitol, Analytical Methods, 7 (2015) 566-572.
[33] N. Malashikhina, G. Garai-Ibabe, V. Pavlov, Unconventional application of conventional enzymatic substrate: first fluorogenic immunoassay based on enzymatic formation of quantum dots, Analytical chemistry, 85 (2013) 6866-6870.
[34] M. Scarpa, F. Momo, P. Viglino, F. Vianello, A. Rigo, Activated oxygen species in the oxidation of glutathione A kinetic study, Biophysical Chemistry, 60 (1996) 53-61.
[35] Y.J. Yang, The thioglycerol catalyzed reaction of metal salts and elemental sulfur: A new approach for the preparation of nanocrystalline metal sulfides, Colloids and Surfaces A: Physicochemical and Engineering Aspects, 276 (2006) 192-196.
[36] G.-L. Wang, J.-J. Xu, H.-Y. Chen, Selective detection of trace amount of Cu2+ using semiconductor nanoparticles in photoelectrochemical analysis, Nanoscale, 2 (2010) 1112-1114.
[37] Q. Shen, X. Zhao, S. Zhou, W. Hou, J.-J. Zhu, ZnO/CdS Hierarchical Nanospheres for Photoelectrochemical Sensing of Cu2+, The Journal of Physical Chemistry C, 115 (2011) 17958-17964.

Conclusions

This PhD thesis represents bioanalytical assays based on modulation of quantum dots *in situ*. A variety of methods were developed for this purpose.

The mayor findings of this PhD thesis are summarized below:

1. Photocatalytical CdS NPs acting as catalysts powered by UV light can be produced *in situ* under mild conditions in aqueous medium suitable for operation of enzymes. These NPs use energy of photons from a standard UV light and do not require hydrogen peroxide for oxidation of commercially available chromogenic enzymatic substrates TMB. The stability of the present photocatalytical system under ambient laboratory light allows applying it for development of sensitive bioanalytical chromogenic assays taking advantage of enzymatic formation of QDs by using UV spectroscopy instead of fluorometry.
2. The biocatalytic process involving bromide, HRP and H_2O_2 decreased the size of semiconductor CdS NPs. Thus, this phenomenon can be applied to resizing of semiconductor CdS NPs under mild physiological conditions and sensitive detection of H_2O_2 and HRP. It was proven that also CdS NPs immobilized on polyvinyl chloride microspheres can be etched biocatalytically. We introduce a new platform for optical detection of analytes based on etching of semiconductor NPs. This finding opens new path for enzymatic modification and modulation of biosensors based on semiconductor NPs.
3. A bead-based immunoassay for the detection of tumor biomarkers such as SOD2 employing enzymatic *in situ* generation and adsorbtion of CdS QDs onto microspheres was developed. It was demonstrated that electrochemical and fluorogenic detection employing enzymatically generated CdS NPs yield new immunoassays with better detection limits in comparison with those of the previously published methods at least by three orders of magnitude. Our methodology allows for the detection of SOD2 in lysates from HepG2 cells.
4. The employment of cysteine (CSH) as a capping agent allows for rapid formation of fluorescent CdS QDs in aqueous solutions at room temperature. H_2O_2, produced in the course of enzymatic oxidation of D-glucose by GOx,

oxidizes CSH to CSSC modulating the growth of QDs. This biocatalytic process can be applied to the development of simple sensitive photoelectrochemical (PEC) assays for GOx activity in buffered solutions and D-glucose in real samples of human serum using the photocatalytic activity of the resulting QDs.

5. The assays for Cu^{2+} ions based on the growth of CdS NPs modulated by oxidation of CSH were developed. The sensitivity of the assays meets the European Union standard limit of Cu^{2+} ions in drinking water. Besides, these assays did not suffer from interference with other ions accompanying Cu^{2+}. The present approach shows high potential for monitoring Cu^{2+} ions in environmental samples. Furthermore, exploiting the photoelectrochemical properties of *in situ* formed QDs opens up new possibilities in the field of nanotechnology exploiting formation of nanoparticles in situ modulated by redox reactions.
6. To summarize, this thesis demonstrates that analtyte-triggered modulation and resizing of CdS QDs change their optical properties studied by fluorescence spectroscopy and TEM. Modulation and resizing also drastically influence photocatalytical and electrochemical properties of CdS QDs manifested by photooxydation of reducing agents such as TMB and 1-thioglycerol. Analytical assays based on above mentioned processes are more sensitive and cost-efficient than the previously published relevant analytical procedures.

Appendix

Chapter 4

Microbead QD-ELISA: microbead ELISA using biocatalytic formation of quantum dots for ultra high sensitive optical and electrochemical detection

TEM and EDX study

The element mapping study by EDX spectroscopy in STEM mode focuses on the detection and colocalization of Cd as an element in the sample, while the conclusion that present Cd is forming nanoparticles is to be derived from the strong fluorescence signal observed in the fluorescence studies.

CdS NPs have not been imaged on the surface of the microbeads because the necessary high microscopy magnification would not automatically result in the needed high image resolution. Actually, high magnification data acquisition on the samples impacts the resolution because of the sample material being prone to beam damages. The beads shrink during the data acquisition in the TEM. This beam damage increases with the applied electron dose. Obtaining higher magnification images at useful signal to noise ratio implies an increase of the electron dose and thus increases the beam damages. As the shrinkage is locally observed as moving material, high magnification images would appear blurred due to the movements of the sample during image acquisition and no high resolution could be obtained.

Materials and Method

For the characterization of microbeads by electron microscopy, a droplet of a freshly prepared sample solution was desiccated on a by plasma treatment hydrophilic rendered carbon surface. Ultrathin carbon film coated TEM grids have been used (Ted Pella, USA). Data was acquired in a TEM of type JEM-2100F-UHR (JEOL, Japan) equipped with a high-angle annular dark field (HAADF) detector and an energy-dispersive X-ray spectroscopy (EDX) system of type INCA (Oxford Instruments Analytical Limited, UK).

The EDX data was processed and analyzed by the same software, which also run the INCA and X-STREAM hardware system (The Microanalysis Suite - Issue 17b (2007); INCA Suite version 4.09, Energy TEM 250 with the modules Analyzer and Mapping + Site Lock). Exported graphs have been color corrected in the software PAINT (Microsoft, USA) and merged into finally presented figures by the public domain software ImageJ 1,51d (National Institutes of Health, USA).

Results and Discussion:

The analysis of the sum EDX spectrum for samples prepared in the presence of 111.5 ng mL^{-1} SOD2 in the assay proves the identification of Cd to be valid: the Figure A4.1A shows the relevant part of the measured sum spectrum (yellow), and simulated spectra assuming the absence (blue) or the presence (red) of Cd. The experimental data can very well be reconstructed if the presence of Cd is considered in the simulation. Alternatively excluding the presence of Cd does not reconstruct the experimental data anymore. Thus, Cd is confirmed to be present in the samples prepared in the presence of SOD2 protein. Mapping for this sample the Cd signal to the corresponding STEM image shows clearly that the excitation occurred where the organic matrix was localized (Figure 4.4**.**, chapter 4).

The Figure A4.1B shows for the sample prepared in the absence of SOD2 in the assay that a same data analysis does not produce evidence for the presence of Cd in this sample. The visible, small signal in the energy range around the Lα line of Cd therefore has to be assigned to Bremsstrahlung not fully corrected for by the automatic spectrum processing. In conclusion of this finding no Cd map (no image) should be elaborated for this sample, because it would falsely map Bremsstrahlung instead of true Cd Lα line counts.

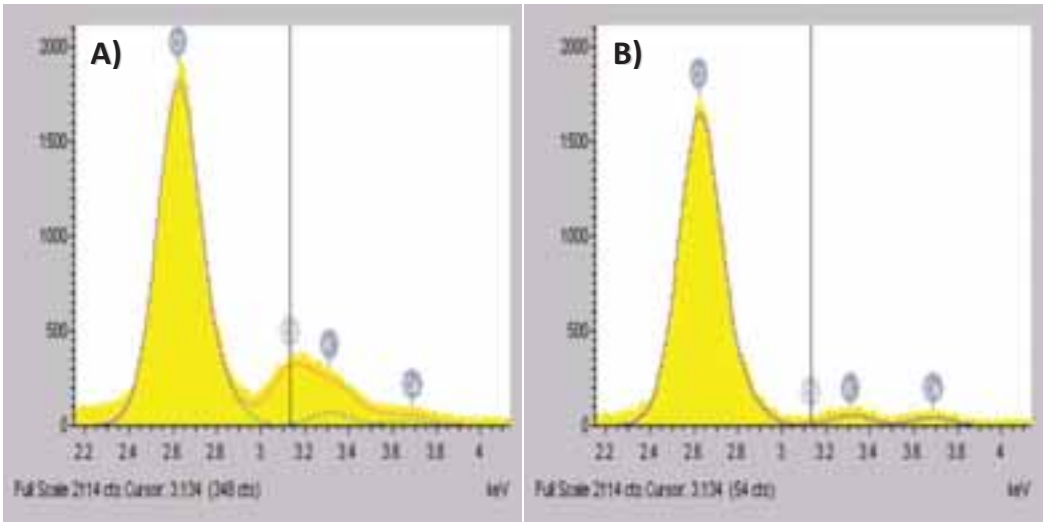

Figure A4.1. Energy Dispersive X-Ray sum spectra: (1A) sample prepared in the presence of 111.5 ng mL^{-1} SOD2; (1B) in the absence of SOD2 protein.

Figure A4.1 legend: In yellow color is shown the for this study relevant part of the experimentally obtained EDX spectrum. In blue color is shown a simulated spectrum taking into account only parameters relevant for the reconstruction of the peaks of the selected elements Cl, K, and Ca (but not Cd!) in the energy range of interest. In red color is shown a simulated spectrum taking additionally into account relevant Cd parameters. The vertical marker at 3,134 keV in the spectrum shows the position for Cadmium Lα emission.

Electrochemical measurements: Cd^{2+} ions deposition

It was confirmed that all the dissolved Cd^{2+} ions were deposited on the surface of the SPE. The following protocol was applied:

First, a 40 µL drop of Cd^{2+} solution (2.5 mM) was placed on the electrode 1 (A) and reduced at 1.2 V vs. Ag/AgCl for 2 minutes. Then, the solution was transferred to another electrode 2 (B) and the reduction process was also applied. Finally, electrochemical SWV measurements were conducted (2 mV step potential, 25 mV amplitude and 25 Hz frequency) and stripping from -1.2 to -0.6 V.

Figure A4.2 shows the square wave voltammograms which confirm that all the dissolved Cd2+ was deposited on the surface of the working electrode and electrochemically oxidized at 0.9 V vs. Ag/AgCl (dark line). In absence of Cd^{2+} (in the solution generated from A) oxidation peak was not observed (dashed line).

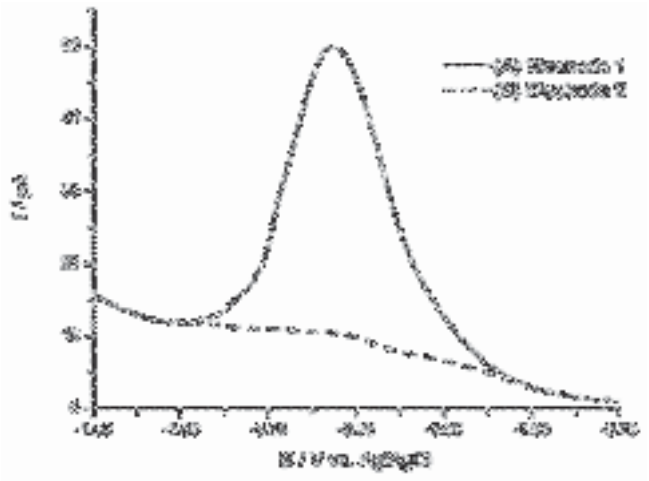

Figure A4.2. Square wave voltammograms obtained for a system containing: (A) oxidized-reduced $Cd(NO_3)_2$ 2.5 mM and (B) free-cadmium solution generated from (A).

Appendix

Chapter 5

Modulation of growth of cysteine-capped cadmium sulfide quantum dots with enzymatically produced hydrogen peroxide

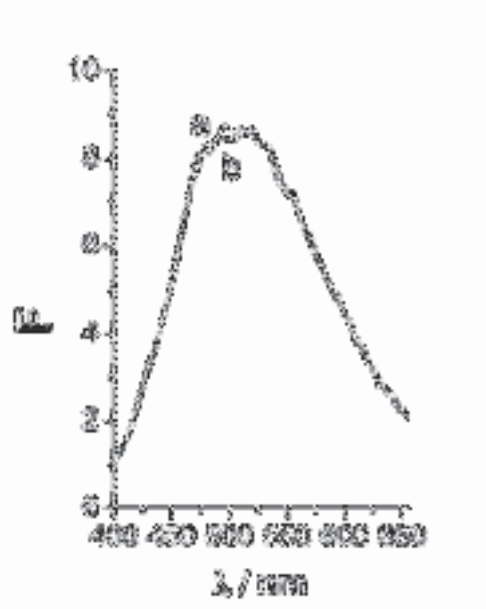

Figure A5.1. The system containing cysteine-stabilized CdS QDs before addition of H_2O_2 (curve a) and after addition of 0.1 mM of H_2O_2 (curve b). Incubation time 5 min, λ_{exc} = 300 nm.

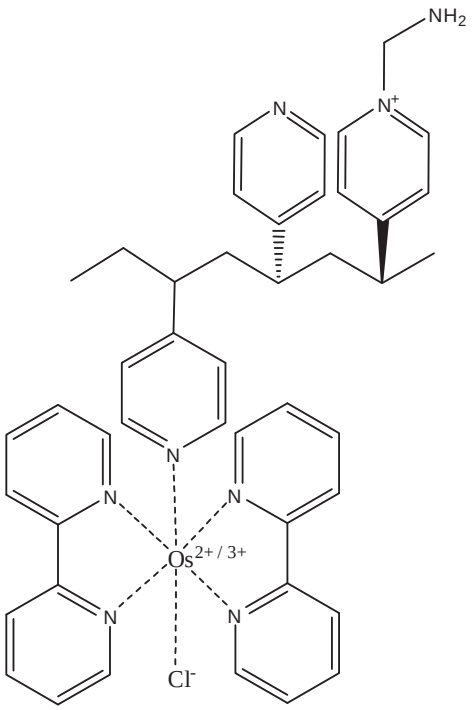

Figure. A5.2 2D structure of poly(vinypyridine) complexed with Os(bipyridine)$_2$Cl$_2$ (Os-PVP complex).

The polymer was synthesized according to the procedure previously published elsewhere (Katakis I., Ye L., Heller A., 1994. J. Am. Chem. Soc. 116, 3617-3618).

Electrochemical characterization of SPCEs

Surface coverage (*Γ)* of electroactive species was determined by cyclic voltammetry (CV) calculating the charge under the areas of peaks depicted in Figure A5.3.

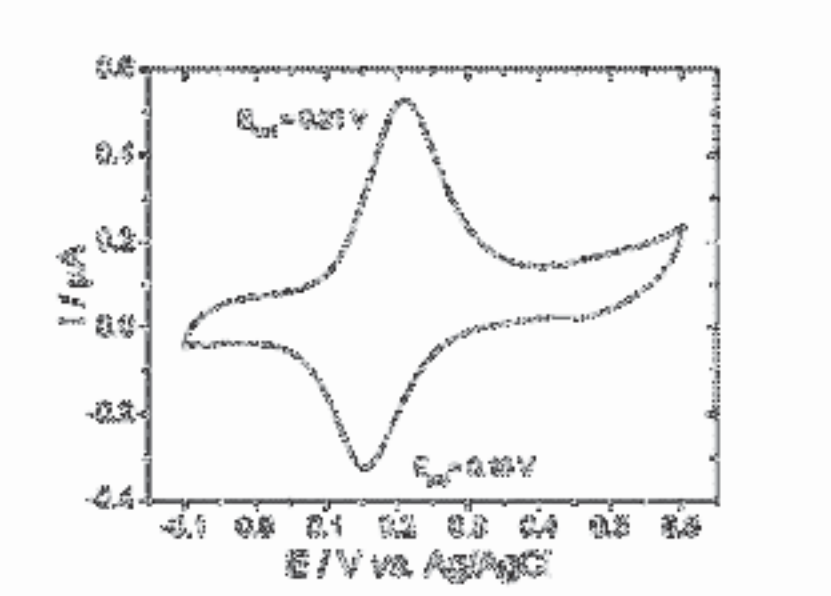

Figure A5.3. Cyclic voltammograms of screen-pirnted carbon electrode (SPCE) modified by Os-PVP complex. Scan rate of 50 mV s^{-1}.

Taking into account the number of exchanged electrons per redox molecule and the Faraday´s constant, the surface concentration was calculated. The peak intensity, I_p, is a function of scan rate υ, charge diffusion coefficient D_0, number of exchanged electrons n, surface concentration of redox active species C_0^*, surface coverage Γ, electrode surface area A, temperature T, Faraday´s constant F and gas constant R according to the equation:

$$I_P = n^2F^2\Gamma A\upsilon(4RT)^{-1}$$

The Randles-Sevčik equation for quasi-reversible electron transfer processes was employed to determine the active electrode area, as follows:

$$I_P = (2.65 * 10^5)n^{3/2}ACD^{1/2}\upsilon^{1/2}$$

where n is the number of electrons participating in the redox process, A is the active electrode area, D is the diffusion coefficient, C is the concentration of probe molecule and υ is the scan rate. The CV were performed in potasium ferricyanide (2mM). The calculations of active area (A) were carried out employing the value of D mentioned by Kadara et al., 2009. The electrochemically active area was 0.099 cm^2. The surface coverage is shown in Table S1 for three independent screen-printed carbon electrodes

(SPCEs) modified by Os-PVP complex. The average coverage was found to be 10.9 ± 1.4 nmol cm^{-2}.

Table A5.1 Surface coverage (Γ / nmol cm^{-2}) of three independent screen-printed carbon electrodes.

Electrode	Γ / nmol cm^{-2}
1	**11.2**
2	**12.1**
3	**9.4**

References

1. Prodromidis M.I., Florou A.B., Tzouwara-Karayanni S.M., Karayannis M.I., 2000. Electroanal. 12, 1498-1501.
2. Gao Z., Binyamin G., Kim H.H., Barton S.C., Zhang Y., Heller A., 2002. Angew. Chem. Int. Ed. 41, 810-813.
3. Kadara R.O., Jenkinson N., Banks C.E., 2009. Sensor Actuat B-Chem. 138,556–562.

Photoelectrochemical control

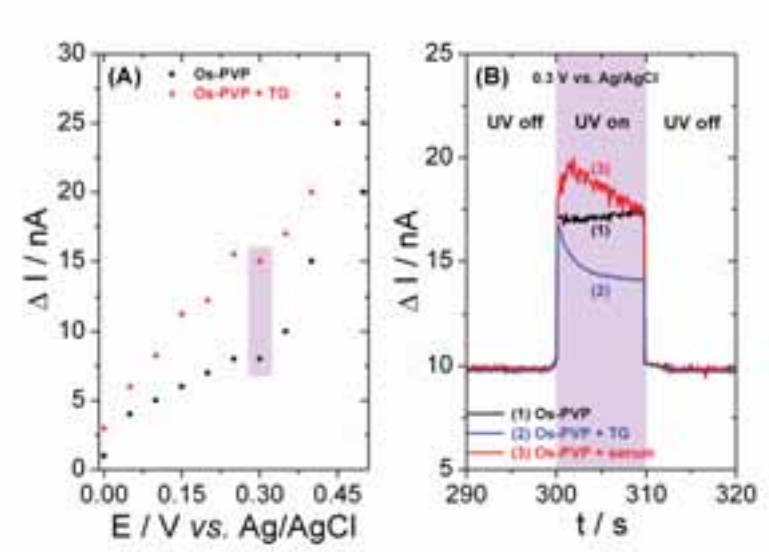

Figure A5.4 (A) Variation in the photocurrent for the modified SPCE sensitized by conductive OS-PVP complex in the presence and in the absence of 1-thioglycerol (TG) in the potential range between from 0 to 0.5 V vs. Ag/AgCl; (B) Photocurrent background responses in the absence of CdS QDs on the SPCE containing (1) only Os-PVP complex; (2) Os-PVP complex, 1-thioglycerol (TG) 20 mM and (3) Os-PVP complex, human serum.

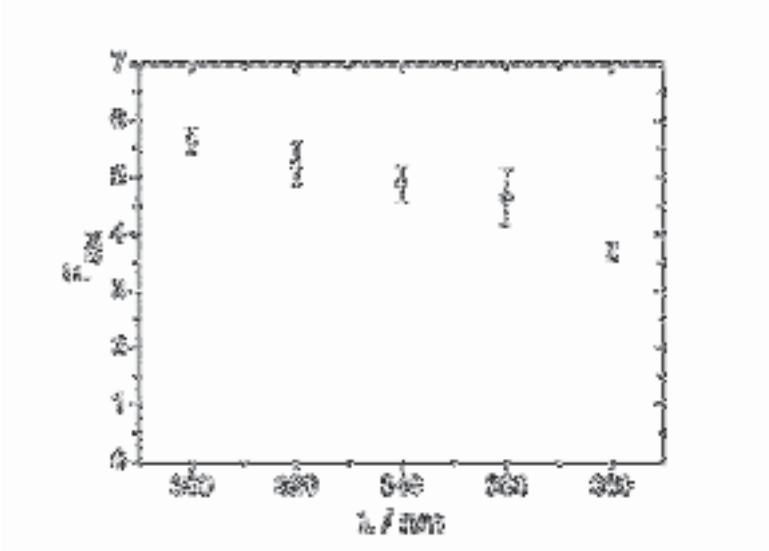

Figure A5.5 The plot showing the dependence of the emission light intensity, registered in the reaction mixture containing CdS QDs, on the wavelength of the excitation light.

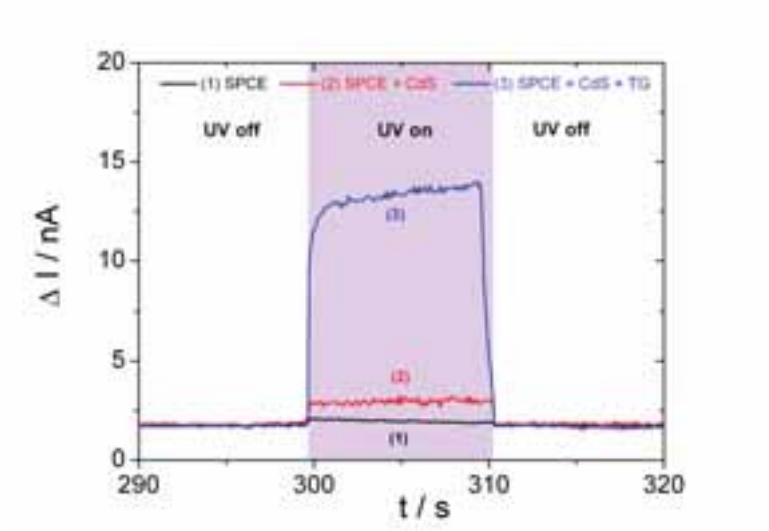

Figure A5.6. Photocurrent background responses in the absence of Os-PVP complex for (1) only SPCE; (2) SPCE and CdS QDs and (3) SPCE, CdS QDs and 1-thioglycerol (TG) 20 mM.

Optimization of 1-thioglycerol concentration

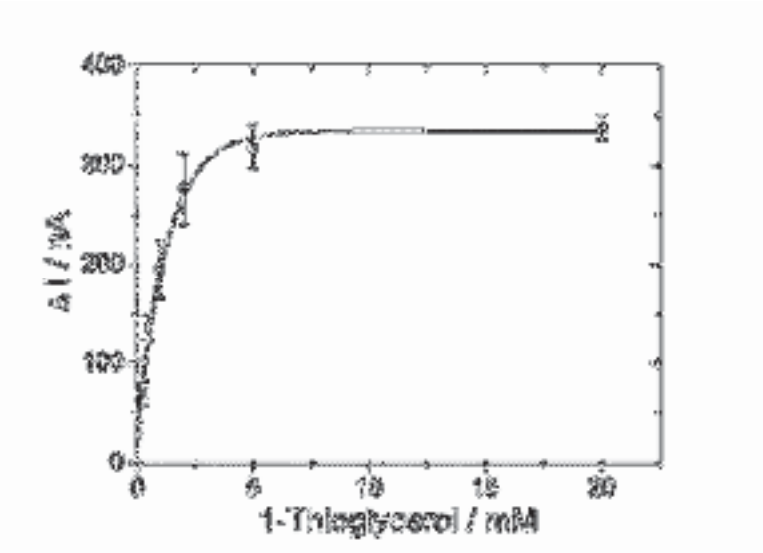

Figure A5.7. Effect of the increasing 1-thioglycerol concentrations (TG) on photocurrent observed in the presence of CdS QDs at 0.3 V (*vs.* Ag/AgCl) and 365 nm excitation light. Concentrations of TG: a) 0 mM; b) 0.25 mM; c) 0.5 mM; d) 1 mM; e) 2 mM; f) 5 mM; g) 20 mM. The the system contains $Cd(NO_3)_2$ (1.25 mM), Na_2S (0.1 mM) and cysteine (0.075 mM). The average relative standard deviation (RSD) calculated from the plot (obtained using at least three independent SPCEs modified by Os-PVP) was 9.75 %.

Appendix

Chapter 6

Modulating growth of CdS nanoparticles with redox process catalyzed by copper ions

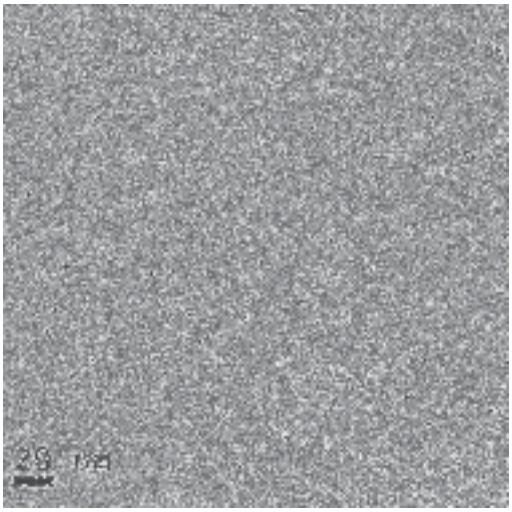

Figure A6.1. TEM image of cysteine stabilized CdS QDs.

Electrochemical characterization of SPCEs

Surface coverage (*Γ)* of electroactive species was determined by cyclic voltammetry (CV) calculating the charge under the areas of peaks depicted in Figure S4.

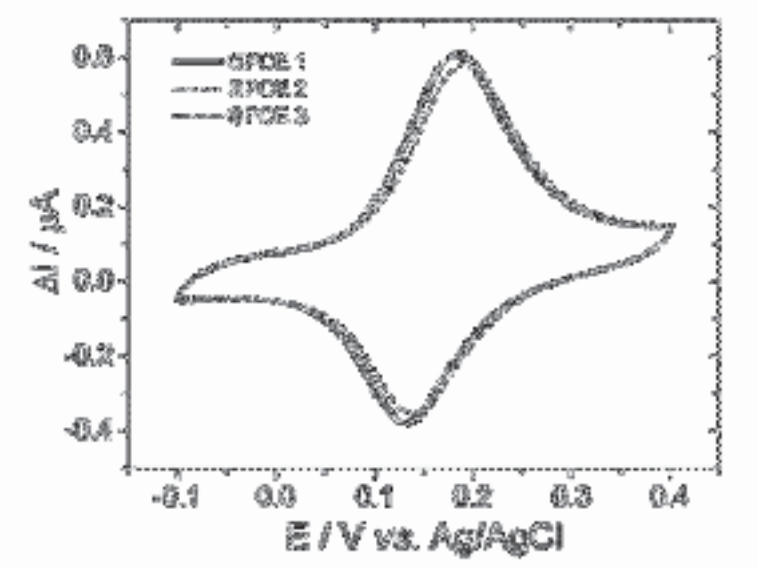

Figure A6.2. Cyclic voltammograms of three independent screen-printed carbon electrodes (SPCEs) modified by Os-PVP complex. Scan rate of 50 mV s^{-1}.

Table A6.1. Surface coverage (Γ / nmol cm^{-2}) of three independent screen-printed carbon electrodes (SCPEs). See calculation in Appendix chapter 5.

Electrode	Γ / **nmol cm^{-2}**
1	12.30
2	11.46
3	12.18

Optimization of 1-thioglycerol (TG) concentration

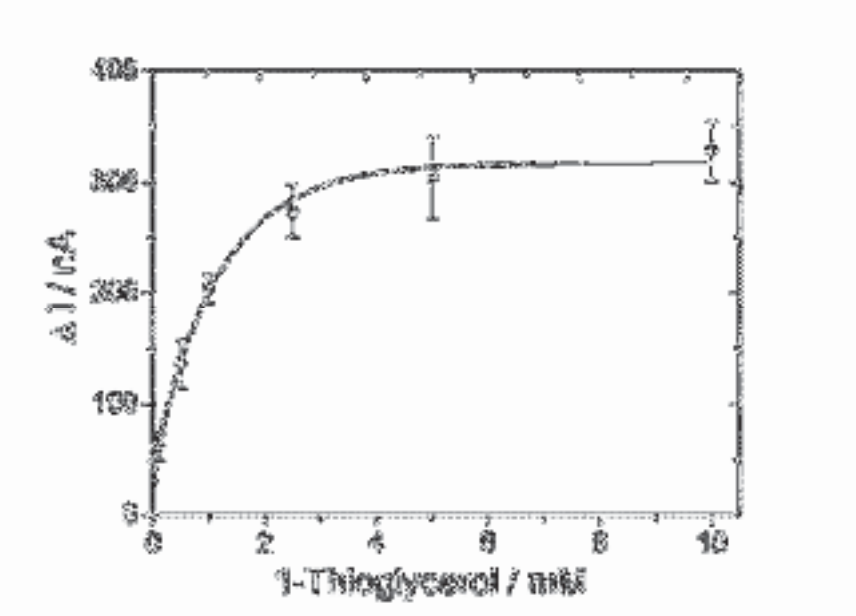

Figure A6.3. Effect of the increasing 1-thioglycerol (TG) concentrations on photocurrent observed in the presence of CdS QDs at 0.3 V (*vs.* Ag/AgCl) and 365 nm excitation light. Concentrations of TG: a) 0 mM; b) 0.25 mM; c) 0.5 mM; d) 1 mM; e) 2 mM; f) 5 mM; g) 20 mM. The the system contains $Cd(NO_3)_2$ (0.18 mM), Na_2S (0.09 mM) and cysteine (0.075 mM). The average relative standard deviation (RSD) calculated from the plot (obtained using at least three independent SPCEs modified by Os-PVP) was 10%.

Photoelectrochemical detection of copper ions in real samples

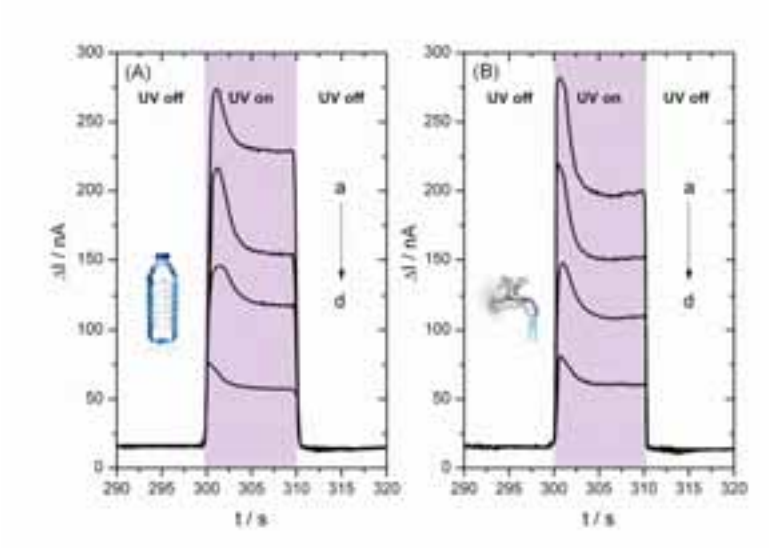

Figure A6.4. Photocurrent responses of the system containing cysteine (0.075 mM), 1-thioglycerol (0.02 M), Na_2S (0.09 mM), $Cd(NO_3)_2$ (0.18 mM) and different concentrations of copper: a) 0 nM; b) 125 nM; c) 250 nM; d) 375 nM for (A) mineral and (B) tap water.

List of Publications

AUTHORS: **Ruta Grinyte**, Javier Barroso, Laura Saa, Valeri Pavlov TITLE: Modulating growth of CdS nanoparticles with redox process catalyzed by copper ions JOURNAL: Nano Letters. 2016 submitted

AUTHORS: **Ruta Grinyte**, Javier Barroso, Laura Saa, Valeri Pavlov TITLE: Modulation of growth of cysteine-capped cadmium sulfide quantum dots with enzymatically produced hydrogen peroxide JOURNAL: Nano Research., 2016 Nov DOI:10.1007/s12274-016-1378-1

AUTHORS: **Ruta Grinyte**, Javier Barroso, Marco Möler, Laura Saa, Valeri Pavlov TITLE: Electrochemical immunoassay for detection of superoxide dismutase 2 employing enzymatic formation and deposition of cadmium sulfide quantum dots on polyvinyl chloride microbeads JOURNAL: ACS Appl. Mater. Interfaces. 2016 Oct DOI:10.1021/acsami.6b08362

AUTHORS: Laura Saa, **Ruta Grinyte**, Ana Sánchez-Iglesias, Luis M. Liz-Marzan, Valeri Pavlov TITLE: Blocked enzymatic etching of gold nanorods: application to colorimetric detection of acetylcholinesterase activity and its inhibitors JOURNAL: ACS Appl Mater Interfaces. 2016 May 4, 8 (17), 11139-11146

AUTHORS: Javier Barroso, Laura Saa, **Ruta Grinyte**, Valeri Pavlov TITLE: Photoelectrochemical detection of enzymatically generated CdS nanoparticles: Application to development of immunoassay JOURNAL: Biosens Bioelectron. 2016 Mar 15, 77, 323-329

AUTHORS: **Ruta Grinyte**, Laura Saa, Gaizka Garai-Ibabe, Valeri Pavlov TITLE: Biocatalytic etching of semiconductor cadmium sulfide nanoparticles as a new platform for the optical detection of analytes JOURNAL: Chem. Commun., 2015, 51, 17152-17155

AUTHORS: **Ruta Grinyte**, Gaizka Garai-Ibabe, Laura Saa, Valeri Pavlov TITLE: Application of photocatalytic cadmium sulfide nanoparticles to detection of enzymatic activities of

glucose oxidase and glutathione reductase using oxidation of 3,3',5,5'-tetramethylbenzidine JOURNAL: Anal Chim Acta. 2015 Jun 30, 881, 131-138

AUTHORS:Maximilien Cottat, Cristiano D'Andrea, Ryohei Yasukuni, Natalia Malashikhina, **Ruta Grinyte**, Nathalie Lidgi-Guigui, Barbara Fazio, Angela Sutton, Olivier Oudar, Nathalie Charnaux, Valery Pavlov, Andrea Toma, Enzo Di Fabrizio, Pietro G. Gucciardi, Marc Lamy de la Chapelle TITLE: Highsensitivity, high selectivity SERS detection of MnSOD using optical nanoantennas functionalized with aptamers. JOURNAL: J. Phys. Chem. C, 2015, 119 (27), 15532–15540

AUTHORS: Gaizka Garai-Ibabe,Laura Saa, **Ruta Grinyte**, Valery Pavlov TITLE: Peroxidase-mimicking DNAzyme modulated growth of CdS nanocrystalline structuresin situ through redox reaction: application to development of genosensors andaptasensors. JOURNAL: AnalChem. 2014 Oct 21, 86(20)

AUTHORS: Paul Marzenell, Helen Hagen, Leopold Sellner, Thorsten Zenz, **Ruta Grinyte**, Valeri Pavlov, SteffenDaum, and Andriy Mokhir TITLE: Aminoferrocene-based prodrugs and their effects on human normal and cancer cells as well as bacterial cells. JOURNAL: J. Med. Chem., 2013, 56 (17), 6935-6944

AUTHORS: Gaizka Garai-Ibabe, **Ruta Grinyte**, Allon Canaan, Valery Pavlov TITLE: Homogeneous assay for detection of active EBNA-1 by thrombin activity modulation. JOURNAL: AnalChem., 2012 Jul 17, 84(14), 5834-5837

AUTHORS: Gaizka Garai; **Ruta Grinyte**; Efim i Golub; AllonCanaan; Marc Lamy de la Chapelle; Robert s Marks; Valery Pavlov TITLE: Detection of cancer marker Ebna-1 by DNA probe based biosensors. JOURNAL: Biosensorsand Bioelectronics, 2011 Dec 15, 30(1), 272-275

Acknowledgments

Seven years ago, after the defense of the thesis of my brother, one professor told me what now is my turn and I said: “I will never be a doctor”. But never say “never”, here I am.

First of all, I would like to thank my supervisor Dr. Valery Pavlov for all his support and understanding in research. Also for a good ideas and inspiration to continue working then sometimes you lose the motivation and for a very beautiful schemes.

I would also like to give special thanks to the group members. First of all to Dr. Laura Saa, I do not know what I would do without your help, always ready to help me with the problems at work and personal, also for nice time together after work. To Dr. Javier Barroso for helping me in research and in euskera and for very nice articles published together. To Beatriz Díez for bringing new vitality to our group. Also to former group member Dr. Gaizka Garai, for a meaningful discussions about the work and about the life.

Big thanks to laboratory members. To Dr. Fernando López, Dr. Susana Velasco and Ana Isabel Benítez for teaching me to shear a lab and for a nice coffee and lunch time together. Also for spending a great time together outside the lab.

During my thesis I spend really nice time here in San Sebastian. I met many people, I made a good friends. Thank you all!! Especially to Silvia Alonso, for being my friend, companion and a flatmate and for unforgettable concerts, terrace time and hours spending together, to Dr. Nina Gómez, for really nice and strange trips and very good time together, and to Manu (Dr. Emmanuel Ruggiero) for organizing all events and making my life more entertaining.

I acknowledge the University of the Basque Country for help in organization of my thesis defense, especially thanks to Dr. Isabel Goñi for the fast responses and help with the documents.

I gratefully acknowledge the funding sources that made my PhD work possible: CIC biomaGUNE for PhD fellowship especially to scientific director Dr. Luis Liz-Marzán to give me an opportunity to start the PhD thesis and the Spanish Ministry of Economy and Competitiveness (Project BIO2014-59741-R) for the financial support.

Galiausiai norėčiau padėkoti savo tėveliams, broliams ir brolenei už supratimą, paramą ir ištvermę visą tą laiką.